

# Chapter 5

## Results and discussion

In this chapter, we present the Raman-scattering and optical reflectivity measurements of single-crystalline thin films  $\text{Na}_x\text{CoO}_2$  ( $x = 0.68$  and  $0.75$ ), single crystal  $\text{Na}_{0.84}\text{CoO}_2$ , powder  $\text{Na}_{0.33}\text{K}_{0.015}\text{CoO}_2 \cdot 1.3\text{H}_2\text{O}$ , and  $\text{Co}_3\text{O}_4$  thin film.

### 5-1 Raman scattering

Fig. 5 - 1 shows the room-temperature unpolarized Raman-scattering spectra (with laser excited wavelength  $\lambda = 514.5$  nm) on  $ab$  - plane of  $\text{Na}_x\text{CoO}_2$  as a function of Na content  $x$  ( $x = 0.68, 0.75,$  and  $0.84$ ). All these samples were fresh or freshly cleaved. Two Raman peaks,  $E_{2g}$  around  $462\text{ cm}^{-1}$  and  $A_{1g}$  around  $576\text{ cm}^{-1}$  are commonly observed in these spectra. These results are consistent with previous studies by M. N. Iliev *et al.* for  $x = 0.7$  single crystal with hexagonal crystal structure,<sup>[23]</sup> J. F. Qu *et al.* for  $x = 0.3$  and  $0.7$  single crystals with hexagonal crystal structure,<sup>[51]</sup> and P. Lemmens *et al.* for  $x = 0.83$  and  $\sim 1$  single crystals.<sup>[49]</sup> According to the group theory analysis,<sup>[23,51]</sup>  $\text{Na}_x\text{CoO}_2$  with hexagonal crystal structure [ $P6_3/mmc$  space group] should have five Raman active phonon modes:

$$\Gamma(\text{Raman}) = A_{1g} + E_{1g} + 3E_{2g}, \quad (5.1.1)$$

where the  $A_{1g}$  and  $E_{1g}$  modes only involve motions from oxygen atoms, and the  $E_{2g}$  vibration modes consist of oxygen and sodium atoms, while Co motions are not Raman active.  $E_{1g}$  and  $E_{2g}$  modes represent the in-plane vibration, and  $A_{1g}$  mode is the

out-of-plane movement. The scheme of these phonon modes are shown in Fig. 5 - 2. The atomic positions, site symmetries, the  $\Gamma$ -point (zone center) phonon modes, and the cross section of Raman phonon modes expected of  $\text{Na}_x\text{CoO}_2$  for hexagonal crystal structure with  $P6_3/mmc$  space group are summarized in Table 5 - 1. It is clear that  $A_{1g}$  mode can be observed only by  $xx$  and  $zz$  polarized scattering from  $ab$  and  $ac$  - planes, respectively.  $E_{2g}$  mode is detectable only by  $xx$  and  $xy$  polarized scattering from  $ab$  - plane, while  $E_{1g}$  mode is observed only by  $zx$  polarized scattering from  $ac$  - plane.

In  $\text{Na}_x\text{CoO}_2$  systems, Na and  $\text{CoO}_2$  layers stack alternately, the Na ions are generally highly mobile among three different lattice sites: in Na(1) the Na ion is placed at (0, 0, 1/4), above the Co site of  $\text{CoO}_2$  layers; in Na(2) it occupies the (2/3, 1/3, 1/4) lattice point above the center of triangular lattice of  $\text{CoO}_2$  layers; the third site Na(2) is similar to the previous Na(2) one but Na is at (2x, x, 1/4).<sup>[1]</sup> The occupation probability of the above sites depends on both Na content and temperature. However, the disordered distribution, small occupation, and high mobility of Na ions can smear out the corresponding two  $E_{2g}$  phonon modes.<sup>[49,51]</sup>

Fig. 5 - 3 shows the polarized Raman-scattering spectra ( $\lambda = 514.5$  nm) of  $\text{Na}_{0.68}\text{CoO}_2$  thin film which were taken from  $ab$  - plane. The intensity of  $A_{1g}$  in unpolarized scattering is almost the same as the one in  $xx$  polarized scattering, but it vanishes in  $xy$  polarized scattering, indicating the contribution of  $A_{1g}$  is mainly due to  $xx$  polarized scattering.  $E_{2g}$  is observed in all three spectra, revealing that  $E_{2g}$  can be detected by both  $xx$  and  $xy$  polarized scattering. These results are consistent with the Raman cross section analysis, as mentioned above in Table 5 - 1.

Interestingly, two other different Raman features can be identified with different spots on  $ab$  - plane of  $x = 0.84$  single crystal sample with 514.5 nm laser

excited wavelength, as shown in Fig. 5 - 4(b). The Raman-scattering spectrum of  $\text{Co}_3\text{O}_4$  is also shown in Fig. 5 - 4(a) for a comparison, and the Raman phonon peaks fitting results are shown in Table 5 - 2. There are three important features to these spectra. First of all, the spectrum of area C shows two Raman peaks at 465 and 582  $\text{cm}^{-1}$ , corresponding to  $E_{2g}$  and  $A_{1g}$  Raman-active modes, consistent with that of our  $\text{Na}_x\text{CoO}_2$  ( $x = 0.68$  and  $0.75$ ) thin films and those reported by three groups that we have mentioned above.<sup>[23,49,51]</sup> This spectrum stands for the  $\text{Na}_x\text{CoO}_2$  systems.

Second, we focus on the Raman-scattering spectrum taken from area A. There are seven Raman phonon peaks at about 194.9, 454.5, 477.9, 519.0, 580.6, 618.3, and 685.2  $\text{cm}^{-1}$ , respectively. The phonon peaks at about 454.5 and 580.6  $\text{cm}^{-1}$ , are  $E_{2g}$  and  $A_{1g}$  Raman-active modes. On the other hand, the rest of five Raman phonon peaks at about 194.9, 477.9, 519.0, 618.3, and 685.2  $\text{cm}^{-1}$  are the signatures of  $\text{Co}_3\text{O}_4$ , which can be almost exactly related to those of  $\text{Co}_3\text{O}_4$  at 196.5, 483.1, 521.9, 620.3, and 691.9  $\text{cm}^{-1}$ , as shown in Fig. 5 - 3(a). This scenario is consistent with J. F. Qu *et al.*<sup>[51]</sup> However, H. X. Yang *et al.* for  $x = 0.75$  polycrystal<sup>[52]</sup> and Y. G. Shi *et al.* for  $x = 0.75$  single crystal<sup>[47]</sup> show conflicting results. They suggest that these five Raman phonon peaks represent the Raman-scattering signals of  $\text{Na}_x\text{CoO}_2$  and named  $\gamma\text{-Na}_{0.75}\text{CoO}_2$  by Yang, corresponding to five Raman-active phonon modes:  $A_{1g}$  at 685.3  $\text{cm}^{-1}$ ,  $E_{1g}$  at 194.9  $\text{cm}^{-1}$ , and  $3E_{2g}$  at 477.9, 519.0, and 618.3  $\text{cm}^{-1}$ . However, according to the Raman cross section analysis, both  $A_{1g}$  and  $E_{2g}$  can be detected from the  $ab$  - plane scattering, but  $E_{1g}$  is only observed from  $ac$  - plane scattering. Hence, it is impossible to observe all these five Raman phonon peaks from  $ab$  - plane at the same time. Therefore, the Raman spectrum from area A is the contribution from both  $\text{Na}_x\text{CoO}_2$  and  $\text{Co}_3\text{O}_4$ .

Third, the spectrum from area B, containing three clear Raman peaks at about

472, 582, and 682  $\text{cm}^{-1}$ , is similar to that reported by H. X. Yang *et al.*, who called as  $\beta\text{-Na}_{0.6}\text{CoO}_2$  for  $x = 0.6$  single crystal.<sup>[52]</sup> H. X. Yang suggests that their  $\text{Na}_{0.6}\text{CoO}_2$  is monoclinic structure with  $C2/m$  space group, nine Raman-active phonon modes ( $5A_g + 4B_g$ ) are possibly visible; this discrepancy could be caused by the overlap of Raman peaks. This result seems to imply that area B is monoclinic structure, different with the hexagonal structure of  $\text{Na}_{0.84}\text{CoO}_2$  single crystal observed from X-ray diffraction analysis. However, we will prove later that these three clear Raman phonon peaks on area B are due to the appearance of  $\text{Co}_3\text{O}_4$ , rather than the monoclinic structure by Raman-scattering ageing experiments.

According to the group theory analysis,<sup>[51,73]</sup>  $\text{Co}_3\text{O}_4$  with cubic crystal structure [ $Fd3m$  space group] should have five Raman active phonon modes:

$$\Gamma (\text{Raman}) = A_{1g} + E_g + 3F_{2g}. \quad (5.1.2)$$

Table 5 - 3 shows factor group analysis and relative Raman scattering cross section of  $\text{Co}_3\text{O}_4$  for cubic crystal structure with  $Fd3m$  space group. In this table,  $A_{1g}$  and  $E_g$  modes can be observed only by  $xx$  and  $zz$  polarized scattering, while  $F_{2g}$  mode is detectable only by  $xy$  and  $zx$  polarized scattering from  $ab$  and  $ac$  - planes. Hence, we can observe five Raman phonon modes in  $ab$  - plane spectrum.

In a short summary, we observe three different spectra on different areas of  $ab$  - plane in  $\text{Na}_{0.84}\text{CoO}_2$  single crystal. The two spectra different with the representative spectrum of  $\text{Na}_x\text{CoO}_2$  are caused by the appearance of  $\text{Co}_3\text{O}_4$ . Such phenomenon is due to the structural inhomogeneities of  $x = 0.84$  single crystal.

Next, we perform our Raman-scattering experiments by using another laser line with its excited wavelength at 632.8 nm. Fig. 5 - 5 shows Raman-scattering spectra of  $\text{Na}_{0.68}\text{CoO}_2$  and  $\text{Co}_3\text{O}_4$  thin films with two laser excitation wavelengths at 514.5 and

632.8 nm. The fitting results are shown in Table 5 - 4. The Raman-scattering spectra of  $\text{Na}_{0.68}\text{CoO}_2$  thin film as showing in Fig. 5 - 5(a), are similar to each other with these two different laser excitation wavelengths. In contract, the Raman-scattering spectra of  $\text{Co}_3\text{O}_4$  show dramatic changes with these two different laser excited wavelengths. In Fig. 5 - 5(b), the Raman phonon modes at about 198 and 620  $\text{cm}^{-1}$  measured with laser excitation wavelength at 632.8 nm are strongly enhanced (especially the 198  $\text{cm}^{-1}$  peak), while the 690  $\text{cm}^{-1}$  peak is monstrously depressed as compared with the other laser excited wavelength at 514.5 nm. Such characteristic provides us another efficient way to study the influence of  $\text{Co}_3\text{O}_4$  on the  $\text{Na}_x\text{CoO}_2$  systems due to the large enhancement of the 198  $\text{cm}^{-1}$  peak.

Fig. 5 - 6(a) shows the Raman-scattering spectra of  $\text{Na}_{0.68}\text{CoO}_2$  thin film and  $\text{Na}_{0.84}\text{CoO}_2$  single crystal which were burned by laser source (9 mW) with 632.8 nm excited wavelength, and the Raman-scattering spectrum of  $\text{Co}_3\text{O}_4$  thin film is also shown in this figure for a comparison. As we can see in Fig. 5 - 6, the appearance of the black spot on the surface of  $\text{Na}_{0.68}\text{CoO}_2$  thin film tells us that the sample had been burned by excess laser power. There are two important features to these spectra. First, the Raman-scattering spectra of these two burned samples show a redshift behavior and their linewidths are broader as compared with those of  $\text{Co}_3\text{O}_4$ . These scenarios can be explained by a looser and strongly disordered structure of these samples due to over-heating. Second, after burning, the Raman-scattering spectra of these two samples show the characteristic of  $\text{Co}_3\text{O}_4$ , similar to that reported by X. N. Zhang *et al.*, who annealed their  $\text{Na}_{0.5}\text{CoO}_2$  single crystal on an in-situ heating stage with  $T_{max} = 550 \text{ K}$ .<sup>[74]</sup> Accordingly, when we heat the  $\text{Na}_x\text{CoO}_2$  sample, it becomes unstable due to the high mobility of Na ion. It is known that the  $\text{Na}_{0.75}\text{CoO}_2$  film instantly react with carbon dioxide and moisture in the ambient environment resulting in loss of

sodium, and then leading to the emersion of  $\text{Co}_3\text{O}_4$ .

Fig. 5 - 7 shows Raman-scattering spectra of  $\text{Na}_{0.68}\text{CoO}_2$  thin film at 300 K and 15 K. The other spectra measured between these two temperatures were smeared by  $\text{Co}_3\text{O}_4$  during the temperature-decreasing process (not shown here). The fitting results are shown in Table 5 - 5. The  $E_{2g}$  mode at about  $460.3\text{ cm}^{-1}$  splits into two peaks at about  $452.2$  and  $473.5\text{ cm}^{-1}$ , while another  $E_{2g}$  mode appears at  $536.5\text{ cm}^{-1}$  when temperature is decreasing to 15 K. Such separation at low temperature is also observed in those reported by J. F. Qu *et al.* for  $x = 0.7$  single crystal below 160 K<sup>[51]</sup> and X. N. Zhang *et al.* for  $x = 0.5$  single crystal below 100 K.<sup>[74]</sup> However, another  $E_{2g}$  mode at  $536.5\text{ cm}^{-1}$  is also observed by P. Lemmens *et al.* for  $x = 0.82$  single crystal,<sup>[49]</sup> while it was not seen by J. F. Qu and X. N. Zhang's groups. This phenomenon reveals that Na ions have higher ordered at 15 K. Moreover, the  $A_{1g}$  mode at  $571.3\text{ cm}^{-1}$  moves to  $577.2\text{ cm}^{-1}$  as temperature lowers to 15 K, indicating the shortening of  $\text{Na}_{0.68}\text{CoO}_2$  lattice with decreasing temperature. The  $A_{1g}$  mode hardens due to anharmonicity at low temperature, while its linewidth is narrowed at low temperature, related to freezing of Na diffusion.

Fig. 5 - 8 shows Raman-scattering spectra of  $\text{Na}_{0.33}\text{K}_{0.015}\text{CoO}_2 \cdot 1.3\text{H}_2\text{O}$  powder measured from fresh one and 1 hour after exposing in humid air with 514.5 nm laser line at room temperature. The fitting results are shown in Table 5 - 6. The Raman-scattering spectrum of the fresh one shows different result with that reported by K. Takada *et al.* for  $\text{Na}_{0.35}\text{CoO}_2 \cdot y\text{H}_2\text{O}$  powder, who assign one  $E_{1g}$  mode at around  $445\text{ cm}^{-1}$  and two  $E_{2g}$  modes at around  $505$  and  $550\text{ cm}^{-1}$  with a frequency range from  $200$  to  $800\text{ cm}^{-1}$ .<sup>[53]</sup> Such difference may be caused by the influence of K ions. However, after exposing the powder in humid air for 1 hour, five clear peaks appear at around  $193.5$ ,  $470.9$ ,  $512.9$ ,  $620.6$ , and  $676.3\text{ cm}^{-1}$ , revealing the emergence

of  $\text{Co}_3\text{O}_4$ . So, it provides the evidence that both single crystal and powder samples show structural inhomogeneities. Moreover, the emergence of  $\text{Co}_3\text{O}_4$  seems to imply that the degradation effects of  $\text{Na}_x\text{CoO}_2$  systems. In order to gain more information, we perform time-dependent Raman-scattering experiments.

Fig. 5 - 9 shows two video images of  $x = 0.84$  single crystal taken by microscopy with a  $50\times$  objective, one is the freshly cleaved surface, while another one has been exposed in humid air for 1 hour. In these figures, we center on a hollow circle as a distinct mark. Obviously, many black spots arose after one hour as we can see in Fig. 5 - 9(b). Similar results have also been found in our  $\text{Na}_x\text{CoO}_2$  thin films. Since  $\text{Na}_x\text{CoO}_2$  instantly reacts with moisture in the ambient environment, these black spots are related to these impurities. Fig. 5 - 10(a) shows the difference between fresh clear point (area A) and black point (area B) which is exposing in humid air for 2 hours in Raman-scattering spectra of  $\text{Na}_{0.75}\text{CoO}_2$  thin film. Their video images are shown in Figs. 5 - 10(b) and (c). The fitting results are shown in Table 5 - 7. Both  $E_{2g}$  and  $A_{1g}$  modes soften and become broader in area B than in area A, indicating an obviously disordered structure due to degradation. The spectral profile of such disorder-induced Raman-scattering qualitatively displays the smeared phonon density-of-states versus phonon energy distribution for the perfect crystalline structure.<sup>[75,76]</sup>

After six days, we measured the Raman-scattering spectra of  $\text{Na}_{0.75}\text{CoO}_2$  thin film again: two spectra different from the original one were observed and shown in Fig. 5 - 11(a). Their video images are shown in Figs. 5 - 11(b) and (c). The fitting results are shown in Table 5 - 8. The spectrum from area C is related to the influence of  $\text{Co}_3\text{O}_4$ , indicating that  $\text{Co}_3\text{O}_4$  may accompany with degradation. Beside, the spectrum from area D shows an interesting feature that the  $E_{2g}$  mode splits into two

peaks, similar to that reported by M. N. Iliev *et al.* in their ageing experiments on *ac* - plane for  $x = 0.7$  single crystal which is measured four days after sample preparation.<sup>[23]</sup> Accordingly, the separation of  $E_{2g}$  mode and the appearance of  $\text{Co}_3\text{O}_4$  show further evidence of lattice disorder and structural inhomogeneities due to degradation.

It is worthy to note that all these Raman-scattering spectra and all groups study on  $\text{Na}_x\text{CoO}_2$  systems so far were measured on different spots of  $\text{Na}_x\text{CoO}_2$  samples. Because of the obviously structural inhomogeneities in  $\text{Na}_x\text{CoO}_2$  systems, the degraded effect will be unclear. So, it is interesting and important to know what happen if we perform in-situ Raman-scattering ageing experiments. Fig. 5 - 12(a) shows Raman-scattering spectra of  $\text{Na}_{0.75}\text{CoO}_2$  thin film measured from fresh and 42 minutes after exposing in humid air with 514.5 nm laser line at room temperature. Their video images are shown in Figs. 5 - 10(b) and 5 - 12(c). The fitting results are shown in Table 5 - 9. Both spectra show two Raman phonon modes:  $E_{2g}$  at about  $462\text{ cm}^{-1}$  and  $A_{1g}$  at about  $577\text{ cm}^{-1}$ . Although the video image seems to remain the same after 42 minutes, we still can obtain a little change from the fitting results: the peaks become hardened and broader after 42 minutes, indicating lattice disorder as time goes by. Accordingly, the band broadening and spectral weight redistribution represent that  $\text{Na}_x\text{CoO}_2$  lattice is getting more disordered with ageing.

In addition, we performed the time-dependent Raman-scattering experiments on area E of aged  $\text{Na}_{0.75}\text{CoO}_2$  thin film, as shown in Fig. 5 - 13, while two video images representing before and after images of our measurements are shown in Figs. 5 - 13(b) and (c), respectively. The 514.5 nm laser source (5 mW) was used for excitation. The spectrum of the initial one shows three Raman phonon modes, similar to our spectrum on area B of  $x = 0.84$  single crystal and that reported by H. X. Yang *et*

*al.* for  $x = 0.6$  single crystal as  $\beta\text{-Na}_{0.6}\text{CoO}_2$ .<sup>[52]</sup> However, after 40 seconds, four clear Raman phonon modes related to  $\text{Co}_3\text{O}_4$  appear, and are getting more hardened with increasing time. This is a strong evidence that within  $\sim 2 \mu\text{m}$  spatial resolution,  $\text{Co}_3\text{O}_4$  emerges under the laser source (5 mW) with 514.5 nm wavelength, resulting in the transition from one spectrum having three Raman phonon modes to another spectrum having seven Raman phonon modes. It is reasonable to infer that the three-modes spectrum is caused by  $\text{Co}_3\text{O}_4$ , and because of the mode at around  $680 \text{ cm}^{-1}$  is much stronger than any other modes else, we can only obtain one mode is contributed by  $\text{Co}_3\text{O}_4$  in this spectrum, while the two others modes are the typical modes of  $\text{Na}_x\text{CoO}_2$ . Hence, we suggest that the  $680 \text{ cm}^{-1}$  peak in the three-modes spectrum is related to  $\text{Co}_3\text{O}_4$  rather than the characteristic of monoclinic structure of  $\text{Na}_x\text{CoO}_2$  that reported by H. X. Yang *et al.*<sup>[52]</sup>

According to our discussions above,  $\text{Na}_x\text{CoO}_2$  systems show structural inhomogeneities behavior and the heterogeneous distribution caused by  $\text{Co}_3\text{O}_4$ . It is interesting and essential to know how the morphology, facial distribution and domain size of  $\text{Co}_3\text{O}_4$  on  $\text{Na}_x\text{CoO}_2$  surface are developing. Raman mapping experiment coupled with the ratioimage method with higher contrast and reliability provides a very attractive way to characterize the compatibility and phase behavior of the  $\text{Na}_x\text{CoO}_2$  systems. Hence, we present Raman mapping experiments on our  $\text{Na}_x\text{CoO}_2$  systems. Fig. 5 - 14(a) shows the video image on *ab* - surface of  $\text{Na}_{0.84}\text{CoO}_2$  single crystal which was freshly cleaved, while our Raman-scattering spectra were taken on each intersection point crossed by grey lines to form a rectangular region. A total of 25 Raman spectra were recorded by point-to-point mapping with a step size of  $10 \mu\text{m}$  within the rectangular region ( $40 \times 40 \mu\text{m}^2$ ), while 514.5 nm laser line was used for excitation. The Raman spectrum taken on the red point is shown in Fig. 5 - 14(b),

while the band  $681\text{ cm}^{-1}$  is marked by a dashed line. Since the band  $681\text{ cm}^{-1}$  stands for the existence of  $\text{Co}_3\text{O}_4$  as we mentioned above, its Raman intensity represents the concentration of  $\text{Co}_3\text{O}_4$ . Fig. 5 - 14(c) shows the Raman mapping ratioimage of band  $681\text{ cm}^{-1}$ . We can obtain five brighter areas in this image, indicating higher  $\text{Co}_3\text{O}_4$  concentration. Accordingly, we know the domain size of  $\text{Co}_3\text{O}_4$  is less than  $10\text{ }\mu\text{m}$ . The distribution of  $\text{Co}_3\text{O}_4$  seems to be unsystematic within our measured region. However, as compared with the video image, the areas of  $\text{Co}_3\text{O}_4$  do not show much different with those areas of pure  $\text{Na}_x\text{CoO}_2$ . That may be due to the larger step size that we chose.

An interesting phenomenon is obtained in another  $\text{Na}_{0.84}\text{CoO}_2$  single crystal which was exposing in ambient environment for 2.5 years by F. C. Chou *et al.* (unpublished). During the exposing process, the sodium ions of fringe region were reacting with carbon dioxide and moisture, resulting in superior loss of sodium. Hence, the sodium content is the lowest ( $x \sim 0.3$ ) close to edge, and then enhances with increasing distance from edge up to impregnate Na content ( $x \sim 0.84$ ) region ( $\sim 50\text{ }\mu\text{m}$  from edge). These results are proved by electron probe X-ray microanalyzer (EPMA). Here, we analyze this sample by using Raman mapping experiment coupled with the ratioimage method. Fig. 5 - 15 shows Raman mapping spectra as a function of distance from edge on *ab* - plane of this  $\text{Na}_{0.84}\text{CoO}_2$  single crystal which was freshly cleaved before measuring. A total of 25 Raman spectra were recorded by point-to-point mapping with a step size of  $2\text{ }\mu\text{m}$  on a  $50\text{ }\mu\text{m}$  straight line, while  $514.5\text{ nm}$  laser line was used for excitation. We obtain that the Raman spectra taken on marginal region from  $5$  to  $7\text{ }\mu\text{m}$  show the characteristic combination with  $\text{Co}_3\text{O}_4$  and  $\text{Na}_x\text{CoO}_2$ .

For the Raman spectrum of  $11\text{ }\mu\text{m}$  shown in Fig. 5 - 16, there are four Raman

peaks at about 437.8, 457.4, 494.1, and 578.3  $\text{cm}^{-1}$ , revealing a spectrum different with neither typical  $\text{Na}_x\text{CoO}_2$  spectrum nor the contribution of  $\text{Co}_3\text{O}_4$ . This spectrum should be corresponding to  $x = 0.5$  compound.<sup>[49,51,74]</sup> It is known that for  $\text{Na}_{0.5}\text{CoO}_2$ , the electron diffraction studies demonstrated that the Na ions become ordered and the insulating charge ordering state is believed to be closely related to the Na ions ordering in this system.<sup>[27]</sup> Moreover, the location of  $x = 0.5$  content obtained by Raman mapping experiment is close to the EPMA result (15 ~ 20  $\mu\text{m}$  from edge), providing another cogent evidence for the diffused effect in aged  $\text{Na}_x\text{CoO}_2$  single crystal.

For the region between 13 and 29  $\mu\text{m}$ , the contribution of  $\text{Co}_3\text{O}_4$  disappears, while  $E_{2g}$  and  $A_{1g}$  modes remain invariant, indicating the spectra in this region is indistinguishable. However, the signal of  $\text{Co}_3\text{O}_4$  emerges again in the region from 31 to 39  $\mu\text{m}$  and then vanishes when the distance from edge is more than 39  $\mu\text{m}$ , revealing unsystematic distribution of  $\text{Co}_3\text{O}_4$ . Moreover, for the region more than 31  $\mu\text{m}$  from edge, it shows slightly redshift for both  $E_{2g}$  and  $A_{1g}$  modes. Since the Na diffused effect in this sample is verified, such phenomenon may be caused by the change of Na concentration after one critical Na content.

## 5-2 Optical reflectance

### 5-2-1 Room temperature spectra

As mentioned above, we identified the  $\text{Co}_3\text{O}_4$  phase in the aged  $\text{Na}_{0.84}\text{CoO}_2$  single crystal and  $\text{Na}_x\text{CoO}_2$  ( $x = 0.68$  and  $0.75$ ) thin films by using micro Raman-scattering technique. In order to gain additional insight into the impurity phase of these samples, the optical reflectance spectra of  $\text{Na}_x\text{CoO}_2$  ( $x = 0.68$  and  $0.75$ ),  $\text{Co}_3\text{O}_4$ ,  $\text{Na}_2\text{CO}_3$  thin films, and  $\text{Al}_2\text{O}_3$  substrate are presented. Figs. 5 - 17(a) and (b) show the room temperature optical reflectance spectra of two  $\text{Na}_x\text{CoO}_2$  ( $x = 0.68$  and  $0.75$ ) thin films. The spectra show the characteristic of a metallic behavior at low frequencies with Drude response, and several phonon peaks in the far-infrared region. With increasing frequency, there are several interband transitions in the visible and ultraviolet frequency range. In contrast, the spectra of  $\text{Co}_3\text{O}_4$ ,  $\text{Na}_2\text{CO}_3$  thin films, and  $\text{Al}_2\text{O}_3$  substrate show the characteristic of an insulator at low frequencies. A number of phonon features are observed in the far-infrared region. For higher frequencies, only the spectrum of  $\text{Co}_3\text{O}_4$  reveals several prominent peaks, whereas the spectra of  $\text{Na}_2\text{CO}_3$  and  $\text{Al}_2\text{O}_3$  are almost dispersionless.

Due to the reststrahlen regions of sapphire overlapping with those of  $\text{Na}_{0.68}\text{CoO}_2$ ,  $\text{Na}_{0.75}\text{CoO}_2$ ,  $\text{Co}_3\text{O}_4$ , and  $\text{Na}_2\text{CO}_3$  thin films, we have used thin-film optics and the Drude-Lorentz analysis to model the optical properties of these samples. The Drude-Lorentz model<sup>[77]</sup> used for the complex dielectric function of each layer may be written as

$$\varepsilon(\omega) = -\frac{\omega_{pD}^2}{\omega^2 + \frac{i\omega}{\tau_D}} + \sum_{j=1}^N \frac{\omega_{pj}^2}{\omega_j^2 - \omega^2 - i\omega\gamma_j} + \varepsilon_\infty, \quad (5.2.1)$$

where  $\omega_{PD}$  and  $1/\tau_D$  are the plasma frequency and the scattering rate of the Drude component;  $\omega_j$ ,  $\gamma_j$ , and  $\omega_{Pj}$  are the frequency, damping, and oscillator strength of the  $j^{\text{th}}$  Lorentzian contribution; and  $\varepsilon_\infty$  is the high frequency limit of  $\varepsilon(\omega)$  which includes interband transitions at frequencies above the measured range. The parameters used to fit the measured optical data are listed in Tables 5 - 10, 11, and 12. The spectra of  $\text{Na}_{0.68}\text{CoO}_2$  and  $\text{Na}_{0.75}\text{CoO}_2$  thin films are reproduced by considering a Drude-type component due to itinerant charge carriers and twelve Lorentzian oscillators representing the phonon peaks and the electronic interband transitions. Five and two Lorentzian oscillators are used to fit the spectra of  $\text{Co}_3\text{O}_4$  and  $\text{Na}_2\text{CO}_3$  thin films.

Fig. 5 - 18 shows the frequency-dependent optical conductivity of  $\text{Na}_{0.68}\text{CoO}_2$ ,  $\text{Na}_{0.75}\text{CoO}_2$ ,  $\text{Co}_3\text{O}_4$ , and  $\text{Na}_2\text{CO}_3$  thin films. For the two  $\text{Na}_x\text{CoO}_2$  thin films, there are three important features to their spectra. First, two prominent peaks are observed and labeled as A and B peaks,<sup>[37]</sup> where A (centered at  $25080 \text{ cm}^{-1}$  for  $x = 0.68$  and  $27040 \text{ cm}^{-1}$  for  $x = 0.75$ ) and B (centered at  $12300 \text{ cm}^{-1}$  for  $x = 0.68$  and  $11000 \text{ cm}^{-1}$  for  $x = 0.75$ ) represent two interband transitions from the occupied Co  $3d t_{2g}$  to the empty Co  $3d e_g$  bands due to the octahedral crystal field splitting. This observation is similar to the results reported by N. L. Wang *et al.*, who observed A and B peaks at  $25000 \text{ cm}^{-1}$  and  $13000 \text{ cm}^{-1}$ , respectively for  $\text{Na}_{0.7}\text{CoO}_2$  single crystal.<sup>[37]</sup> The local density approximation calculation of  $\text{NaCo}_2\text{O}_4$ , reveals that the energy difference between the  $t_{2g}$  and  $e_g$  bands is estimated to be  $2.5 \text{ eV}$  ( $20165 \text{ cm}^{-1}$ ),<sup>[32]</sup> which lies between these two peaks. The inelastic neutron scattering measurements of  $\text{Na}_{0.75}\text{CoO}_2$  ferromagnetic spin fluctuations existing within the cobalt-oxygen,<sup>[38]</sup> and thereby the actual effect of the exchange splitting would be a broadening of the  $t_{2g}$  and  $e_g$  band widths. On one hand, it reduces the minimum excitation gap between the  $t_{2g}$  and  $e_g$  bands (leading to the B peak); on the other hand, it leads to further increase of the

largest energy separation between the  $t_{2g}$  and  $e_g$  bands (A transition). Second, the difference of center frequency between A and B bands of  $x = 0.75$  is larger than that of  $x = 0.68$ , indicating strong spin fluctuation in  $x = 0.75$ . Third, C (centered at  $3700 \text{ cm}^{-1}$  for  $x = 0.68$  and  $3030 \text{ cm}^{-1}$  for  $x = 0.75$ ) is a weak absorption in the midinfrared region. N. L. Wang *et al.* reported that the C band is around  $3300 \text{ cm}^{-1}$  for  $\text{Na}_{0.7}\text{CoO}_2$  single crystal, similar to our data. The C band is likely due to a transition from occupied  $e_g$  bands to some partially un-filled  $a_{1g}$  bands within  $t_{2g}$  manifold,<sup>[37]</sup> as shown in Fig. 2 - 14(b). In Fig. 5 - 18(b),  $\text{Co}_3\text{O}_4$  thin film reveals 4 obvious peaks (labeled as 1<sup>st</sup>, 2<sup>nd</sup>, 3<sup>rd</sup>, and 4<sup>th</sup>) at about  $6742 \text{ cm}^{-1}$  (0.84 eV),  $11329 \text{ cm}^{-1}$  (1.40 eV),  $20653 \text{ cm}^{-1}$  (2.56 eV) and  $35918 \text{ cm}^{-1}$  (4.45 eV). Our results differ from those reported by H. Yamamoto *et al.*, they observed the optical absorption peaks at about 0.75, 0.9, 1.7, and 3.0 eV.<sup>[78]</sup> It has been reported that  $\text{Co}_3\text{O}_4$  has band gaps at 0.8, 1.3, and 2.1 eV by optical absorption spectra, and these energy gaps are associated with charge transfers from  $\text{Co}^{2+} (\pi^*e)$  to  $\text{Co}^{2+} (\pi^*t_2)$ , from  $\text{Co}^{3+} (\pi^2t_2)$  to  $\text{Co}^{2+} (\sigma^*t_2)$ , and from  $\text{O}^{2-} (\pi^*\Gamma)$  to  $\text{Co}^{2+} (\sigma^*t_2)$ , respectively.<sup>[78-82]</sup> It is important to note that since the optical conductivity spectra of two  $\text{Na}_x\text{CoO}_2$  thin films and  $\text{Co}_3\text{O}_4$  thin film are so different neither mid-infrared nor far-infrared region, there is no  $\text{Co}_3\text{O}_4$  contribution in our conductivity spectra of  $\text{Na}_x\text{CoO}_2$  thin films.

Fig. 5 - 19 illustrates the far-infrared optical conductivity of  $\text{Na}_{0.68}\text{CoO}_2$ ,  $\text{Na}_{0.75}\text{CoO}_2$ ,  $\text{Co}_3\text{O}_4$ , and  $\text{Na}_2\text{CO}_3$  thin films at room temperature. For  $\text{Na}_x\text{CoO}_2$ , the  $P6_3/mmc$  space group with 2 f.u. per unit cell and two occupied Na Wyckoff sites,<sup>[57]</sup> the modes grouped according to their optical activity are  $\Gamma_{\text{IR}} = 4 A_{2u} + 4 E_{1u}$ ,  $\Gamma_{\text{Raman}} = A_{1g} + E_{1g} + 3 E_{2g}$ ,  $\Gamma_{\text{acoustic}} = A_{2u} + E_{1u}$ , and  $\Gamma_{\text{silent}} = 2 B_{2u} + 2 E_{2u} + 3 B_{1g}$ . In Fig. 5 - 19 (a), we can identify five phonon peaks at about  $358, 434, 518, 542,$  and  $632 \text{ cm}^{-1}$  for  $x = 0.68$  sample, while  $379, 435, 510, 537,$  and  $632 \text{ cm}^{-1}$  for  $x = 0.75$  sample. M. Schubert

*et al.* reported four  $E_{1u}$  vibration modes of  $Al_2O_3$  at about 385, 439, 569, and 634  $cm^{-1}$ .<sup>[35]</sup> The observed three phonon peaks at about 358, 434 and 632  $cm^{-1}$  of our  $Na_xCoO_2$  spectra are due to the contribution of  $Al_2O_3$  substrate. Moreover, according to first principle analysis,  $E_{1u}$  is the in-plane phonon mode assigned to Na-Co and Co-O stretching and  $A_{1u}$  is the out-of-plane phonon mode caused by Na-Co and Co-O vibrations.<sup>[83,84]</sup> Therefore, we assign the modes at about 518 and 542  $cm^{-1}$  to  $E_{1u}$  vibrations of  $Co^{4+}$  against O and  $Co^{3+}$  against O, respectively. The splitting of the Co-O in-plane mode can be explained by  $Co^{3+}$  and  $Co^{4+}$  ordering as sketched in Fig. 5 - 20.

Fig. 5 - 21 shows the far-infrared optical conductivity data of fresh and aged  $Na_{0.68}CoO_2$  and  $Na_{0.75}CoO_2$  thin films at room temperature. These aged samples were exposed in humid air over than 30 days and 10 days, respectively. In Fig. 5 - 21, the spectra of both aged  $x = 0.68$  and  $0.75$  samples show dramatic change in comparison with fresh ones. First, there is no Drude response of aged samples at low frequency, indicating the sample has degraded into insulator. Second, there are four clear phonon peaks at around 385, 437, 565 and 632  $cm^{-1}$  of the aged samples, all of them can be exactly relative to  $E_{1u}$  vibration modes of  $Al_2O_3$  substrate. Third, the phonon peaks of aged samples at around 408, 518 and 542  $cm^{-1}$  are strongly suppressed and even vanished, especially the  $x = 0.68$  owing to Na ion has reacted with humidity. The aged  $Na_{0.75}CoO_2$  thin films has less time exposing in air, leading to the less extent of signals of substrate.

There is a striking feature observed in Fig. 5 - 19(a), especially  $Na_{0.75}CoO_2$  thin films, the conductivity drops at very low frequencies, resulting in a low-frequency peak at 191  $cm^{-1}$  for  $x = 0.68$  and 163  $cm^{-1}$  for  $x = 0.75$  component. Such peak has also been observed by Bernhard *et al.* on  $Na_{0.82}CoO_2$  single crystal, N. L. Wang *et al.*, and

G. Caimi *et al.* on  $\text{Na}_{0.7}\text{CoO}_2$  single crystal.<sup>[37,57,60]</sup> Therefore, the metallic component of  $\sigma_1(\omega)$  cannot be fully reproduced by a simple Drude term, the most common description for simple metals, also successfully applied in several oxides. The effective metallic component of the optical conductivity can be alternatively described in terms of an "anomalous-Drude" model,<sup>[56]</sup> where both the effective mass  $m^*(\omega)/m_b$  and the scattering rate  $1/\tau(\omega)$  of the itinerant charge carriers are allowed to depend on frequency. The detailed behavior and corresponding charge dynamic analysis of this interesting feature will be canvassed later with temperature dependence optical conductivity spectra.

Moreover, Fig. 5 - 19(b) is the far-infrared optical conductivity data of  $\text{Co}_3\text{O}_4$  and  $\text{Na}_2\text{CO}_3$  thin films at room temperature. For  $\text{Co}_3\text{O}_4$  thin films, there is an absorption peak at  $670\text{ cm}^{-1}$ , which is associated with the vibration of the Co-O bond in the oxide's octahedral sublattice.<sup>[85]</sup>

## 5-2-2 Temperature dependence

The temperature-dependent infrared reflectance spectra of  $\text{Na}_{0.68}\text{CoO}_2$  and  $\text{Na}_{0.75}\text{CoO}_2$  thin films are presented in Fig. 5 - 22. First of all, the spectra of both  $\text{Na}_x\text{CoO}_2$  thin films do not change significantly with temperature, which implies that there is no structural phase transition within the temperature range investigated. Besides, we can recognize the quite sharp plasma edge feature with onset at about  $7800\text{ cm}^{-1}$  for  $\text{Na}_{0.68}\text{CoO}_2$  thin film and  $6400\text{ cm}^{-1}$  for  $\text{Na}_{0.75}\text{CoO}_2$  thin film. The intensity of reflectance spectra increases with decreasing temperature below  $1700\text{ cm}^{-1}$ , indicative for the metallic character of for both  $\text{Na}_x\text{CoO}_2$  thin films. In order to qualitatively analyze the temperature-dependent behavior, we have fitted the reflectance data with the Drude-Lorentz model;<sup>[77]</sup> the fitting parameters are shown in Tables 5 - 13 and 14.

Figs. 5 - 23 and 24 show the temperature-dependent infrared conductivity spectra of  $\text{Na}_x\text{CoO}_2$  ( $x = 0.68$  and  $0.75$ ) thin films. As expected from the reflectance spectra of both  $\text{Na}_x\text{CoO}_2$  thin films, the effective intraband metallic components in  $\sigma_1(\omega)$  are enhanced below  $100\text{ cm}^{-1}$  and the  $\sigma_1(\omega \rightarrow 0)$  limit obtained by extrapolating the conductivity spectra to  $0\text{ cm}^{-1}$  increase with decreasing temperature, as typical for metallic systems. Moreover, the linewidths of  $\gamma$  peaks at around  $3000\text{ cm}^{-1}$  of both  $\text{Na}_x\text{CoO}_2$  thin films are getting broader as decreasing temperature, while their central frequencies and spectral weights show temperature-independent behavior. Fig. 5 - 25 shows the temperature dependence of the far-infrared conductivity of two thin films. There are three important features to these spectra. First, two phonon peaks (labeled as 3<sup>rd</sup> and 4<sup>th</sup>) at around  $504$  and  $533\text{ cm}^{-1}$  of shift to higher frequency with decreasing temperature, while the phonon peaks (labeled as 1<sup>st</sup>, 2<sup>nd</sup>, and 5<sup>th</sup>) of substrate at around

360, 416, and 632  $\text{cm}^{-1}$  show temperature-independent behavior. For 3<sup>rd</sup> and 4<sup>th</sup> peaks of both  $\text{Na}_x\text{CoO}_2$  ( $x = 0.68$  and  $0.75$ ) thin films, Figs. 5 - 26 and 27 illustrate their temperature dependence of frequency ( $\omega_j$ ), linewidth ( $\gamma_j$ ), and spectral weight ( $S_j$ ). The linewidth and spectral weight do not change a lot, while the frequency blueshifts with decreasing temperature. Such phenomenon can be explained by the lattice is getting squeezed with decreasing temperature. Anharmonic interactions are relevant to the high-order terms of the atomic vibrations beyond traditional harmonic terms. The temperature-dependent phonon frequency and linewidth can be written as,<sup>[65,86,87]</sup>

$$\omega(T) = \omega^0 + a \left( \frac{2}{e^{\omega^0/2k_B T} - 1} + 1 \right), \quad (5.2.2)$$

and

$$\Gamma(T) = \Gamma^0 + b \left( \frac{2}{e^{\omega^0/2k_B T} - 1} + 1 \right), \quad (5.2.3)$$

where  $\omega^0$  and  $\Gamma^0$  are the harmonic frequency of the optical mode and the line broadening due to defect. The parameters,  $a$  and  $b$ , are the anharmonic coefficients, and  $1/(e^{\omega^0/2k_B T} - 1)$  corresponds to the thermal population factor of the acoustic modes. Table 5 - 15 lists the fitting parameters of two samples. The parameters  $a$  are negative, which indicate the peaks shift to higher frequency with decreasing temperature due to anharmonic phonon decay. In contrast, the parameters  $b$  are positive revealing the linewidths narrowing with decreasing temperature. The agreement between the experimental data points and fitting curves is reasonably good.

Second, the Drude plasma frequency  $\omega_{PD}$  (spectral weight) of  $\text{Na}_{0.68}\text{CoO}_2$  and

Na<sub>0.75</sub>CoO<sub>2</sub> thin films at 300 K are about 3010 and 3071 cm<sup>-1</sup>, while the scattering rate of the free carriers 1/τ<sub>D</sub> are about 60.5 and 198.0 cm<sup>-1</sup>, respectively. The Drude resistivity ρ<sub>Drude</sub> can be written as:

$$\rho_{Drude} = \frac{4\pi}{\omega_{PD}^2 \tau_D}, \text{ in unit } \Omega\text{-cm} \quad (5.2.4)$$

Here, we obtain ρ<sub>Drude</sub> are 0.40 and 1.26 mΩ-cm for Na<sub>0.68</sub>CoO<sub>2</sub> and Na<sub>0.75</sub>CoO<sub>2</sub> thin films at room temperature, while the resistivity obtained from the ρ-*T* measurement (Fig. 4 - 4) are 0.80 and 1.08 mΩ-cm, respectively. Such difference may be caused by the different way we measured these thin films. Fig. 5 - 28 shows temperature dependence of the ω<sub>PD</sub> and 1/τ<sub>D</sub> of Na<sub>0.68</sub>CoO<sub>2</sub> and Na<sub>0.75</sub>CoO<sub>2</sub> thin films. The development of an extremely narrow and sharp Drude component at low temperature which corresponds to the well-defined quasiparticles in angle-resolved photoemission spectroscopy experiment (ARPES).<sup>[35]</sup> These scenarios show metallic behavior of the two fresh thin films and consistent with the four probe dc measurements. Notably, for *x* = 0.68 thin film, the 1/τ<sub>D</sub> (20 K) is about 6 cm<sup>-1</sup> compared with 1/τ<sub>D</sub> (300 K) = 61 cm<sup>-1</sup>, consistent with the small residual resistivity. Since the residual resistivity and 1/τ<sub>D</sub> (20 K) is proportional to the concentration of impurities or defects in the thin films, the transport and optical conductivity results indicate high quality of the Na<sub>0.68</sub>CoO<sub>2</sub> thin film. However, for *x* = 0.75 thin film, the 1/τ<sub>D</sub> (10 K) is about 100 cm<sup>-1</sup> compared with 1/τ<sub>D</sub> (300 K) = 198 cm<sup>-1</sup>, revealing less metallic behavior of this compound.

A numerical calculation can provide more convinced evidence. First, the effective carrier density *n* can be obtained by

$$n = \frac{m^* \omega_{PD}^2}{4\pi e^2}, \quad (5.2.5)$$

where  $m^* \sim 5m_e$ .<sup>[56,60]</sup>

Second, we substitute  $n$  into equation (5.2.5) to get mean free path  $l$

$$l = \frac{\tau_D \hbar (3\pi^2 n)^{1/3}}{m^*} \quad (5.2.6)$$

We can obtain the carrier mean free path of  $\text{Na}_{0.68}\text{CoO}_2$  and  $\text{Na}_{0.75}\text{CoO}_2$  thin films at 300 K to be around 19 and 6 Å, respectively. In addition, we also calculate the carrier mean free path of  $\text{Na}_{0.68}\text{CoO}_2$  and  $\text{Na}_{0.75}\text{CoO}_2$  thin films from 10 K to 300 K, as shown in Fig. 5 - 29. With decreasing temperature, the carrier mean free path is getting longer for both  $\text{Na}_{0.68}\text{CoO}_2$  and  $\text{Na}_{0.75}\text{CoO}_2$  thin films. Moreover, the carrier electron mean free path of  $\text{Na}_{0.68}\text{CoO}_2$  thin film increase rapidly below 100 K, and reach to nearly 250 Å, revealing electric conductivity is fiercely strengthened below 100 K.

Third, as mentioned above, there is a suppression of the optical conductivity at around  $150 \text{ cm}^{-1}$  in both  $\text{Na}_x\text{CoO}_2$  thin films, especially the  $x = 0.68$  one below a typical constant energy scale  $\sim 200 \text{ cm}^{-1}$ , as shown in Fig. 5 - 25. Since the dc resistivity is purely metallic as we can see in Fig. 4 - 4, it is not a signature of charge localization. Such phenomenon is irrespective of temperature, and is suggested to be the infrared signature of the pseudogap state.<sup>[88-91]</sup> Fig. 5 - 30 shows frequency ( $\omega_j$ ), linewidth ( $\gamma_j$ ), and spectral weight ( $S_j$ ) versus temperature of the  $150 \text{ cm}^{-1}$  peak of  $\text{Na}_{0.68}\text{CoO}_2$  and  $\text{Na}_{0.75}\text{CoO}_2$  thin films. With decreasing temperature, the  $150 \text{ cm}^{-1}$  peak shifts to lower frequencies, similar trend can be seen in those reported by N. L. Wang *et al.* for  $\text{Na}_{0.7}\text{CoO}_2$  single crystal,<sup>[37]</sup> C. Bernhard *et al.* for  $\text{Na}_{0.82}\text{CoO}_2$  single crystal,<sup>[57]</sup> D. Wu *et al.* for  $\text{Na}_x\text{CoO}_2$  ( $x = 0.18, 0.32, 0.36, \text{ and } 0.85$ ) single crystals,<sup>[58]</sup> and D. Wu *et al.* for  $\text{Na}_{0.7}\text{CoO}_2$  single crystal.<sup>[59]</sup> However, S. Lupi *et al.* reported that a strong far-infrared peak develops at nearly  $100 \text{ cm}^{-1}$  below 160 K and due to spin density wave instability, it blueshifts to  $200 \text{ cm}^{-1}$  below 30 K for  $\text{Na}_{0.85}\text{CoO}_2$  and

Na<sub>0.95</sub>CoO<sub>2</sub> single crystals.<sup>[55]</sup> We emphasize that there is no detectable spectral weight loss found in the *ab* - plane conductivity spectra of both Na<sub>x</sub>CoO<sub>2</sub> thin films with decreasing temperature according to Fig. 5 - 30, such behavior is the signature of a pseudogap,<sup>[91]</sup> and significantly resembles with our results above. However, the observed loss in optical conductivity at low-frequency is balanced by the increasing of spectral weight of Drude response at low temperature. Hence, in order to understand the low-frequency dynamics, including the rapid narrowing behavior of the low-frequency component and the pseudogap-like suppression readily seen at all temperature range, we derive the spectrum of the  $\omega$ -dependent scattering rate  $1/\tau(\omega)$  from the extended Drude model:<sup>[88]</sup>

$$\frac{1}{\tau(\omega)} = \left(\frac{\omega_p^2}{4\pi}\right) \text{Re}\left[\frac{1}{\sigma(\omega)}\right] \quad (5.2.7)$$

Here, the plasma frequency  $\omega_p$  (in  $\text{cm}^{-1}$ ) was obtained by integrating the optical conductivity from the partial sum rule:

$$N_{eff}(\omega_c) = \frac{2mV_c}{(\pi e^2) \int_0^{\omega_c} \sigma_1(\omega) d\omega} \quad (5.2.8)$$

where  $m$  is the mass of an electron,  $V_c$  is the unit cell volume of Na<sub>x</sub>CoO<sub>2</sub>,  $e$  is the charge of an electron, and  $\sigma_1(\omega)$  is the optical conductivity. Fig. 5 - 31 shows the frequency-dependent partial sum rule for the two Na<sub>x</sub>CoO<sub>2</sub> thin films. This figure shows that the Drude weight grows with Na concentration and that the Drude absorption becomes sharper and hence better defined as the Na content level increases. Furthermore, the flat region between 5000 and 8000  $\text{cm}^{-1}$  separates the Drude weight from the  $\beta$ -band weight, and we get  $N_{effD}(\infty)$  to be 0.1 for Na<sub>0.68</sub>CoO<sub>2</sub> and 0.07 for Na<sub>0.75</sub>CoO<sub>2</sub> by extrapolating this flat region to infinite frequency. Accordingly, we can get the plasma frequency  $\omega_p$  from

$$\omega_p^2 = \frac{4\pi N_{effD} e^2}{V_c m^*} \quad (5.2.9)$$

Hence, the observed plasma frequency  $\omega_p$  are  $10800 \text{ cm}^{-1}$  for  $\text{Na}_{0.68}\text{CoO}_2$  and  $7600 \text{ cm}^{-1}$  for  $\text{Na}_{0.75}\text{CoO}_2$ . Next, we substitute these into equation (5.2.7) to get  $\omega$ -dependent scattering rate  $1/\tau(\omega)$  of two  $\text{Na}_{0.68}\text{CoO}_2$  and  $\text{Na}_{0.75}\text{CoO}_2$  thin films between 20 k and 300 K, and the results are shown in Figs. 5 - 32 and 33 (two  $E_{1u}$  phonon modes of  $\text{Na}_x\text{CoO}_2$  and three  $E_u$  phonon modes of  $\text{Al}_2\text{O}_3$  substrate between  $350 \text{ cm}^{-1}$  and  $632 \text{ cm}^{-1}$  have been removed). As shown in Figs. 5 - 23, 24, 32, and 33, the suppression in  $1/\tau(\omega)$  appears at lower frequency than that in  $\sigma_1(\omega)$  spectra. This is a generic behavior for pseudogap, and was discussed by N. L. Wang *et al.* for  $\text{Nd}_{2-x}\text{Ce}_x\text{CuO}_4$  single crystal.<sup>[92]</sup> In Figs. 5 - 32 and 33, we can see that the low frequency scattering rate is dominated by a bosonic mode with an onset frequency of scattering rate at about  $600 \text{ cm}^{-1}$ . At low frequency,  $1/\tau(\omega)$  can be fitted with power law expression:

$$\frac{1}{\tau(\omega)} \sim \omega^\alpha \quad (5.2.10)$$

Figs. 5 - 34 and 35 show  $1/\tau(\omega)$  of  $\text{Na}_x\text{CoO}_2$  ( $x = 0.68$  and  $0.75$ ) thin films at low frequency, while the power law fitting curve are also included. We can establish that for  $x = 0.68$  thin film,  $\alpha_{300\text{K}} \sim 1.46$  and  $\alpha_{20\text{K}} \sim 1.50$ , in consistent with that reported by S. Lupi *et al.* for  $x = 0.57$  single crystal,<sup>[56]</sup> revealing a  $1/\tau(\omega) \sim \omega^{3/2}$  law at low temperature. It is interesting to note that the temperature-dependent resistivity  $\rho_{ab}(T)$  of  $x = 0.57$  also has the same trend  $\rho_{ab}(T) \sim T^{3/2}$  at low temperature.<sup>[93]</sup> However, it is different with the Fermi-liquid theory ( $1/\tau(\omega) \sim \omega^2$ ).<sup>[94]</sup> These phenomena reveal  $\text{Na}_x\text{CoO}_2$  ( $x = 0.68$  and  $0.75$ ) are not a simple metal oxide, which closely correlate with the characteristics of its phase diagram.

Table 5 - 1. Atomic position, site symmetries, and relative Raman scattering cross section for crystal orientations of  $\text{Na}_x\text{CoO}_2$  for hexagonal structure with space group  $P6_3/mmc$ ;  $xx$ ,  $xy$ ,  $zz$ , and  $zx$  refer to the different polarization combinations for the incident and scattered light.

Atomic position	Wyckoff index	Site symmetry	Irreducible representations	Raman modes	Displacement direction			
					$xx$	$xy$	$zz$	$zx$
$\text{O}(\frac{1}{3}, \frac{2}{3}, z)$	$4f$	$C_{3v}^d$	$A_{1g} + A_{2u} + B_{1g} + B_{2u} + E_{1g} + E_{1u} + E_{2g} + E_{2u}$	$A_{1g}$	$a^2$	0	$b^2$	0
				$E_{1g}$	0	0	0	$e^2$
				$E_{2g}$	$f^2$	$f^2$	0	0
$\text{Na1}(\frac{2}{3}, \frac{1}{3}, \frac{1}{4})$	$2d$	$D_{3h}^l$	$A_{2u} + B_{1g} + E_{1u} + E_{2g}$	$E_{2g}$	$f^2$	$f^2$	0	0
$\text{Na2}(0, 0, \frac{1}{4})$	$2b$	$D_{3h}^l$	$A_{2u} + B_{1g} + E_{1u} + E_{2g}$	$E_{2g}$	$f^2$	$f^2$	0	0
$\text{Co}(0, 0, 0)$	$2a$	$D_{3d}$	$A_{2u} + B_{2u} + E_{1u} + E_{2u}$					

Table 5 - 2. The Raman phonon peaks position of  $\text{Na}_x\text{CoO}_2$  ( $x = 0.68$  and  $0.75$  thin films, and  $x = 0.84$  single crystal) and  $\text{Co}_3\text{O}_4$  thin film. The 514.5 nm laser line was used for excitation.

Na content x			Raman phonon modes ( $\text{cm}^{-1}$ )						
			$E_{2g}$			$A_{1g}$			
Thin films	0.68		462.1				575.3		
	0.75		462.3				577.0		
Single crystal	0.84	Area A	194.8	454.6	478.0	519.0	580.4	619.0	685.2
		Area B		471.8			581.2		685.2
		Area C		465.3			582.0		
$\text{Co}_3\text{O}_4$			196.5		481.3	521.9		620.3	691.9

Table 5 - 3. Factor group analysis and relative Raman scattering cross section for crystal orientations of  $\text{Co}_3\text{O}_4$  for cubic structure with space group  $Fd\bar{3}m$ ;  $xx$ ,  $xy$ ,  $zz$ , and  $zx$  refer to the different polarization combinations for the incident and scattered light.

Atom	Irreducible representations	Raman modes	Displacement direction			
			$xx$	$xy$	$zz$	$zx$
O	$A_{1g} + A_{2u} + E_u + E_g + F_{1g} + 2F_{2g} + F_{2u} + 2F_{1u}$	$A_{1g}$	$a^2$	0	$a^2$	0
		$E_g$	$b^2$	0	$4b^2$	0
		$F_{2g}$	0	$2d^2$	0	$2d^2$
		$F_{2g}$	0	$2d^2$	0	$2d^2$
Co	$A_{2u} + E_u + F_{2g} + F_{2u} + 3F_{1u}$	$F_{2g}$	0	$2d^2$	0	$2d^2$

Table 5 - 4. The Raman phonon peaks position of burned  $\text{Na}_x\text{CoO}_2$  ( $x = 0.68$  thin film and  $x = 0.84$  single crystal) and  $\text{Co}_3\text{O}_4$  thin film. The 632.8 nm laser line was used for excitation.

$\lambda = 632.8 \text{ nm}$	Raman phonon modes ( $\text{cm}^{-1}$ )				
$\text{Co}_3\text{O}_4$	195.7	482.0	521.3	619.4	690.9
$\text{Na}_{0.68}\text{CoO}_2$	189.7	466.1	508.9	606.0	667.7
$\text{Na}_{0.84}\text{CoO}_2$	191.2	471.2	514.1	610.3	675.2

Table 5 - 5. The Raman phonon peaks position of  $\text{Na}_{0.68}\text{CoO}_2$  thin film at 300 and 15 K. The 514.5 nm laser line was used for excitation.

$\text{Na}_{0.68}\text{CoO}_2$	Raman phonon modes ( $\text{cm}^{-1}$ )			
	$E_{2g}$	$E_{2g}$	$E_{2g}$	$A_{1g}$
300 K		460.3		571.3
15 K	452.2	473.5	536.5	577.2

Table 5 - 6. The Raman phonon peaks position of fresh and 1 hour after exposing in humid air of  $\text{Na}_{0.33}\text{K}_{0.015}\text{CoO}_2 \cdot 1.3\text{H}_2\text{O}$  powder at room temperature. The 514.5 nm laser line was used for excitation.

Condition	Raman phonon modes of $\text{Na}_{0.33}\text{K}_{0.015}\text{CoO}_2 \cdot 1.3\text{H}_2\text{O}$ ( $\text{cm}^{-1}$ )								
Fresh			489.3		572.4			645.0	
After 1 hour exposed in humid air	193.5	470.9	489.3	512.9	573.8	620.6	640.0	676.3	

Table 5 - 7. The Raman phonon peaks position of fresh and 2 hours after exposing in humid air of  $\text{Na}_{0.75}\text{CoO}_2$  thin film at room temperature. The 514.5 nm laser line was used for excitation.

$\text{Na}_{0.75}\text{CoO}_2$		Area A	Area B
		Fresh	After 2 hours
$E_{2g}$	$\omega_{P1}$	7317.2	4955.5
	$\omega_1$	462.1	461.6
	$\gamma_1$	18.5	39.3
$A_{1g}$	$\omega_{P2}$	12987.8	8328.1
	$\omega_2$	576.8	576.2
	$\gamma_2$	52.6	65.3

Table 5 - 8. The Raman phonon peaks position of fresh and 2 hours after exposing in humid air of  $\text{Na}_{0.75}\text{CoO}_2$  thin film at room temperature. The 514.5 nm laser line was used for excitation.

$\text{Na}_{0.75}\text{CoO}_2$	Raman phonon modes ( $\text{cm}^{-1}$ )					
Area C	467.1	482.6	524.4	576.0	617.6	684.0
Area D	445.8	467.2		574.7		

Table 5 - 9. The Raman phonon peaks position of fresh and 42 minutes after exposing in humid air on area A of  $\text{Na}_{0.75}\text{CoO}_2$  thin film at room temperature. The 514.5 nm laser line was used for excitation.

$\text{Na}_{0.75}\text{CoO}_2$		Fresh (area A)	After 42 minutes
$E_{2g}$	$\omega_{P1}$	7317.2	7943.3
	$\omega_1$	462.1	462.3
	$\gamma_1$	18.5	22.0
$A_{1g}$	$\omega_{P2}$	12987.8	13949.6
	$\omega_2$	576.8	577.8
	$\gamma_2$	52.6	59.9

Table 5 - 10. Parameters of a Drude-Lorentz fit for the room-temperature optical reflectance data of  $\text{Na}_{0.68}\text{CoO}_2$  and  $\text{Na}_{0.75}\text{CoO}_2$  thin films. All units are in  $\text{cm}^{-1}$ .

	$\text{Na}_{0.68}\text{CoO}_2$	$\text{Na}_{0.75}\text{CoO}_2$
$\omega_{\text{PD}}$	3010	3071
$1/\tau_{\text{D}}$	60.5	198.0
$\omega_{\text{P1}}$	3600	4000
$\omega_1$	202.0	240.0
$\gamma_1$	280.0	800.0
$\omega_{\text{P2}}$	1330	645
$\omega_2$	356.7	379.2
$\gamma_2$	60.3	33.6
$\omega_{\text{P3}}$	1059	908
$\omega_3$	415.2	417.5
$\gamma_3$	20.4	20.9
$\omega_{\text{P4}}$	1059	770
$\omega_4$	507.3	504.3
$\gamma_4$	20.4	19.7
$\omega_{\text{P5}}$	1038	1205
$\omega_5$	537.2	532.6
$\gamma_5$	17.2	20.1
$\omega_{\text{P6}}$	162	162
$\omega_6$	632.0	632.0
$\gamma_6$	3.6	3.6
$\omega_{\text{P7}}$	19639	13097
$\omega_7$	2481.3	2341.7
$\gamma_7$	8584.5	4721.4
$\omega_{\text{P8}}$	16936	8409
$\omega_8$	12273.9	11592.6
$\gamma_8$	5109.2	2312.8
$\omega_{\text{P9}}$	32850	22757
$\omega_9$	24681.2	26722.0
$\gamma_9$	10946.7	5545.6
$\omega_{\text{P10}}$	41906	49848
$\omega_{10}$	37358.5	38567.2
$\gamma_{10}$	21664.5	17801.6
$\omega_{\text{P11}}$	43896	59828
$\omega_{11}$	55622.0	59302.0
$\gamma_{11}$	68048.1	52733.3
$\epsilon_{\infty}$	2.07	3.77

Table 5 - 11. Parameters of a Lorentz fit for the room-temperature far-infrared optical reflectance data of  $\text{Co}_3\text{O}_4$  thin films. All units are in  $\text{cm}^{-1}$ .

$\text{Co}_3\text{O}_4$	
$\omega_{p1}$	450
$\omega_1$	670
$\gamma_1$	19.2
$\omega_{p2}$	8128
$\omega_2$	6742
$\gamma_2$	3301.3
$\omega_{p3}$	18312
$\omega_3$	11329
$\gamma_3$	3340.4
$\omega_{p4}$	26078
$\omega_4$	20654
$\gamma_4$	16355.0
$\omega_{p5}$	34597
$\omega_5$	35919
$\gamma_5$	26144.9
$\epsilon_\infty$	1.10

Table 5 - 12. Parameters of a Lorentz fit for the room-temperature far-infrared optical reflectance data of  $\text{Na}_2\text{CO}_3$  thin films. All units are in  $\text{cm}^{-1}$ .

$\text{Na}_2\text{CO}_3$	
$\omega_{p1}$	2600
$\omega_1$	20
$\gamma_1$	30.0
$\omega_{p2}$	4467
$\omega_2$	3569
$\gamma_2$	2599.7
$\epsilon_\infty$	1.85

Table 5 - 13. Parameters of a Drude-Lorentz fit for the temperature-dependent infrared optical reflectance data of  $\text{Na}_{0.68}\text{CoO}_2$  thin films. All units are in  $\text{cm}^{-1}$ .

	300 K	250 K	200 K	150 K	100 K	75 K	50 K	20 K
$\omega_{\text{PD}}$	3010	2980	3002	2956	3000	3230	3194	3190
$1/\tau_{\text{D}}$	60.5	46.7	39.2	20.8	19.7	18.0	10.0	6.3
$\omega_{\text{P1}}$	3600	3418	3418	3428	3700	3880	3838	3884
$\omega_1$	202.0	194.2	189.5	164.4	158.0	136.9	124.0	117.9
$\gamma_1$	280.0	249.4	244.9	237.4	280.0	239.7	216.3	214.8
$\omega_{\text{P2}}$	1330	1330	1344	1243	1243	1231	1569	1229
$\omega_2$	356.7	357.6	357.6	357.6	357.6	357.6	357.6	357.6
$\gamma_2$	60.3	56.0	56.0	56.0	56.0	57.0	61.0	53.0
$\omega_{\text{P3}}$	1059	1057	1046	1041	1041	1041	1002	1050
$\omega_3$	415.2	415.3	415.3	415.3	415.3	415.3	415.3	415.3
$\gamma_3$	20.4	19.7	20.0	20.0	20.0	20.0	19.8	20.0
$\omega_{\text{P4}}$	1059	1116	1208	1091	1158	1159	1153	1145
$\omega_4$	507.3	506.2	509.0	509.0	512.5	512.6	512.8	513.3
$\gamma_4$	20.4	23.7	24.5	23.0	23.9	23.5	23.1	22.3
$\omega_{\text{P5}}$	1038	1117	959	1087	1023	1043	1048	1038
$\omega_5$	537.2	535.4	539.5	539.5	542.3	542.2	542.1	542.5
$\gamma_5$	17.2	19.8	14.2	17.3	15.0	15.2	15.3	14.5
$\omega_{\text{P6}}$	162	162	162	162	162	162	162	162
$\omega_6$	632.0	632.0	632.0	632.0	632.0	632.0	632.0	632.0
$\gamma_6$	3.6	3.6	3.6	3.6	3.6	3.6	3.6	3.6
$\omega_{\text{P7}}$	19639	19725	19808	19737	20127	20618	20635	20095
$\omega_7$	2481.3	2487.9	2473.1	2423.3	2480.8	2579.2	2574.9	2500.0
$\gamma_7$	8584.5	8711.4	8836.4	8893.9	9387.0	9943.5	9963.5	9650.7
$\omega_{\text{P8}}$	16936	16936	16936	16936	16936	16936	16936	16936
$\omega_8$	12273.9	12273.9	12273.9	12273.9	12273.9	12273.9	12273.9	12273.9
$\gamma_8$	5109.2	5109.2	5109.2	5109.2	5109.2	5109.2	5109.2	5109.2
$\omega_{\text{P9}}$	32850	32850	32850	32850	32850	32850	32850	32850
$\omega_9$	24681.2	24681.2	24681.2	24681.2	24681.2	24681.2	24681.2	24681.2
$\gamma_9$	10946.7	10946.7	10946.7	10946.7	10946.7	10946.7	10946.7	10946.7
$\omega_{\text{P10}}$	41906	41906	41906	41906	41906	41906	41906	41906
$\omega_{10}$	37358.5	37358.5	37358.5	37358.5	37358.5	37358.5	37358.5	37358.5
$\gamma_{10}$	21664.5	21664.5	21664.5	21664.5	21664.5	21664.5	21664.5	21664.5
$\omega_{\text{P11}}$	43896	43896	43896	43896	43896	43896	43896	43896
$\omega_{11}$	55622.0	55622.0	55622.0	55622.0	55622.0	55622.0	55622.0	55622.0
$\gamma_{11}$	68048.1	68048.1	68048.1	68048.1	68048.1	68048.1	68048.1	68048.1
$\epsilon_{\infty}$	2.07	2.04	2.03	2.03	2.00	1.99	2.00	1.97

Table 5 - 14. Parameters of a Drude-Lorentz fit for the temperature-dependent infrared optical reflectance data of Na<sub>0.75</sub>CoO<sub>2</sub> thin films. All units are in cm<sup>-1</sup>.

	300 K	250 K	200 K	150 K	100 K	75 K	50 K	30 K	10 K
$\omega_{PD}$	3071	3022	3116	3140	3080	3100	3080	3050	3080
$1/\tau_D$	198.0	188.9	184.8	169.0	150.0	142.0	135.0	120.8	100.0
$\omega_{P1}$	4000	3993	4002	4058	4000	4145	4100	4102	4100
$\omega_1$	240.0	194.8	192.1	185.0	182.0	180.0	177.0	175.0	164.0
$\gamma_1$	800.0	920.1	974.5	970.0	954.4	1035.8	970.6	801.8	832.2
$\omega_{P2}$	645	645	645	645	645	645	645	790	884
$\omega_2$	379.2	379.2	379.2	379.2	379.2	379.2	379.2	379.2	379.2
$\gamma_2$	33.6	33.6	33.6	33.6	33.6	33.6	33.6	33.6	33.6
$\omega_{P3}$	908	908	908	908	908	908	908	985	994
$\omega_3$	417.5	417.5	417.5	417.5	417.5	417.5	417.5	417.5	417.5
$\gamma_3$	20.9	20.9	20.9	20.9	20.9	20.9	20.9	20.9	20.9
$\omega_{P4}$	770	771	772	772	824	863	861	863	903
$\omega_4$	504.3	505.0	505.5	506.1	506.9	508.8	509.2	509.6	509.9
$\gamma_4$	19.7	19.9	20.2	20.5	20.9	21.5	21.2	21.2	21.8
$\omega_{P5}$	1205	1203	1200	1192	1237	1233	1226	1231	1189
$\omega_5$	532.6	532.5	532.9	534.0	534.9	535.9	536.1	536.3	536.5
$\gamma_5$	20.1	20.3	20.5	20.6	20.9	20.4	19.3	19.2	18.8
$\omega_{P6}$	162	162	162	162	162	162	162	162	162
$\omega_6$	632.0	632.0	632.0	632.0	632.0	632.0	632.0	632.0	632.0
$\gamma_6$	3.6	3.6	3.6	3.6	3.6	3.6	3.6	3.6	3.6
$\omega_{P7}$	13097	13131	13113	13126	13095	13027	12921	13163	13134
$\omega_7$	2341.7	2321.7	2321.6	2299.1	2319.4	2318.8	2388.3	2280.1	2269.0
$\gamma_7$	4721.4	4746.9	4781.2	4874.6	4922.7	4987.8	5006.0	5065.4	5064.9
$\omega_{P8}$	8409	8409	8409	8409	8409	8409	8409	8409	8409
$\omega_8$	11592.6	11592.6	11592.6	11592.6	11592.6	11592.6	11592.6	11592.6	11592.6
$\gamma_8$	2312.8	2312.8	2312.8	2312.8	2312.8	2312.8	2312.8	2312.8	2312.8
$\omega_{P9}$	22757	22757	22757	22757	22757	22757	22757	22757	22757
$\omega_9$	26722.0	26722.0	26722.0	26722.0	26722.0	26722.0	26722.0	26722.0	26722.0
$\gamma_9$	5545.6	5545.6	5545.6	5545.6	5545.6	5545.6	5545.6	5545.6	5545.6
$\omega_{P10}$	49848	49848	49848	49848	49848	49848	49848	49848	49848
$\omega_{10}$	38567.2	38567.2	38567.2	38567.2	38567.2	38567.2	38567.2	38567.2	38567.2
$\gamma_{10}$	17801.6	17801.6	17801.6	17801.6	17801.6	17801.6	17801.6	17801.6	17801.6
$\omega_{P11}$	59828	59828	59828	59828	59828	59828	59828	59828	59828
$\omega_{11}$	59302.0	59302.0	59302.0	59302.0	59302.0	59302.0	59302.0	59302.0	59302.0
$\gamma_{11}$	52733.3	52733.3	52733.3	52733.3	52733.3	52733.3	52733.3	52733.3	52733.3
$\epsilon_\infty$	3.77	3.75	3.74	3.68	3.69	3.64	3.62	3.60	3.64

Table 5 - 15. The resulting parameters obtained by anharmonic effect model. All units are in  $\text{cm}^{-1}$ .

Na content	Peak	$\omega_0$	$\Gamma_0$	$a$	$b$
$x = 0.68$	3 <sup>rd</sup>	517.41	22.79	-4.71	0.03
	4 <sup>th</sup>	545.41	14.33	-3.58	0.04
$x = 0.75$	3 <sup>rd</sup>	511.92	19.93	-3.3	0.03
	4 <sup>th</sup>	538.65	19.8	-2.9	0.01

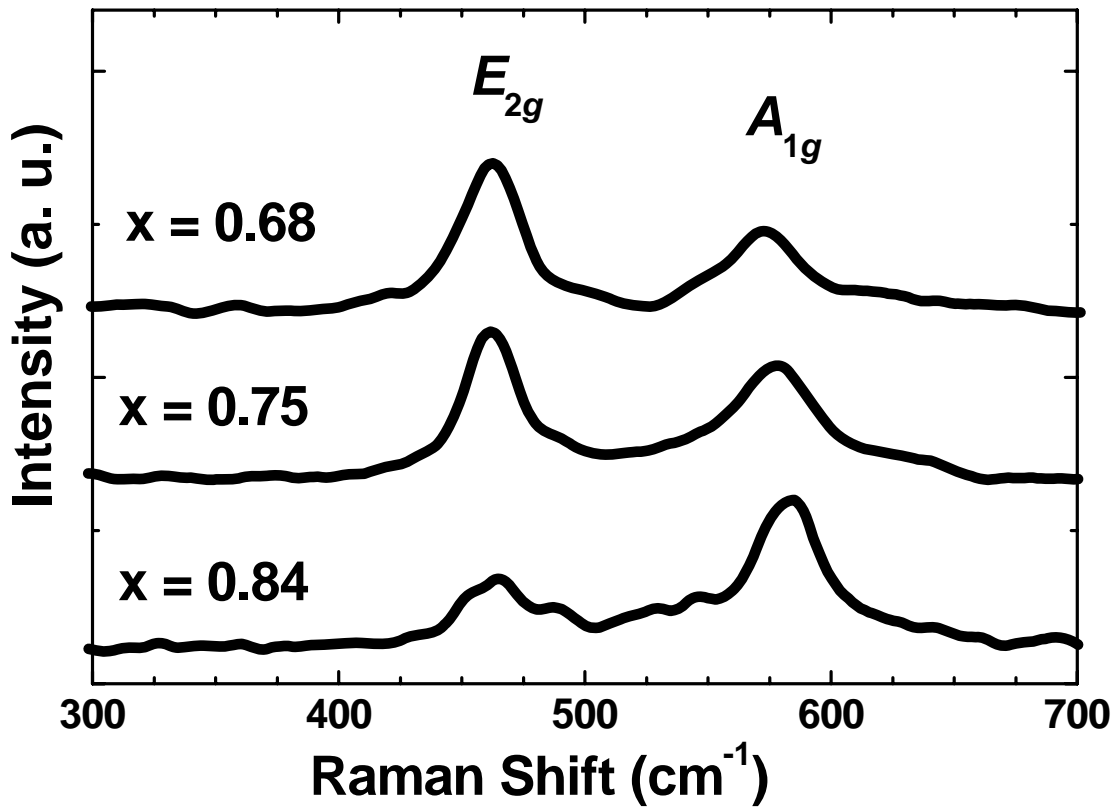


Fig. 5 - 1. Raman-scattering spectra taken from the  $ab$  - plane of  $\text{Na}_x\text{CoO}_2$  ( $x = 0.68, 0.75,$  and  $0.84$ ) at room temperature. All samples were fresh or freshly cleaved. The 514.5 nm laser line was used for excitation. The curves are shifted for clarity.

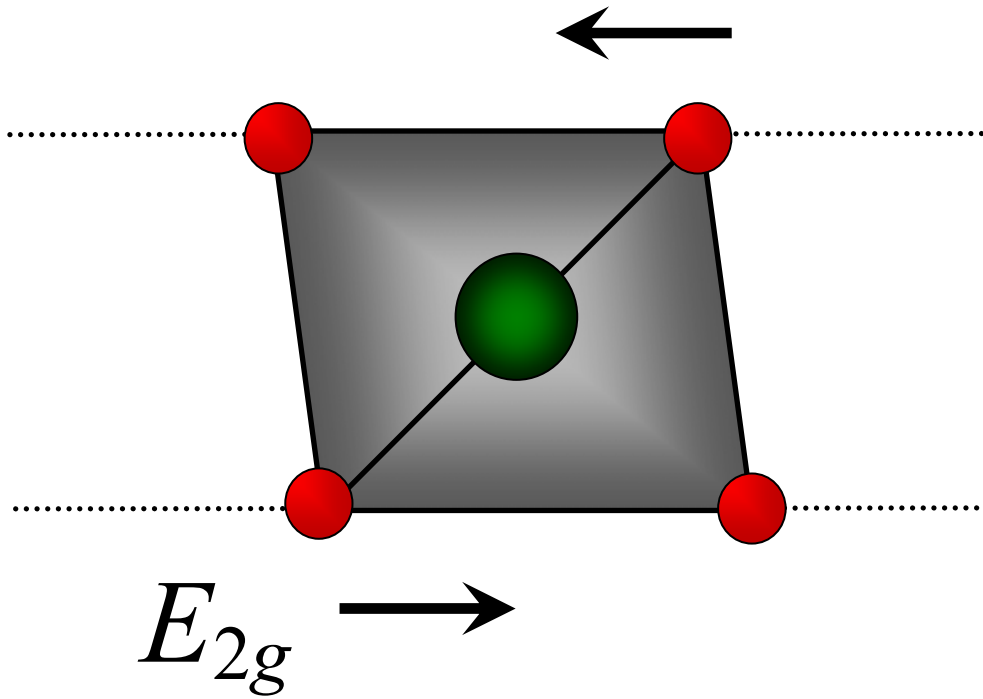


Fig. 5 - 2. (a) Sketch of the oxygen displacements in  $\text{CoO}_6$  octahedra of the  $E_{2g}$  Raman phonon mode. The smaller circles and the larger circles represent oxygen ( $\text{O}_{\text{octa}}$ ) and cobalt ions, respectively. In this figure, the  $\text{O}_z$  on the top of  $\text{CoO}_6$  octahedra are overlap with cobalt ion, hence we do not show  $\text{O}_z$  for clarity.

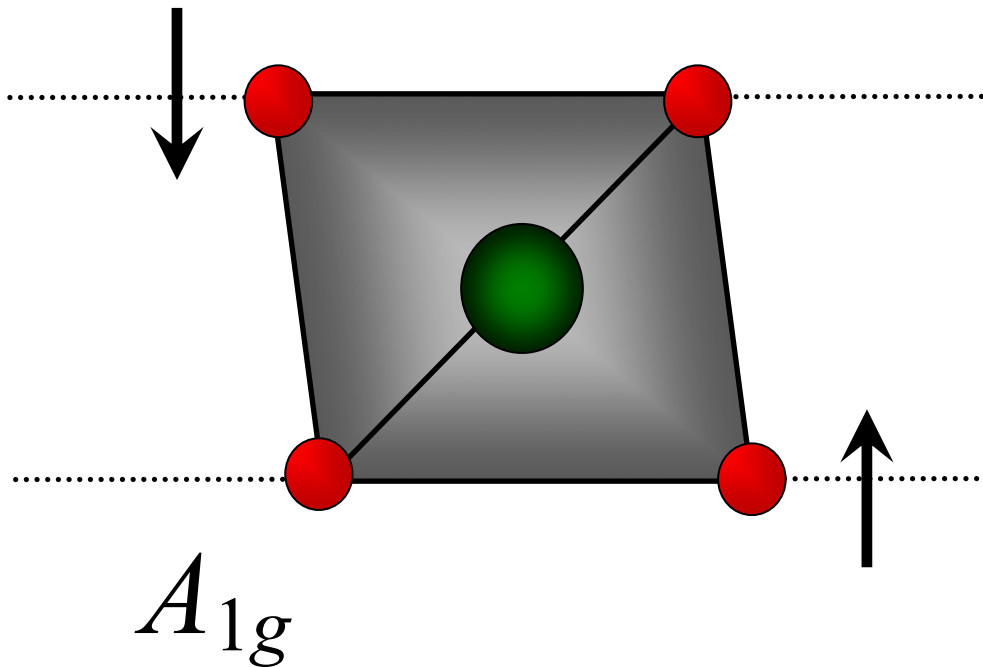


Fig. 5 - 2. (b) Sketch of the oxygen displacements in  $\text{CoO}_6$  octahedra of the  $A_{1g}$  Raman phonon mode. The smaller circles and the larger circles represent oxygen ( $\text{O}_{\text{octa}}$ ) and cobalt ions, respectively. In this figure, the  $\text{O}_z$  on the top of  $\text{CoO}_6$  octahedra are overlap with cobalt ion, hence we do not show  $\text{O}_z$  for clarity.

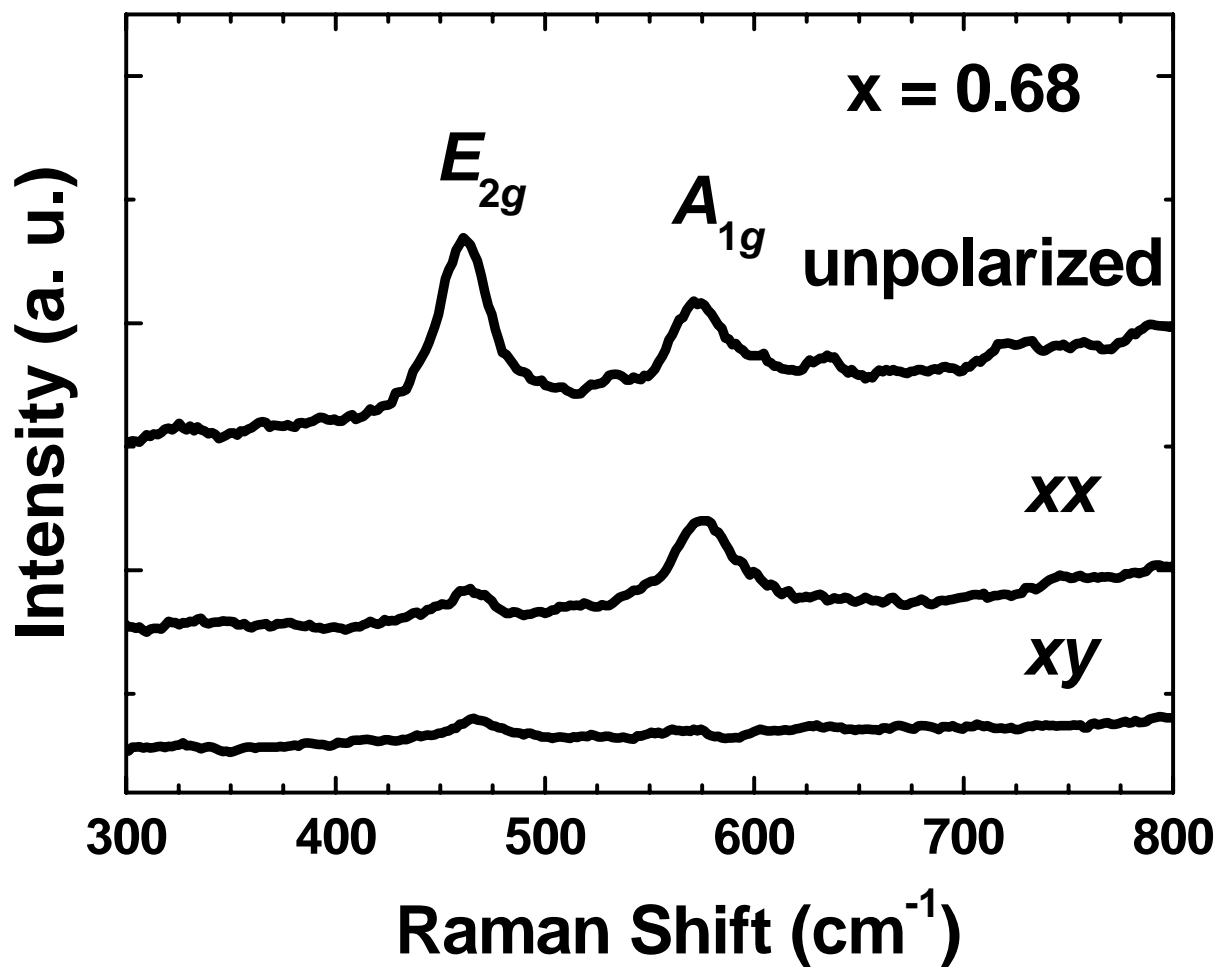


Fig. 5 - 3. Polarized Raman-scattering spectra taken from the  $ab$  - plane of  $\text{Na}_{0.68}\text{CoO}_2$  thin film at room temperature. The 514.5 nm laser line was used for excitation. The curves are shifted for clarity.

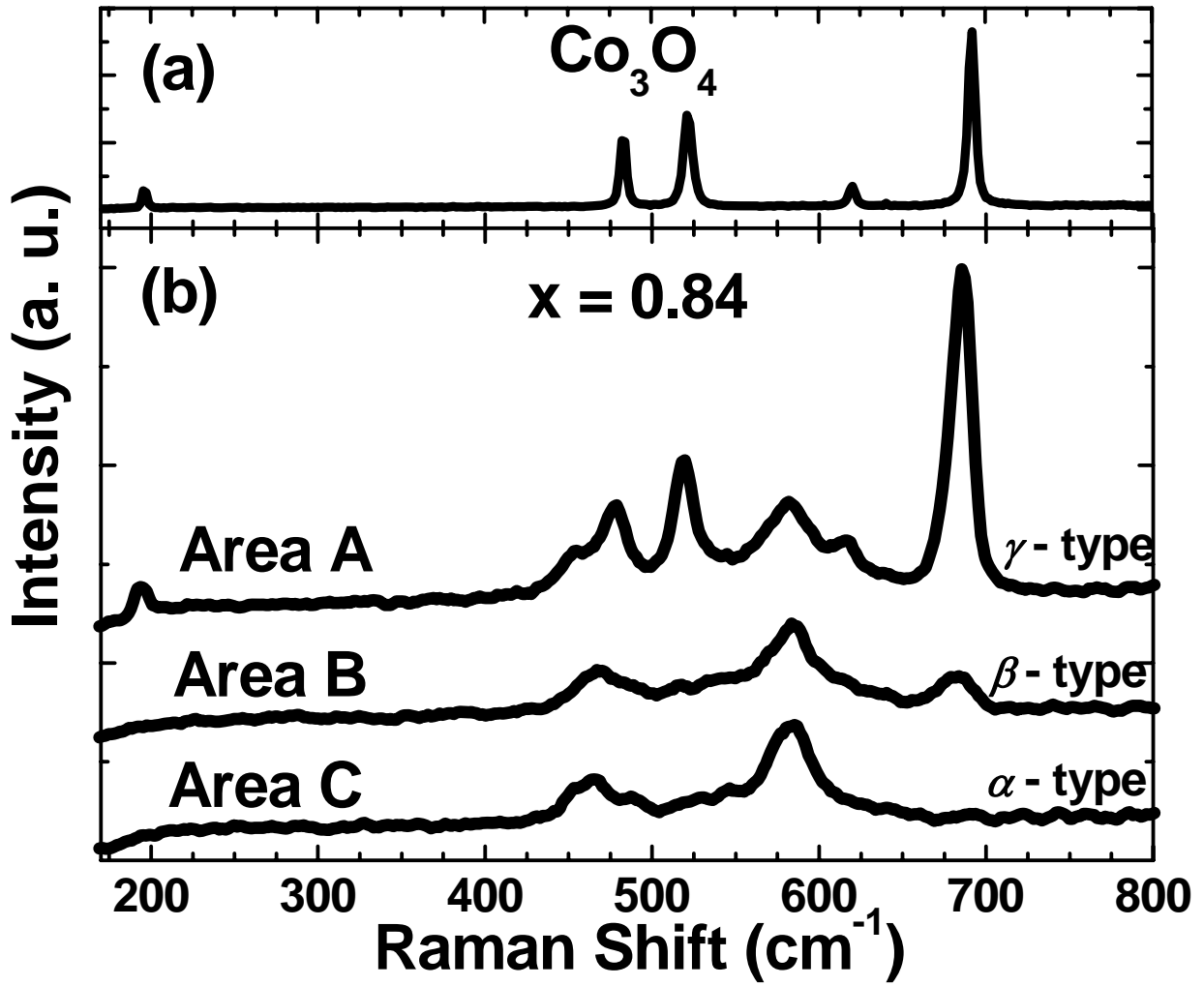


Fig. 5 - 4. Raman-scattering spectra taken from the  $ab$  - plane of (a)  $\text{Co}_3\text{O}_4$  thin film on sapphire (0001) and (b) the three different areas on  $\text{Na}_{0.84}\text{CoO}_2$  single crystal. The 514.5 nm laser line was used for excitation. The curves are shifted for clarity.

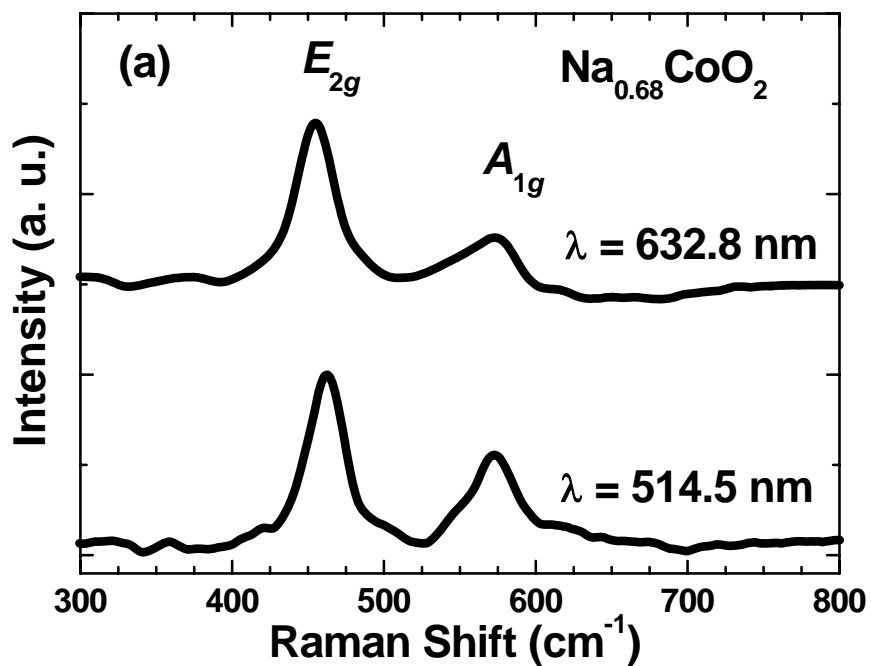


Fig. 5 - 5. (a) Raman-scattering spectra taken from the *ab* - plane of  $\text{Na}_{0.68}\text{CoO}_2$  thin film. The 514.5 and 632.8 nm laser lines were used for excitations. The curves are shifted for clarity.

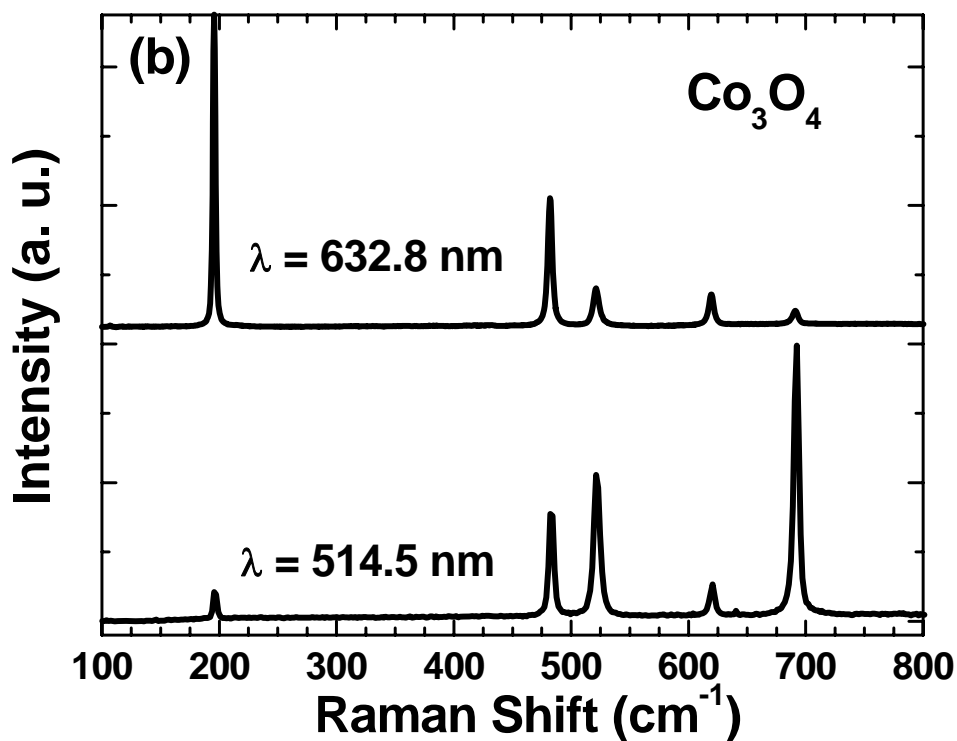


Fig. 5 - 5. (b) Raman-scattering spectra taken from the *ab* - plane of  $\text{Co}_3\text{O}_4$  thin film. The 514.5 and 632.8 nm laser lines were used for excitations. The curves are shifted for clarity.

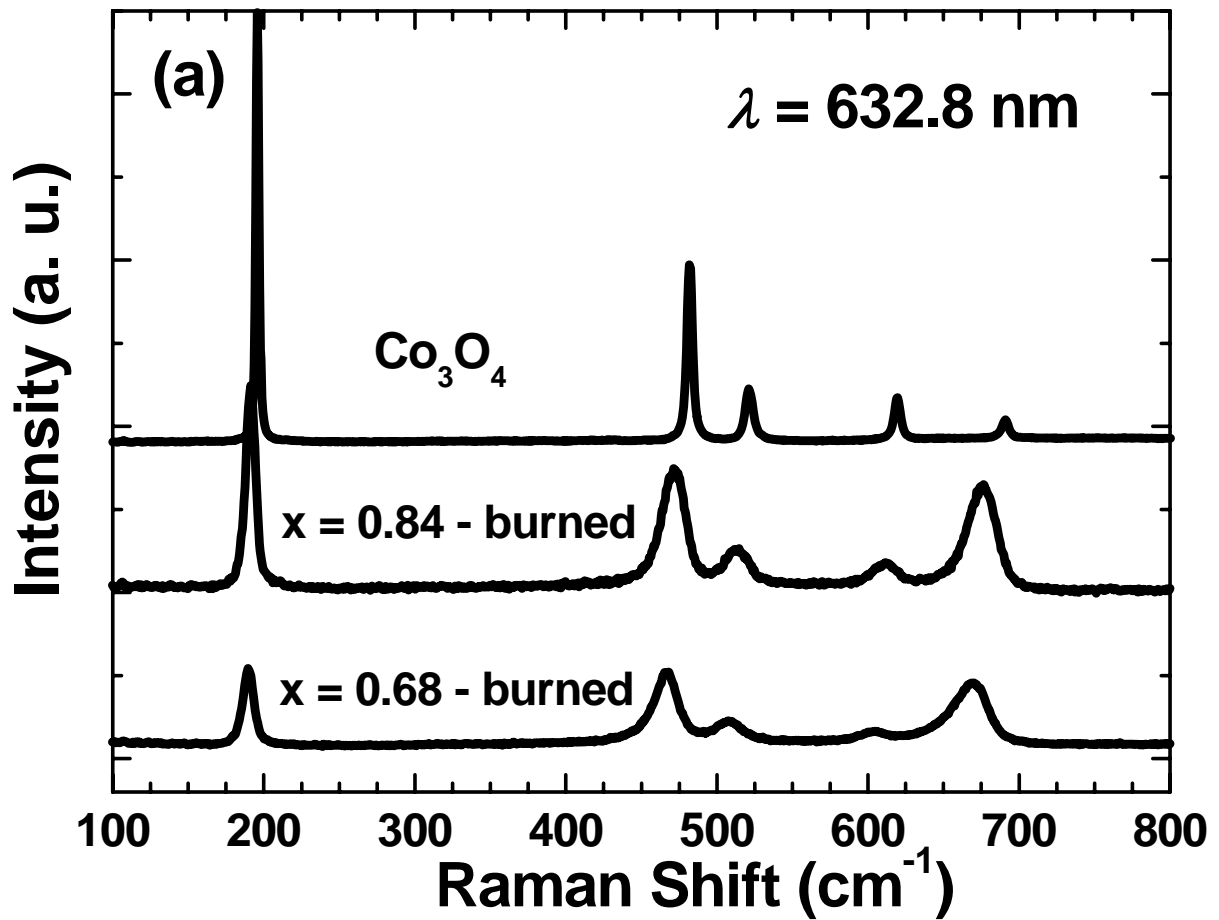


Fig. 5 - 6. (a) Raman-scattering spectra of  $\text{Co}_3\text{O}_4$  thin film, burned  $\text{Na}_{0.68}\text{CoO}_2$  thin film, and burned  $\text{Na}_{0.84}\text{CoO}_2$  single crystal. The 632.8 nm laser line was used for excitation. The curves are shifted for clarity.

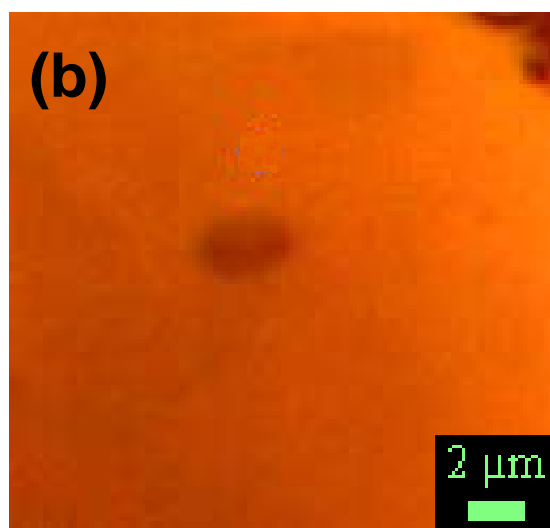


Fig. 5 - 6. (b) The video image showing the burned spot (center) on the surface of  $\text{Na}_{0.68}\text{CoO}_2$  thin film.

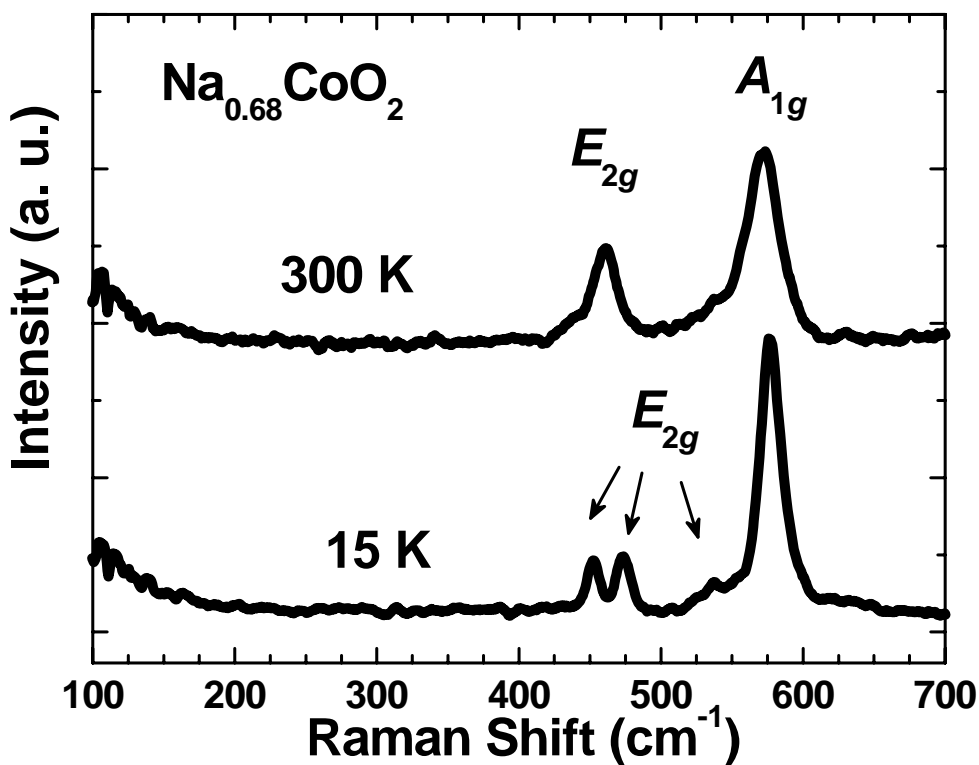


Fig. 5 - 7. Raman-scattering spectra taken from the *ab* - plane of  $\text{Na}_{0.68}\text{CoO}_2$  thin film at 300 and 15 K. The 514.5 nm laser line was used for excitation. The curves are shifted for clarity.

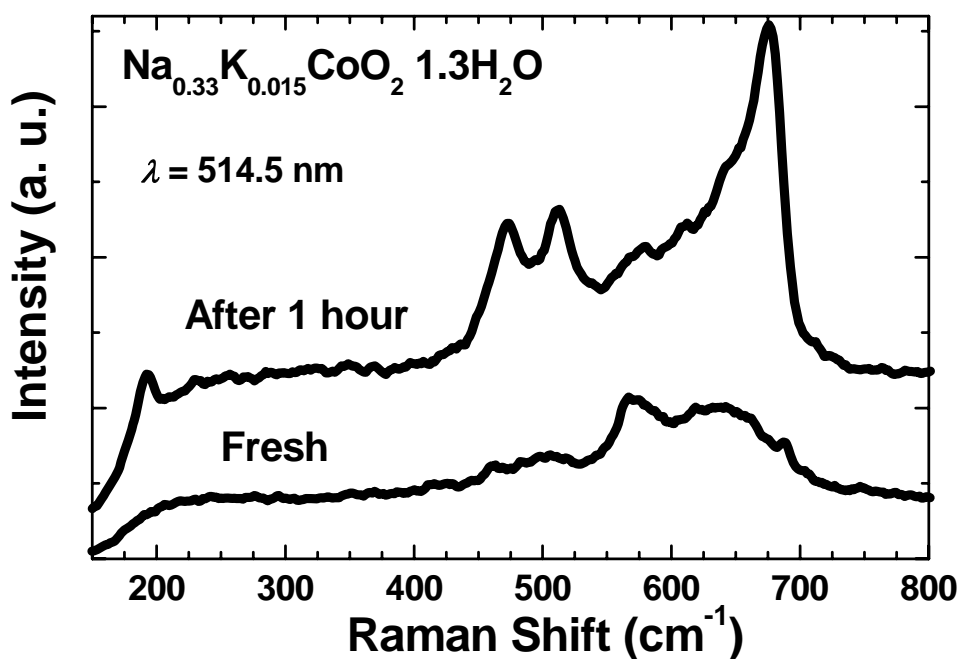


Fig. 5 - 8. Raman-scattering spectra of  $\text{Na}_{0.33}\text{K}_{0.015}\text{CoO}_2 \cdot 1.3\text{H}_2\text{O}$  powder measured from fresh one and 1 hour after exposing in humid air. The 514.5 nm laser line was used for excitation. The curves are shifted for clarity.

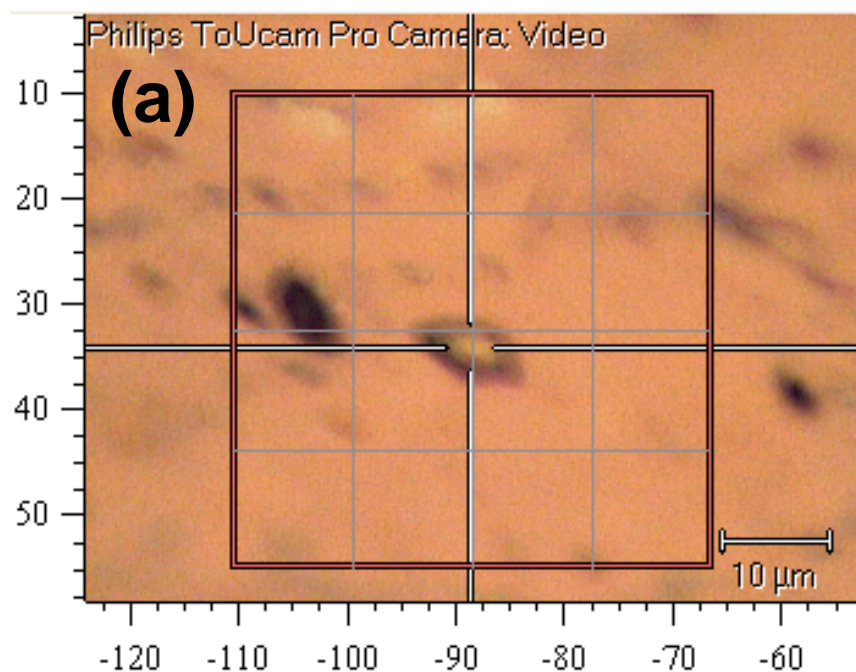


Fig. 5 - 9. (a) The image showing the freshly cleaved  $ab$  - surface of  $\text{Na}_{0.84}\text{CoO}_2$  single crystal.

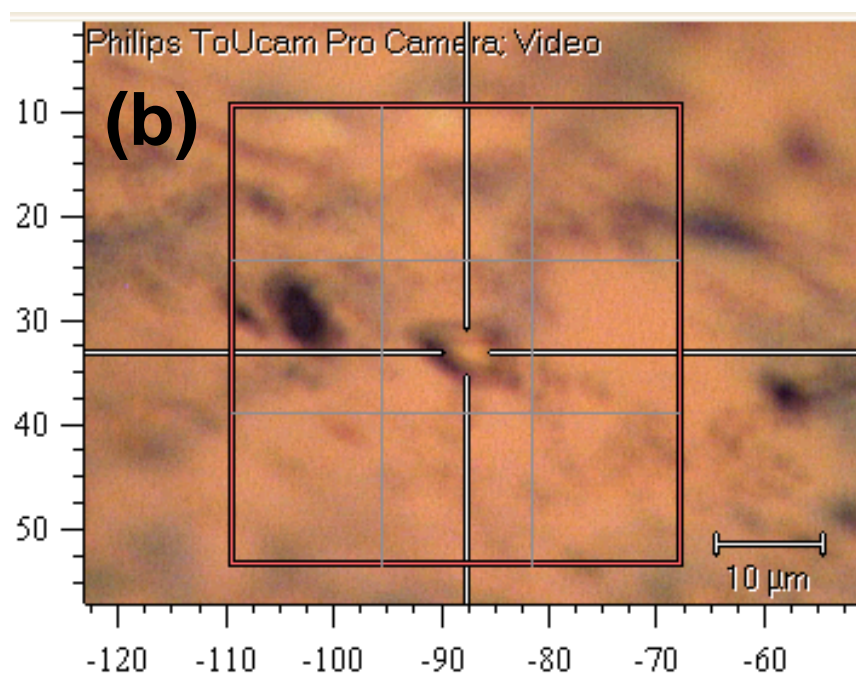


Fig. 5 - 9. (b) The image showing the  $ab$  - surface of  $\text{Na}_{0.84}\text{CoO}_2$  single crystal after exposing in ambient humid air for 2 hours.

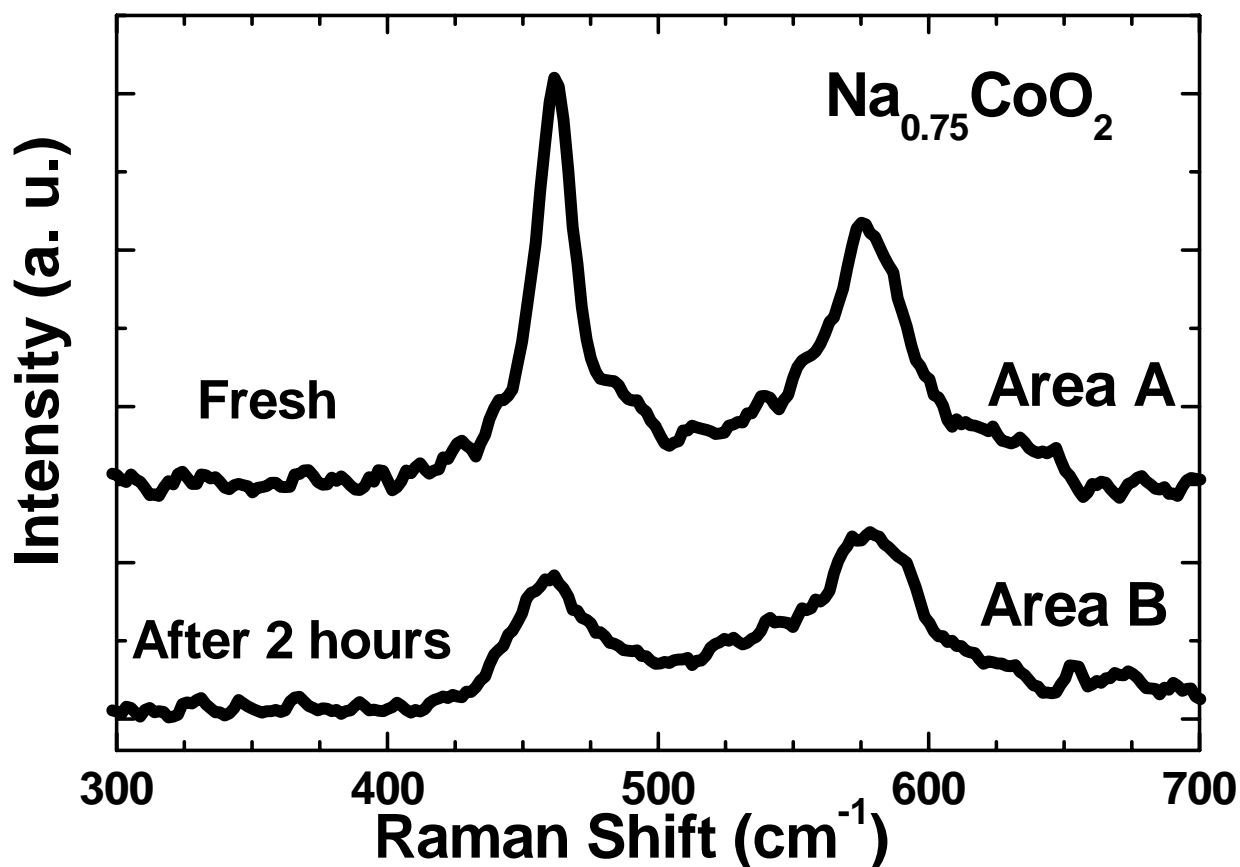


Fig. 5 - 10. (a) Raman-scattering spectra of  $\text{Na}_{0.75}\text{CoO}_2$  single crystal measured from fresh one (area A) and 2 hours after exposing in humid air (area B). The 514.5 nm laser line was used for excitation. The curves are shifted for clarity.

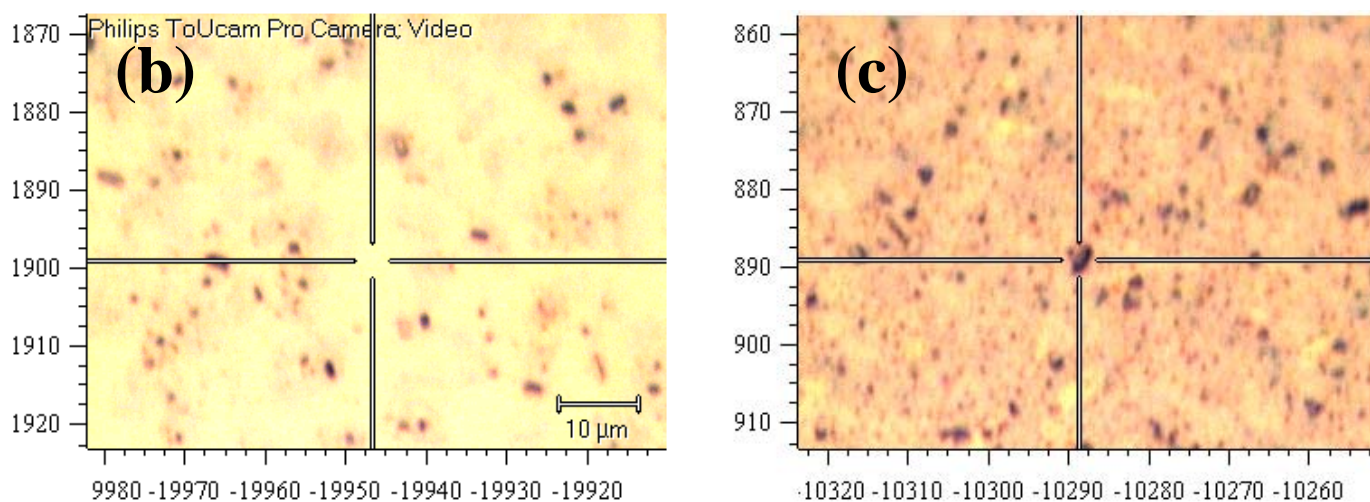


Fig. 5 - 10. These images showing the surfaces of  $\text{Na}_{0.75}\text{CoO}_2$  thin film taken from (b) clear spot (area A) of fresh sample and (c) black spot (area B) of aged sample which is 2 hours after exposing in humid air.

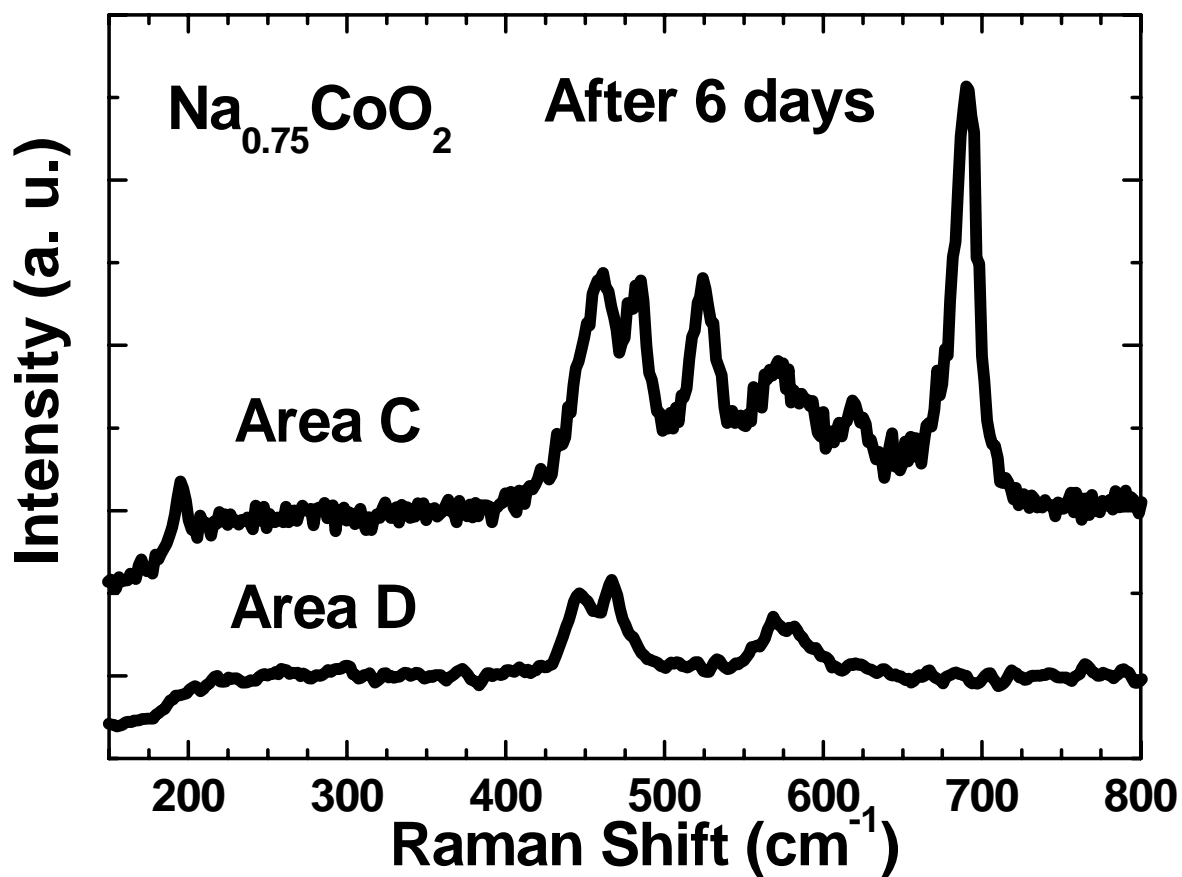


Fig. 5 - 11. (a) Raman-scattering spectra of  $\text{Na}_{0.75}\text{CoO}_2$  thin film measured from two different areas after six days. The 514.5 nm laser line was used for excitation. The curves are shifted for clarity.

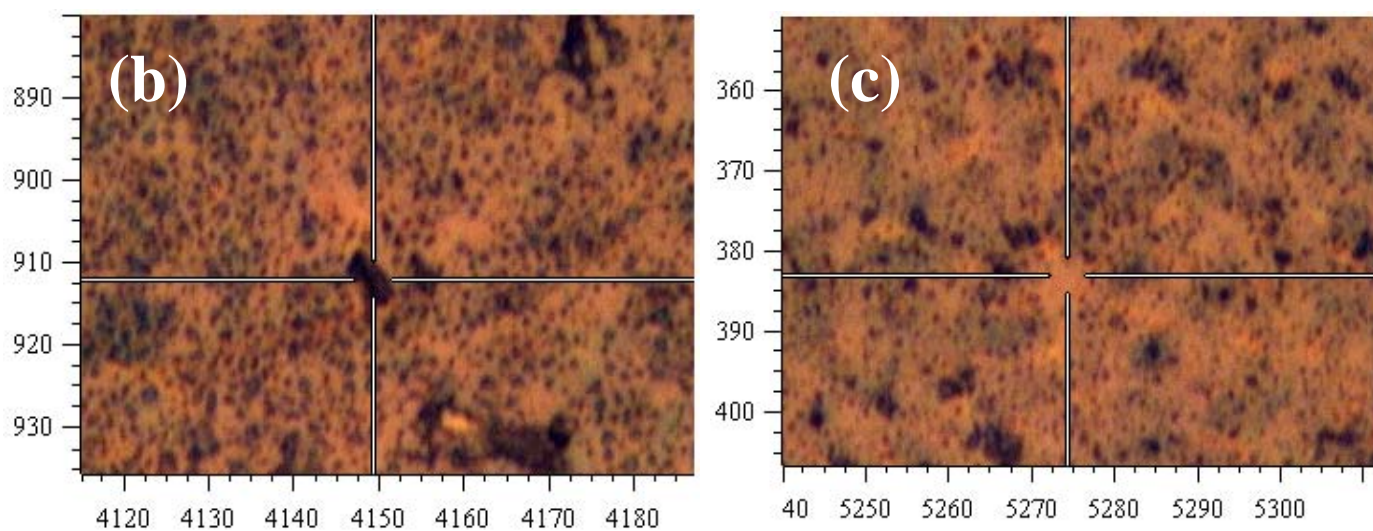


Fig. 5 - 11. These images showing the surfaces of  $\text{Na}_{0.75}\text{CoO}_2$  thin film taken from (b) area C and (c) area D.

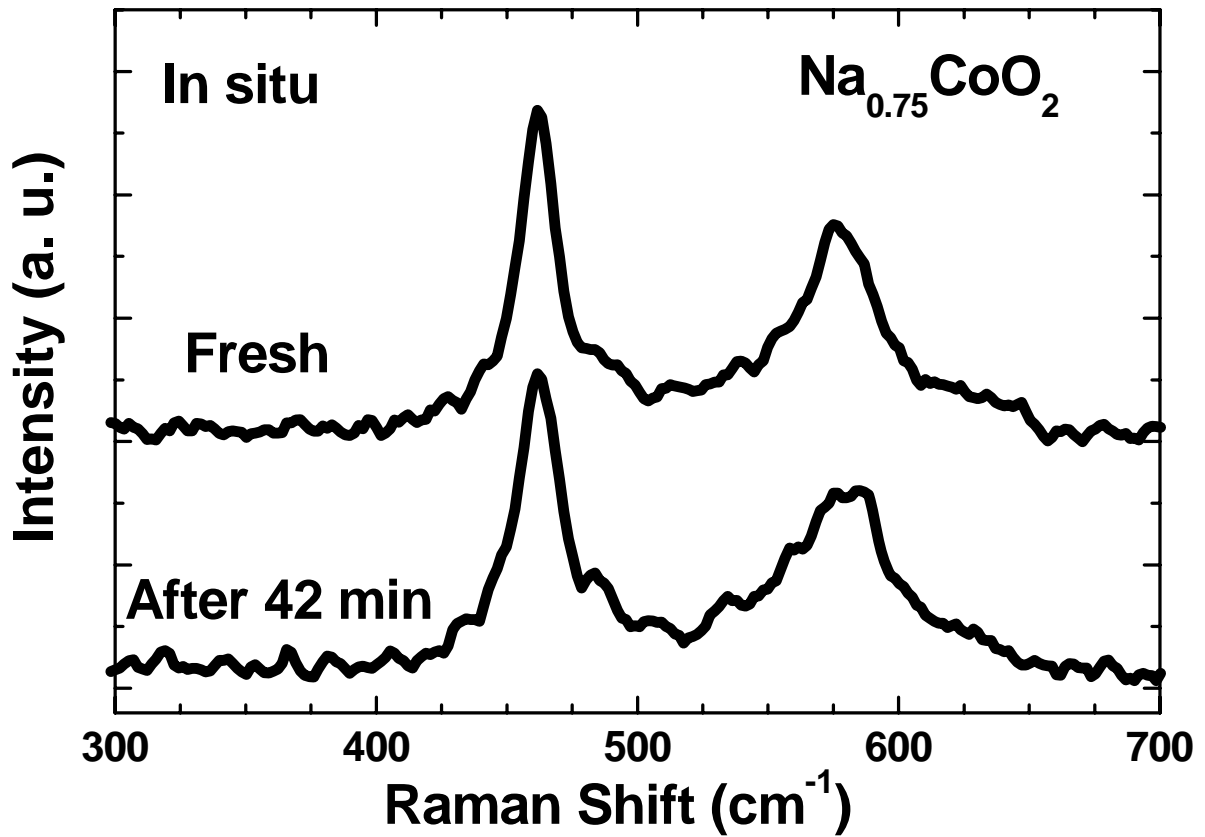


Fig. 5 - 12. (a) Raman-scattering spectra of  $\text{Na}_{0.75}\text{CoO}_2$  thin film measured in situ on area A for fresh and 42 minutes after exposing in humid air at room temperature. The 514.5 nm laser line was used for excitation. The curves are shifted for clarity.

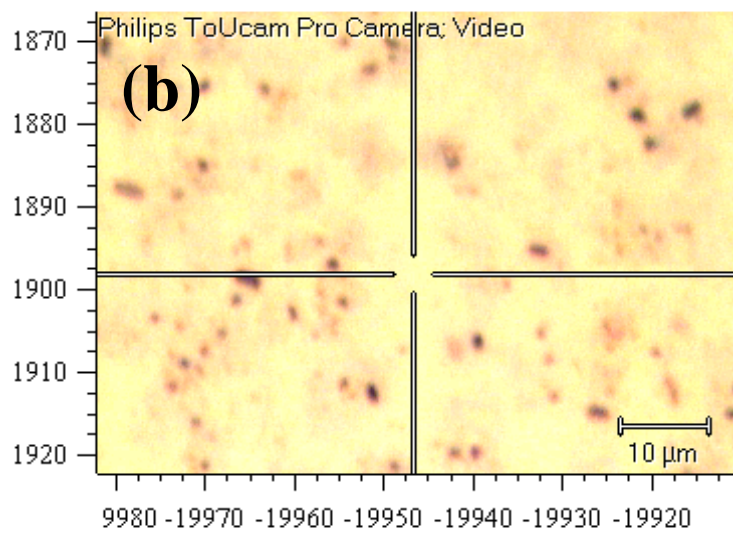


Fig. 5 - 12. (b) The image showing the surface of  $\text{Na}_{0.75}\text{CoO}_2$  thin film taken from area A for 42 minutes after exposing in humid air at room temperature.

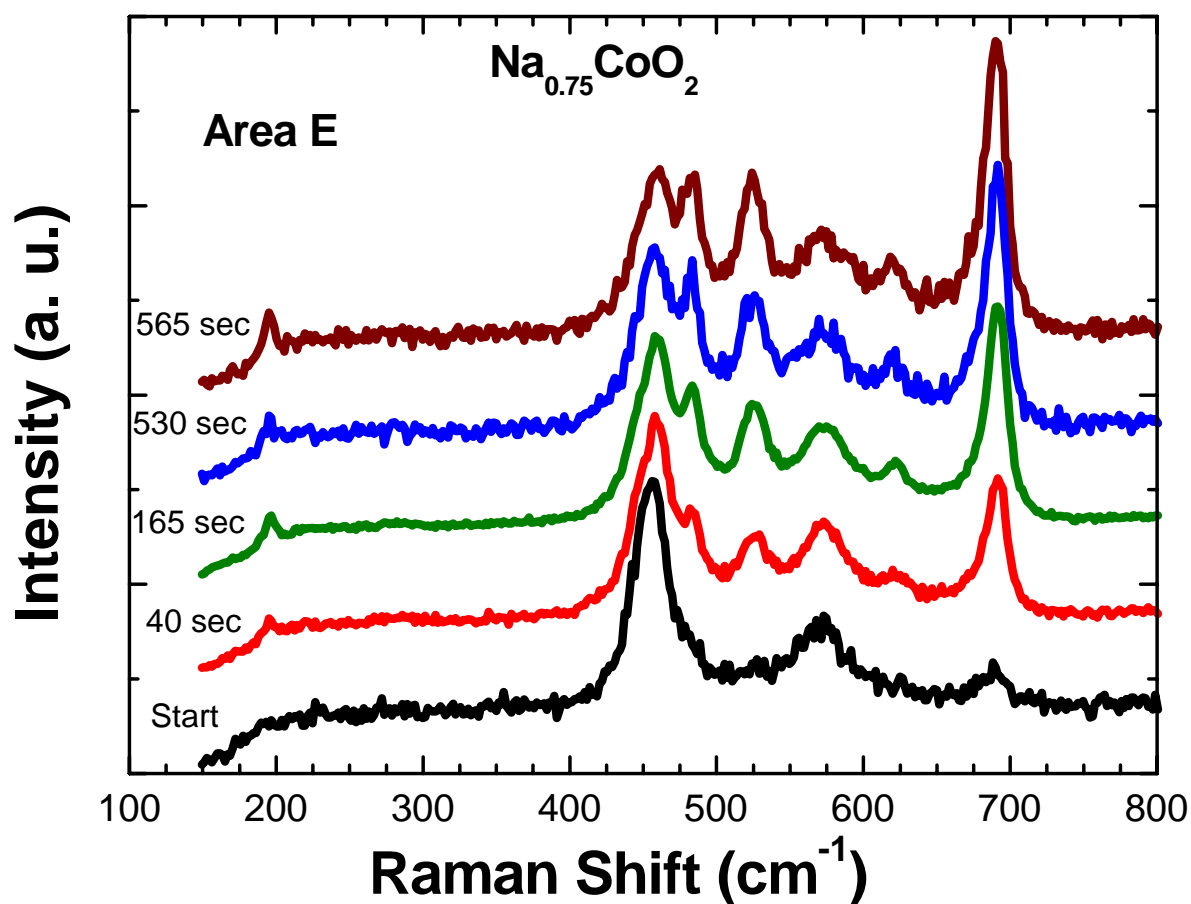


Fig. 5 - 13. Time-dependent Raman-scattering spectra of aged  $\text{Na}_{0.75}\text{CoO}_2$  thin film measured in situ on area E at room temperature. The 514.5 nm laser line was used for excitation. The curves are shifted for clarity.

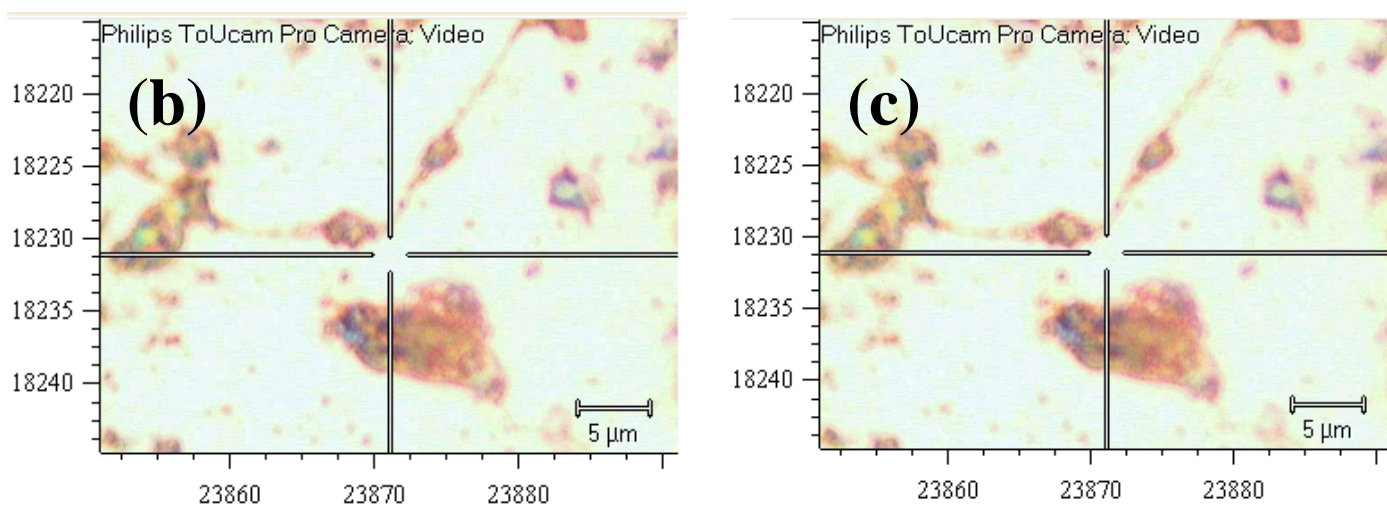


Fig. 5 - 13. These images showing the surface of  $\text{Na}_{0.75}\text{CoO}_2$  thin film (b) before and (c) after our measurements.

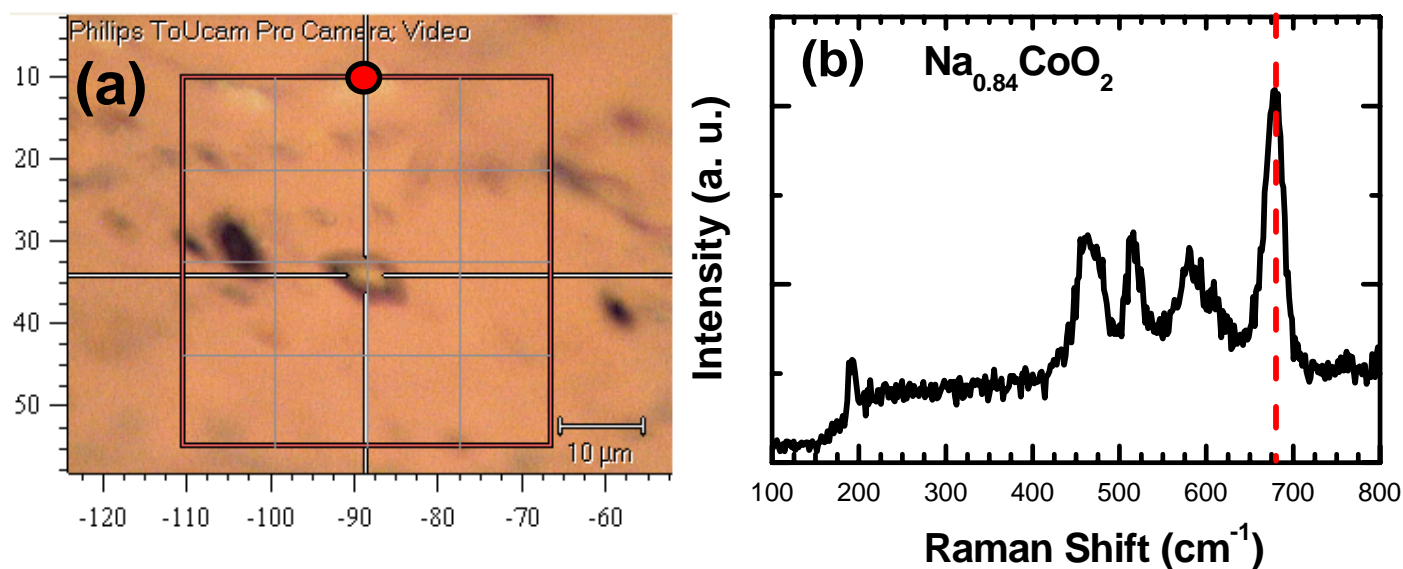


Fig. 5 - 14. (a) The image of the  $ab$  - surface on  $\text{Na}_{0.84}\text{CoO}_2$  single crystal, while our Raman-scattering spectra were taken on each intersection point of the large rectangular region. A total of 25 Raman spectra were recorded by point-to-point mapping with a step size of  $10\ \mu\text{m}$ , while (b) is the Raman spectrum taken on red point as an example. The band  $681\ \text{cm}^{-1}$  is marked by a dashed line, while its intensity represents the concentration of  $\text{Co}_3\text{O}_4$ . The  $514.5\ \text{nm}$  laser line was used for excitation.

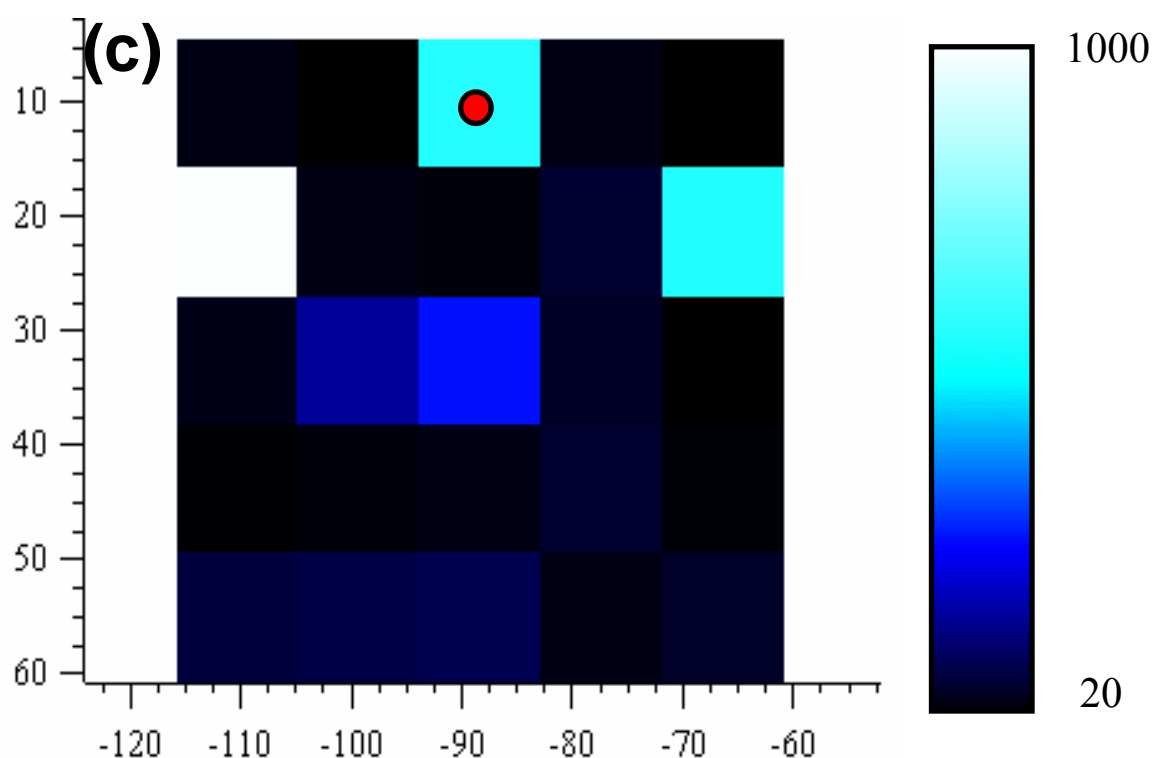


Fig. 5 - 14. (c) Raman mapping image at band  $681\ \text{cm}^{-1}$ , while the brighter color means the stronger Raman intensity.

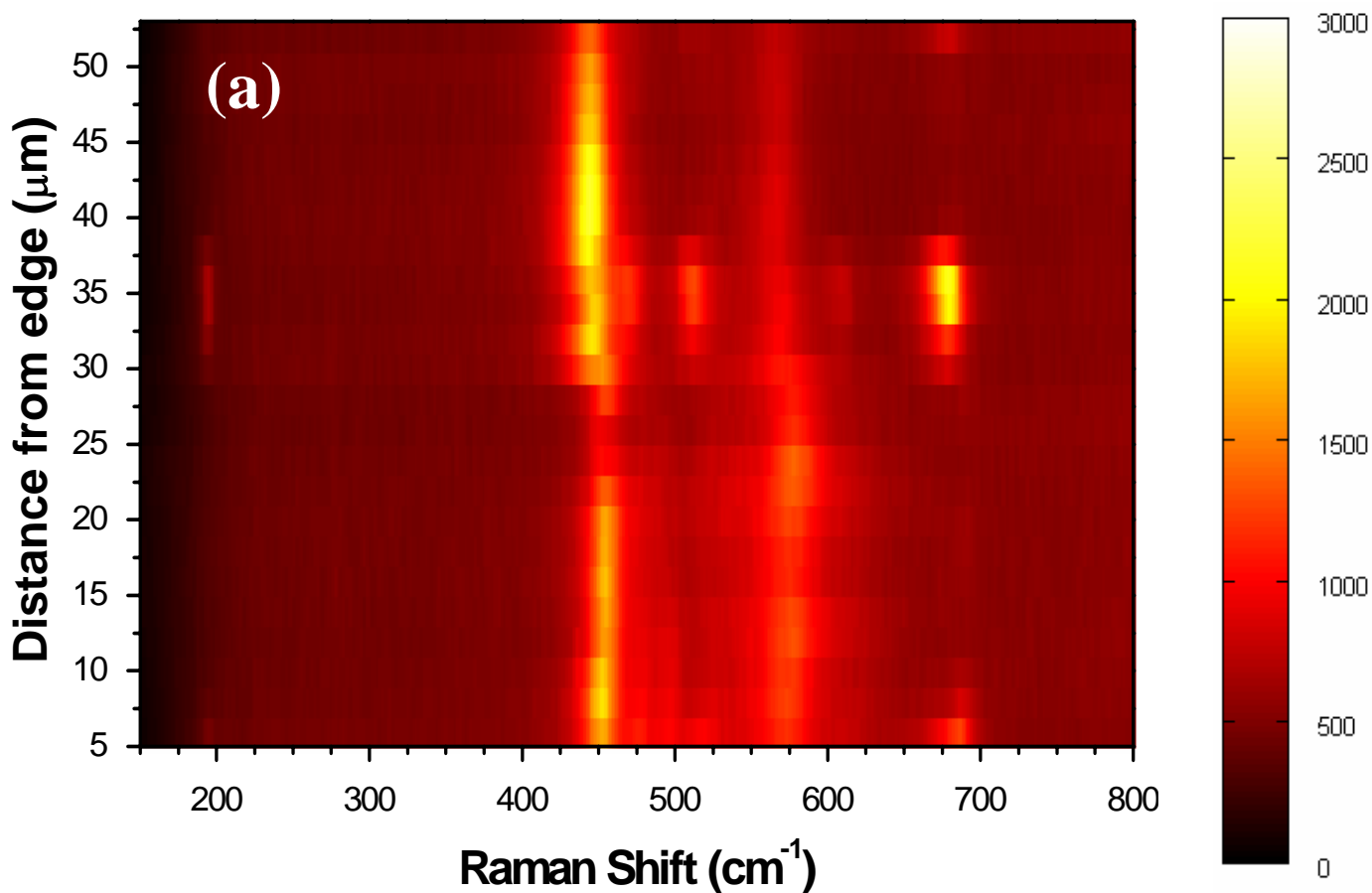


Fig. 5 - 15. (a) Raman mapping spectra as a function of distance from edge on  $ab$  - surface of aged  $\text{Na}_{0.84}\text{CoO}_2$  single crystal which was freshly cleaved before measuring. A total of 25 Raman spectra were recorded by point-to-point mapping with a step size of  $2 \mu\text{m}$ . The  $514.5 \text{ nm}$  laser line was used for excitation.

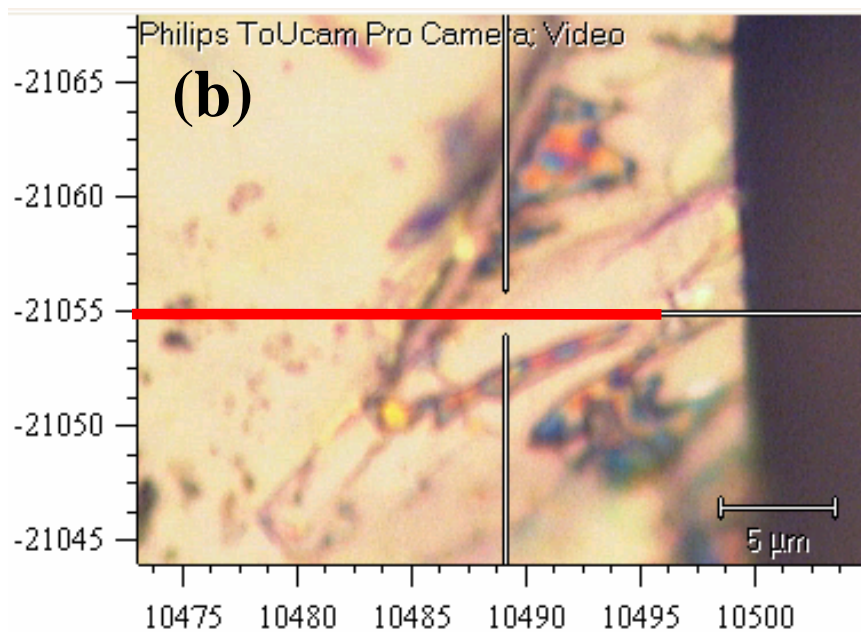


Fig. 5 - 15. (b) The image shows the  $ab$  - surface of  $\text{Na}_{0.84}\text{CoO}_2$  single crystal. The red line is the mapping path.

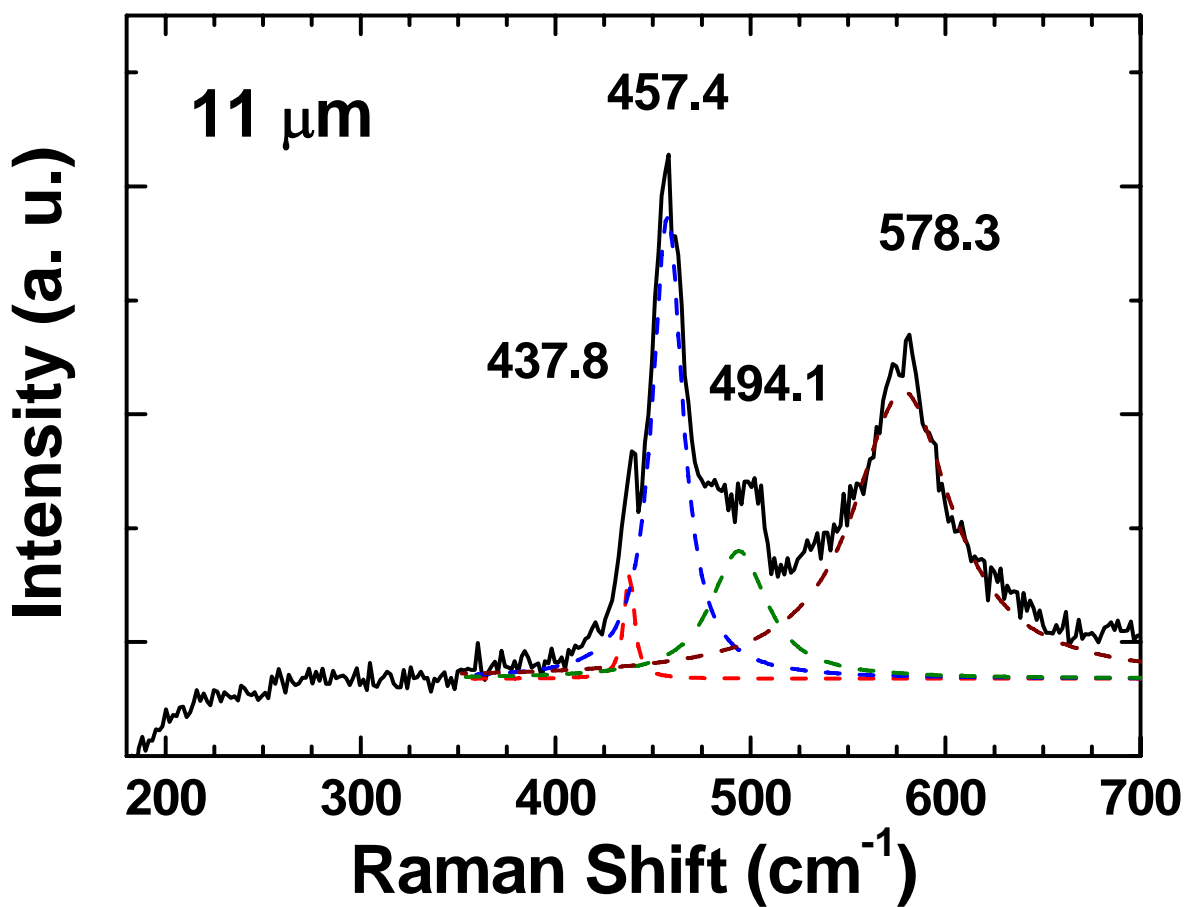


Fig. 5 - 16. Raman-scattering spectrum of 11  $\mu\text{m}$  from edge of aged  $\text{Na}_{0.84}\text{CoO}_2$  single crystal, representing the  $x = 0.5$  compound, while 514.5 nm laser line was used for excitation. The dashed lines are the Lorentzian fitting for the data.

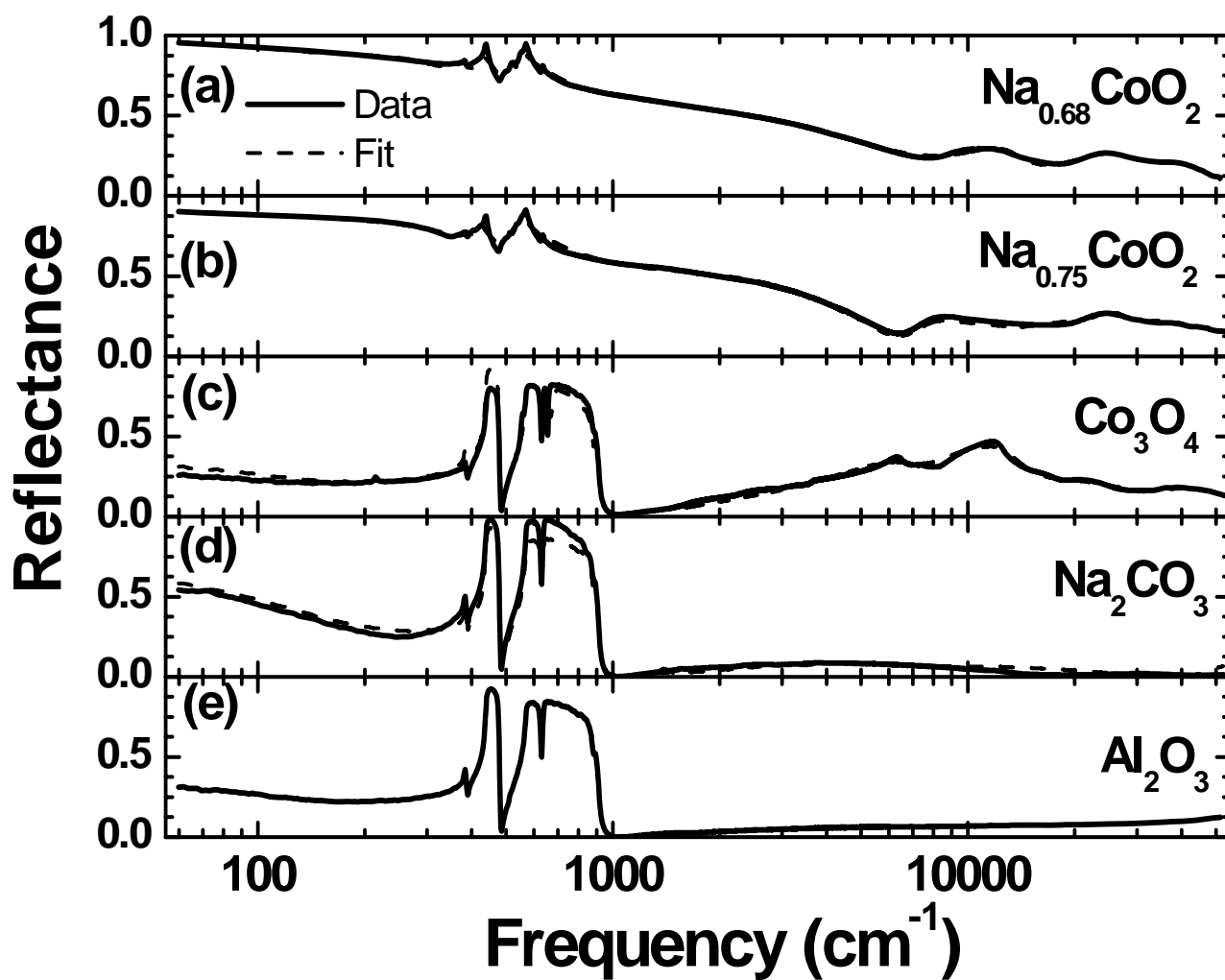


Fig. 5 - 17. Optical reflectance spectra (solid lines) of (a) Na<sub>0.68</sub>CoO<sub>2</sub>, (b) Na<sub>0.75</sub>CoO<sub>2</sub>, (c) Co<sub>3</sub>O<sub>4</sub>, (d) Na<sub>2</sub>CO<sub>3</sub>, and (e) Al<sub>2</sub>O<sub>3</sub> at room temperature. The dashed lines are the best fit using the Drude-Lorentz model.

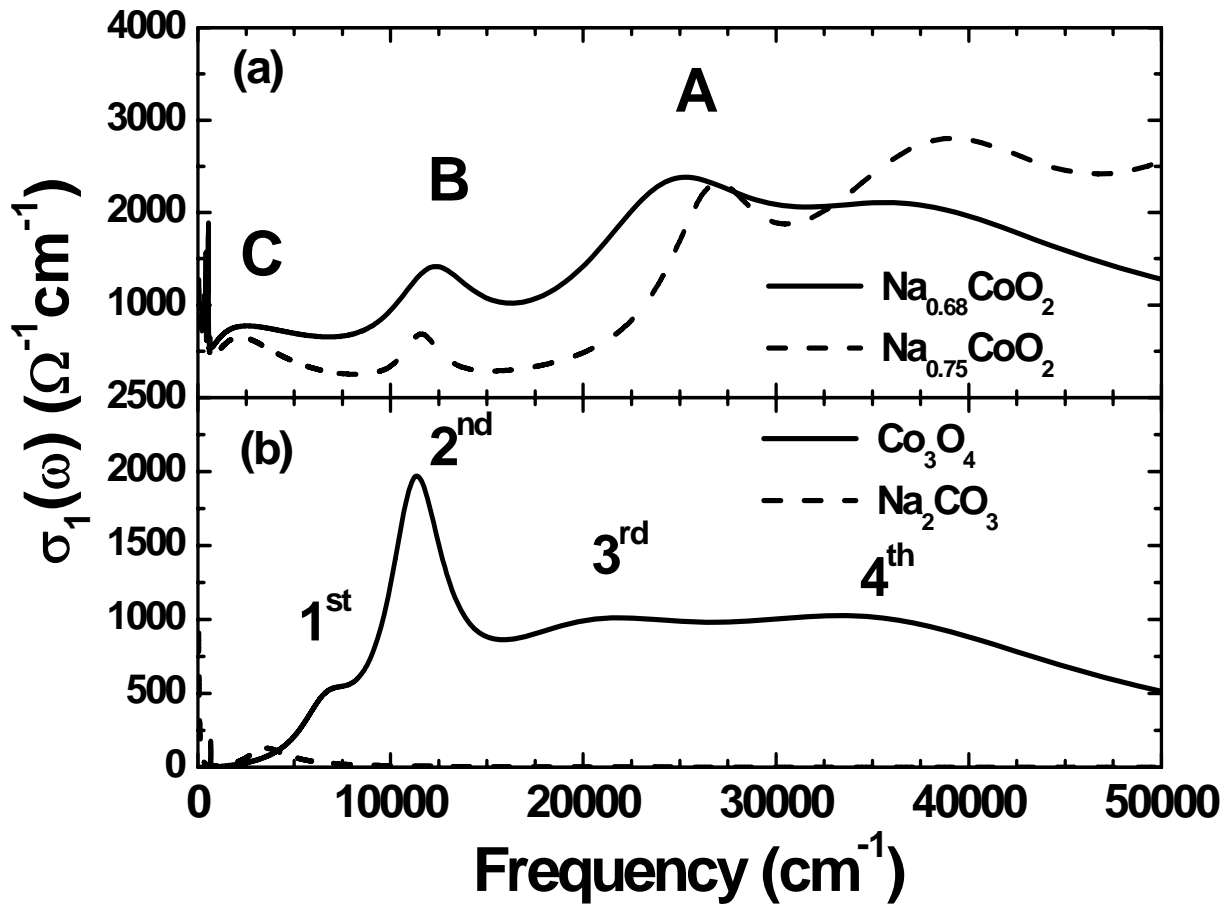


Fig. 5 - 18. Optical conductivity spectra of (a)  $\text{Na}_x\text{CoO}_2$  ( $x = 0.68$  and  $0.75$ ), (b)  $\text{Co}_3\text{O}_4$ , and  $\text{Na}_2\text{CO}_3$  thin films at room temperature.

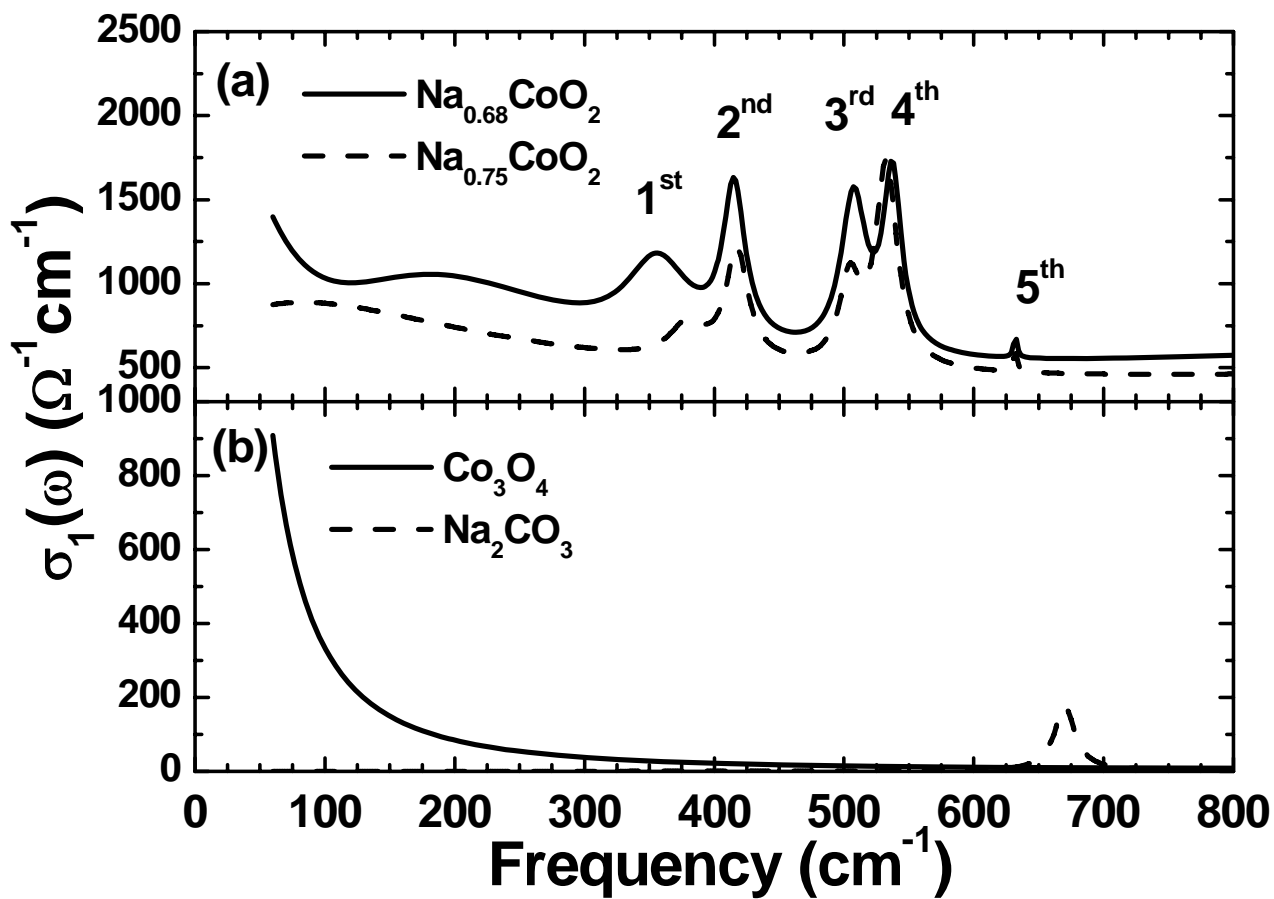


Fig. 5 - 19. Far-infrared conductivity spectra of (a)  $\text{Na}_x\text{CoO}_2$  ( $x = 0.68$  and  $0.75$ ) and (b)  $\text{Co}_3\text{O}_4$  and  $\text{Na}_2\text{CO}_3$  thin films at room temperature.

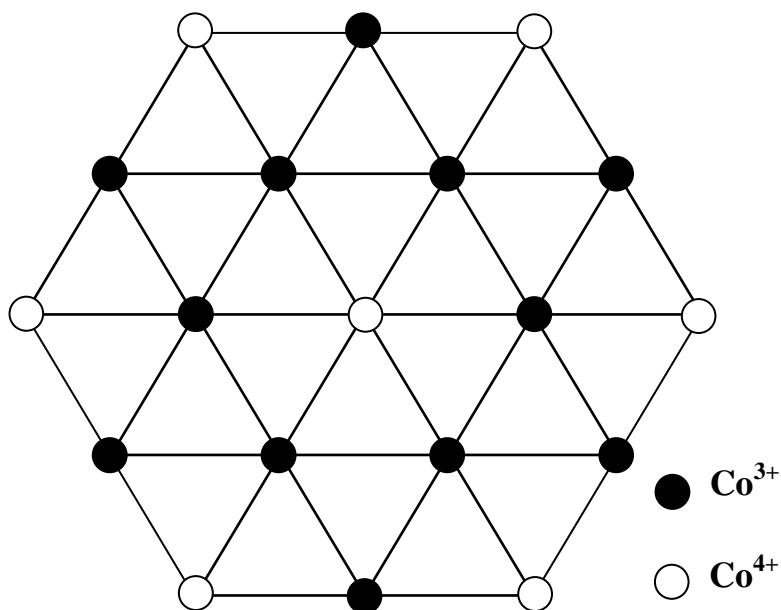


Fig. 5 - 20. A sketch of the suggested charge ordering pattern at the  $\text{CoO}_2$  layer of  $\text{Na}_x\text{CoO}_2$  ( $x = 0.68$  and  $0.75$ ).

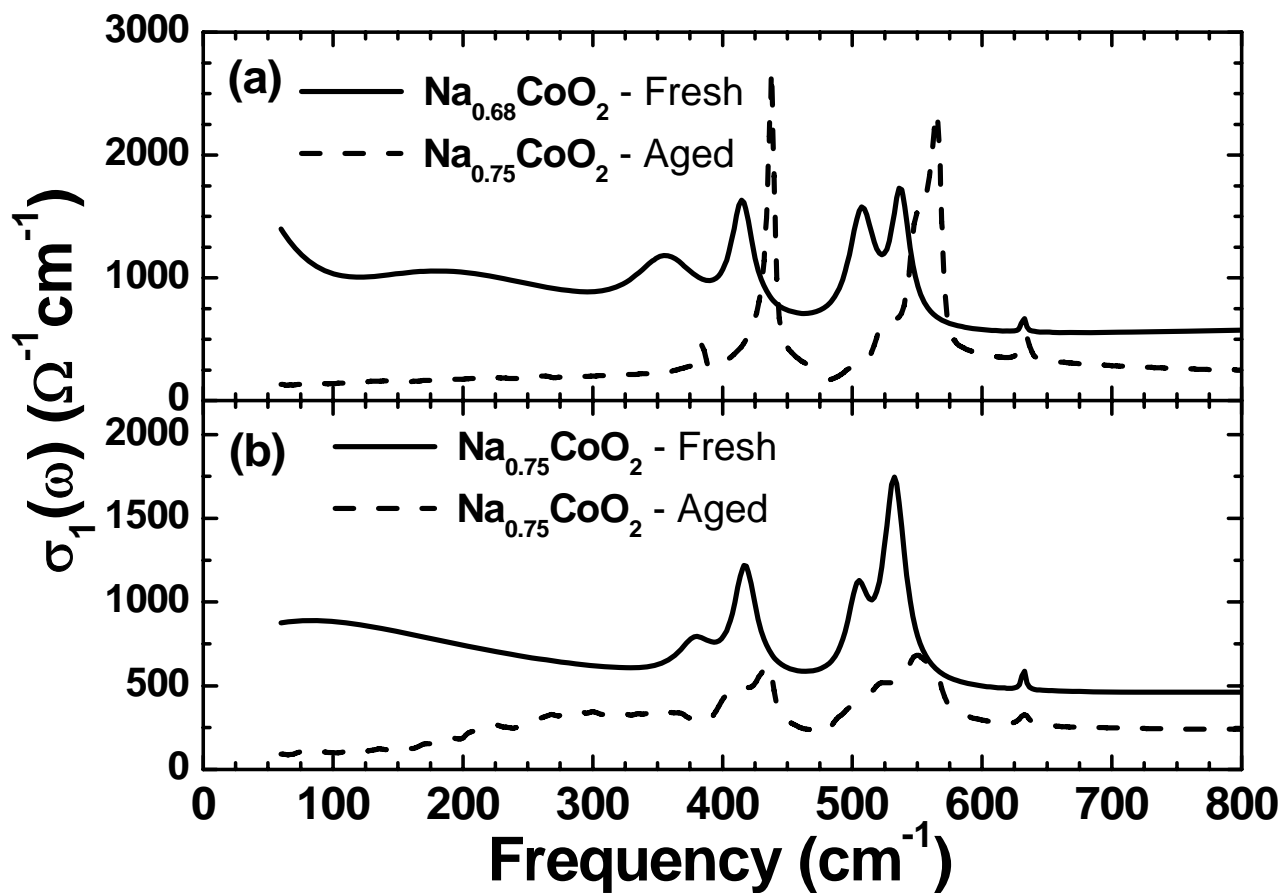


Fig. 5 - 21. Far-infrared conductivity spectra of (a)  $\text{Na}_{0.68}\text{CoO}_2$  (fresh sample and aged sample are shown in solid and dashed lines, respectively) and (b)  $\text{Na}_{0.75}\text{CoO}_2$  (fresh sample and aged sample are shown in solid and dashed lines, respectively) thin films at room temperature.

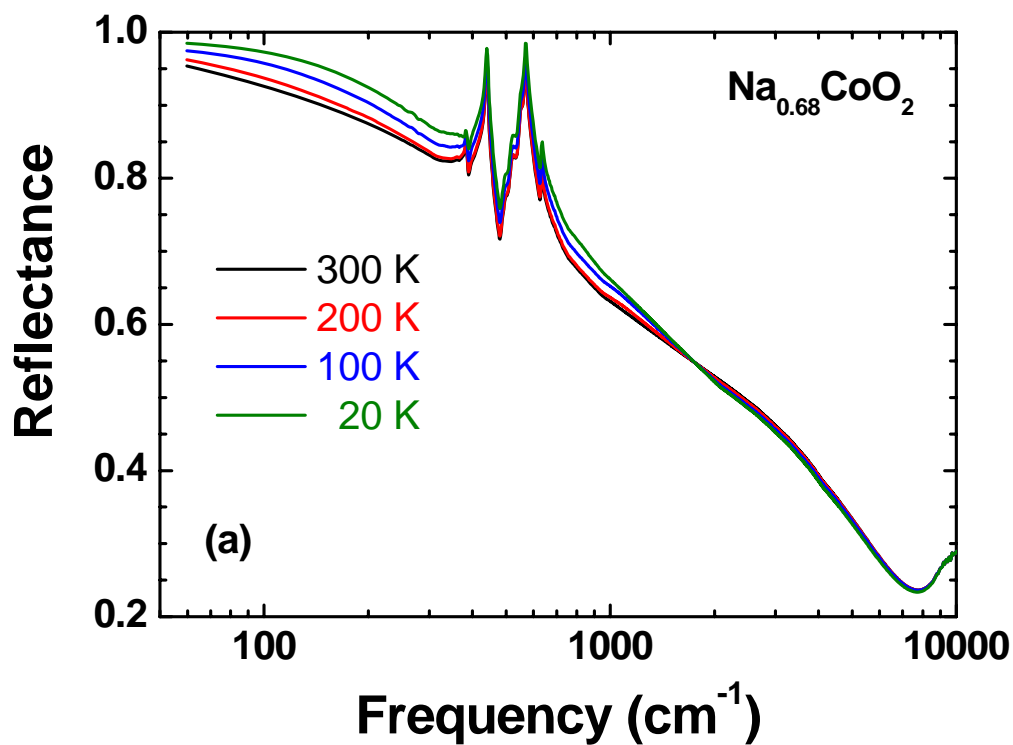


Fig. 5 - 22(a). Temperature dependent infrared reflectance spectra of  $\text{Na}_{0.68}\text{CoO}_2$  thin film.

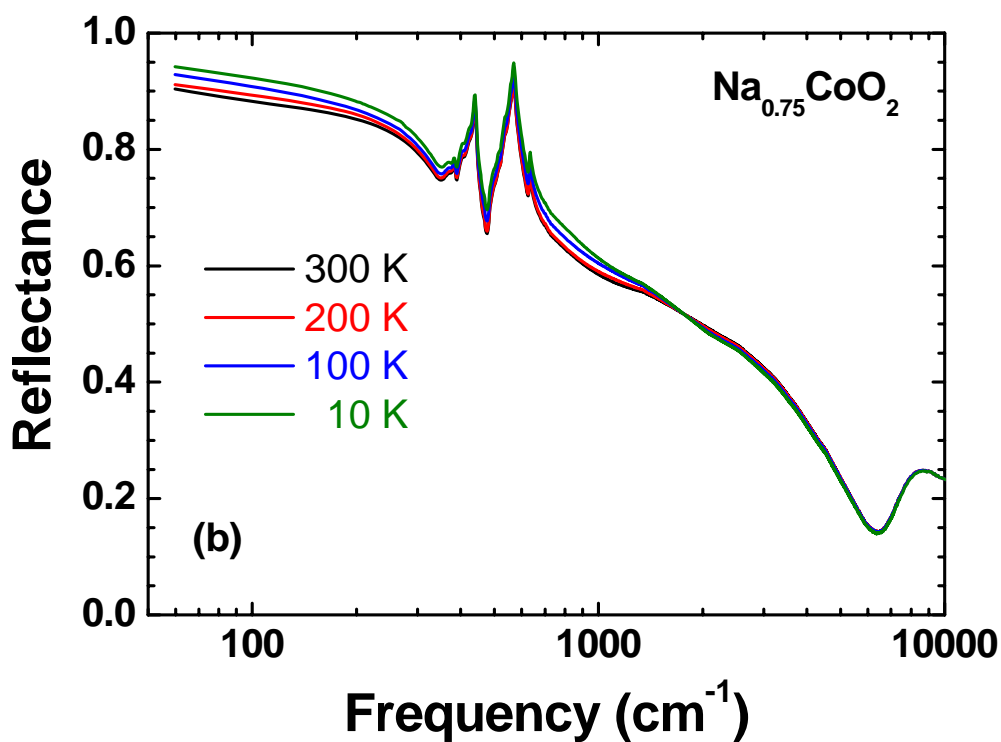


Fig. 5 - 22(b). Temperature dependent infrared reflectance spectra of  $\text{Na}_{0.75}\text{CoO}_2$  thin film.

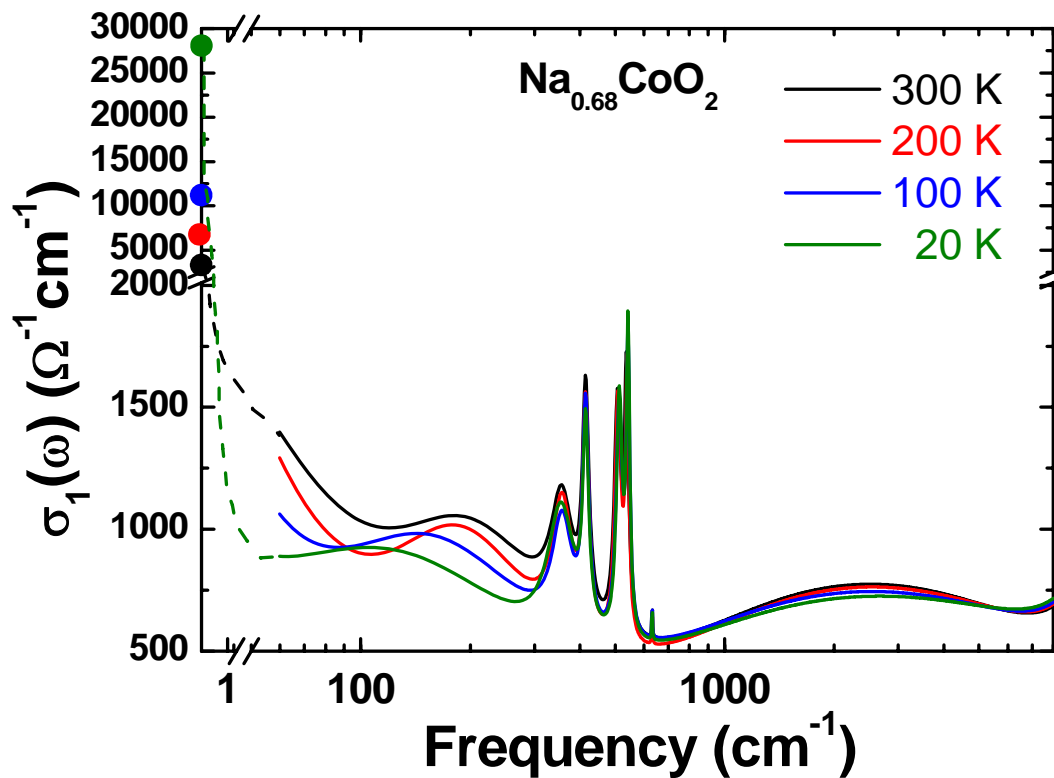


Fig. 5 - 23. Temperature dependent infrared conductivity spectra of  $\text{Na}_{0.68}\text{CoO}_2$  thin film. The dc conductivity values are shown by symbols, low-frequency extrapolations by dashed lines.

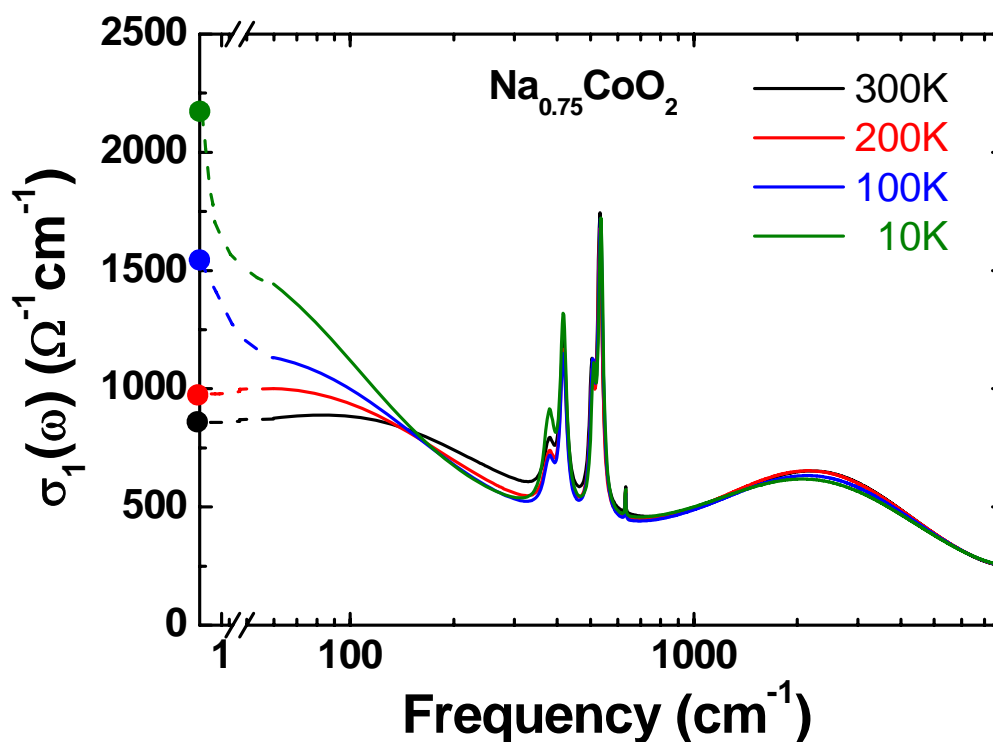


Fig. 5 - 24. Temperature dependent infrared conductivity spectra of  $\text{Na}_{0.75}\text{CoO}_2$  thin film. The dc conductivity values are shown by symbols, low-frequency extrapolations by dashed lines.

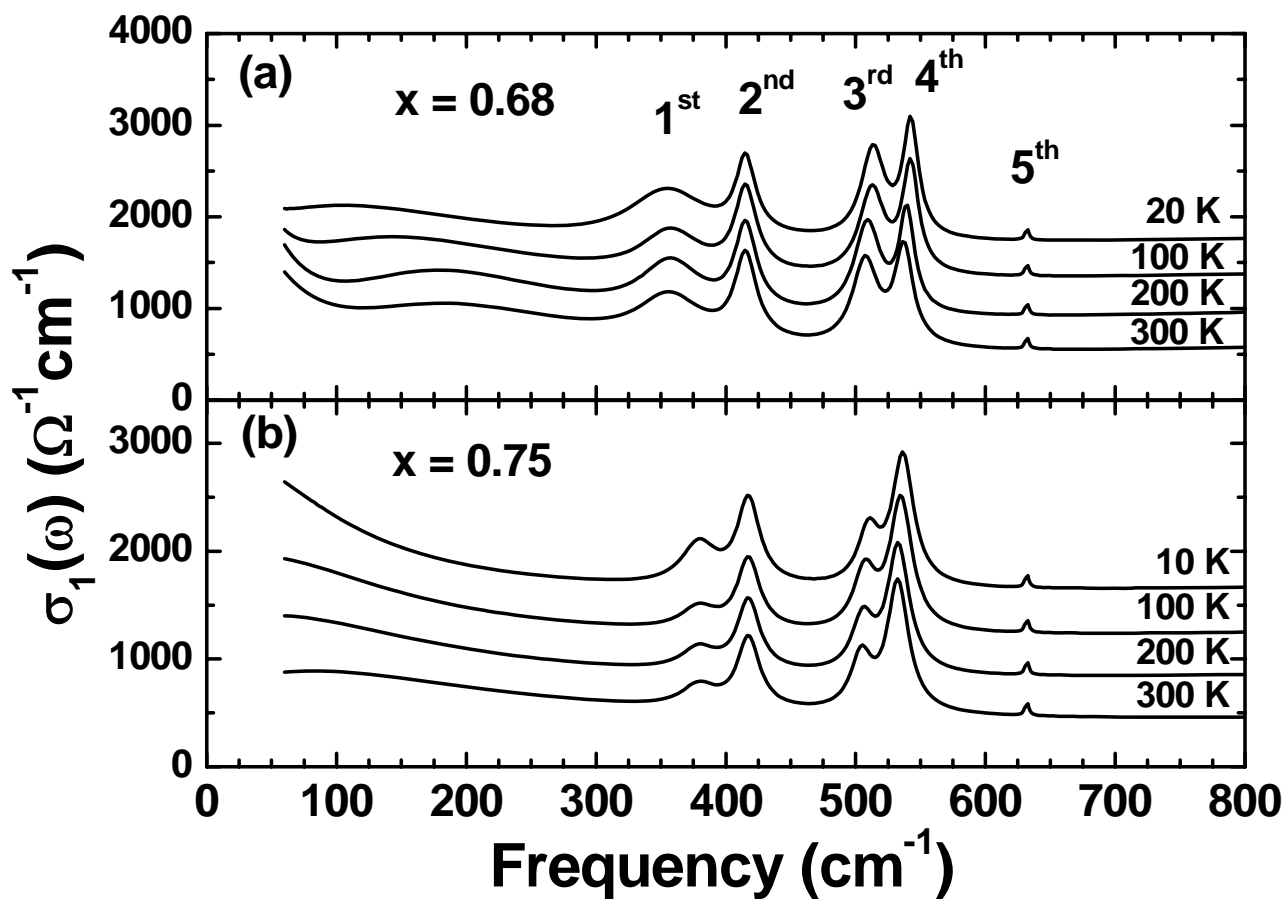


Fig. 5 - 25. Temperature dependent far-infrared conductivity spectra of  $\text{Na}_x\text{CoO}_2$  thin films (a)  $x = 0.68$  and (b)  $x = 0.75$ . For clarity, the ordinate has been offset by 20% of the maximum of  $Y$  - axis for the successive spectra.

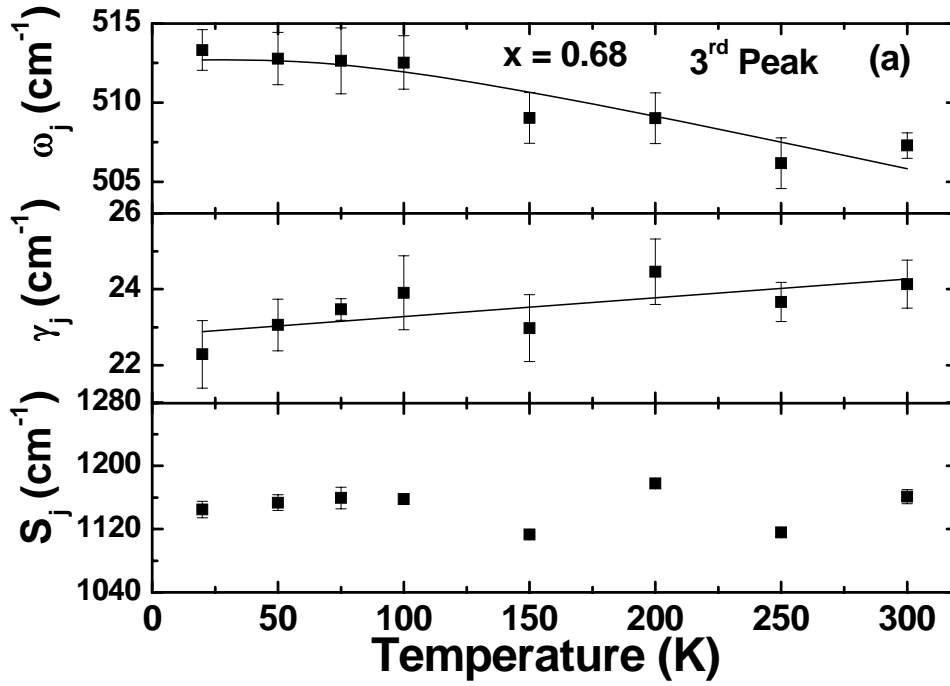


Fig. 5 - 26. (a) Temperature dependence of the frequency ( $\omega_j$ ), linewidth ( $\gamma_j$ ), and spectral weight ( $S_j$ ) of the 3<sup>rd</sup> peak of  $\text{Na}_{0.68}\text{CoO}_2$  thin film. The solid lines are the expected behavior of the phonon frequencies and linewidths according to anharmonic effect.

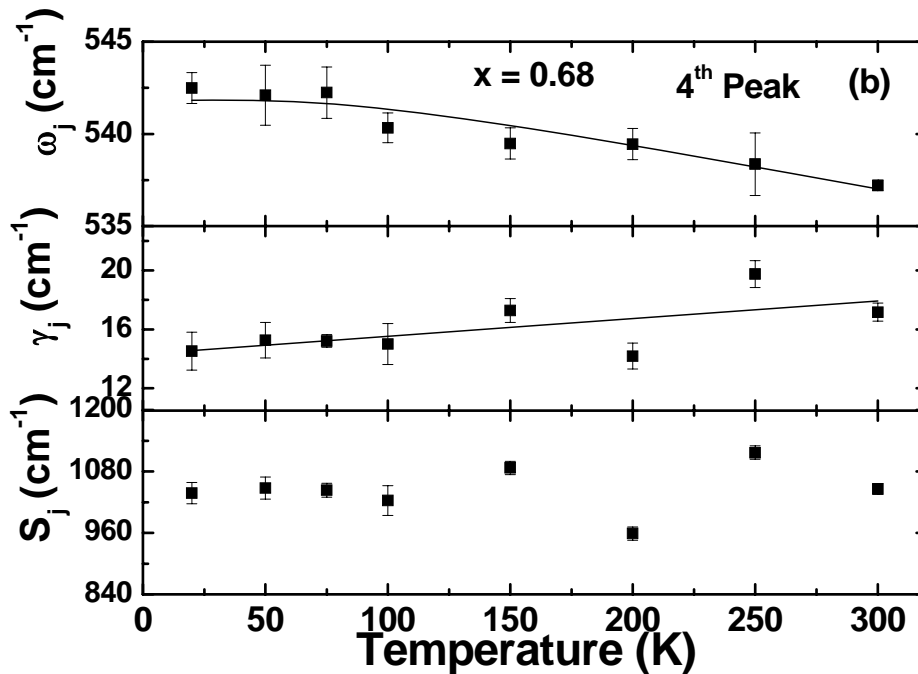


Fig. 5 - 26. (b) Temperature dependence of the frequency ( $\omega_j$ ), linewidth ( $\gamma_j$ ), and spectral weight ( $S_j$ ) of the 4<sup>th</sup> peak of  $\text{Na}_{0.68}\text{CoO}_2$  thin film. The solid lines are the expected behavior of the phonon frequencies and linewidths according to anharmonic effect.

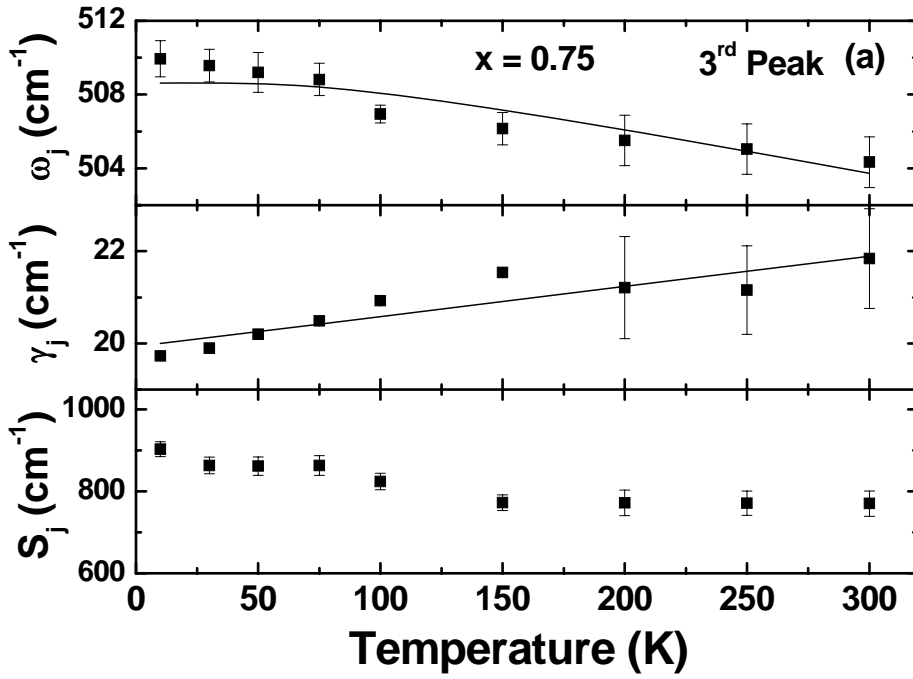


Fig. 5 - 27. (a) Temperature dependence of the frequency ( $\omega_j$ ), linewidth ( $\gamma_j$ ), and spectral weight ( $S_j$ ) of the 3<sup>rd</sup> peak of  $\text{Na}_{0.75}\text{CoO}_2$  thin film. The solid lines are the expected behavior of the phonon frequencies and linewidths according to anharmonic effect.

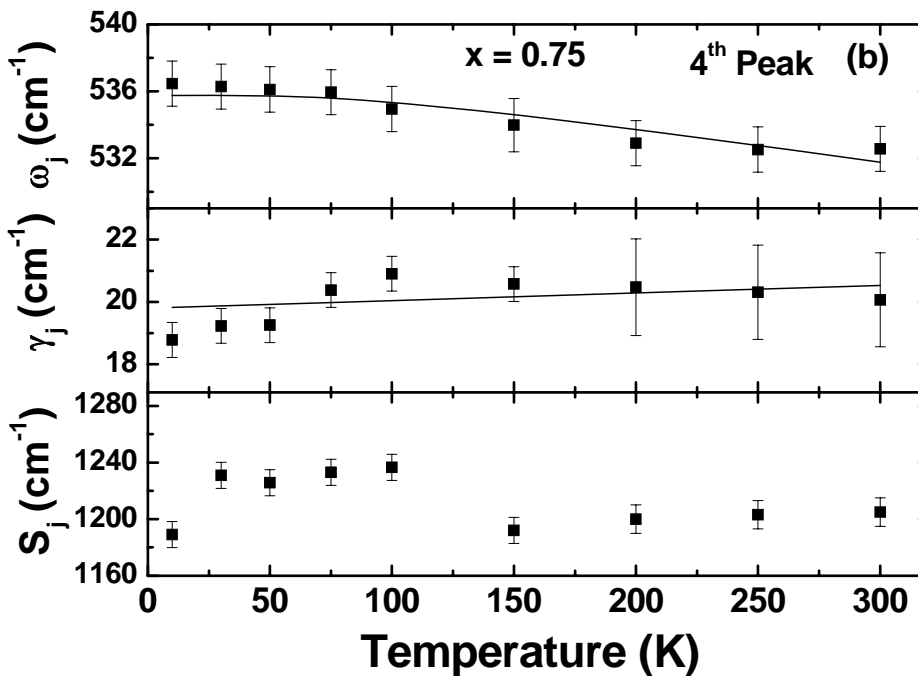


Fig. 5 - 27. (b) Temperature dependence of the frequency ( $\omega_j$ ), linewidth ( $\gamma_j$ ), and spectral weight ( $S_j$ ) of the 4<sup>th</sup> peak of  $\text{Na}_{0.75}\text{CoO}_2$  thin film. The solid lines are the expected behavior of the phonon frequencies and linewidths according to anharmonic effect.

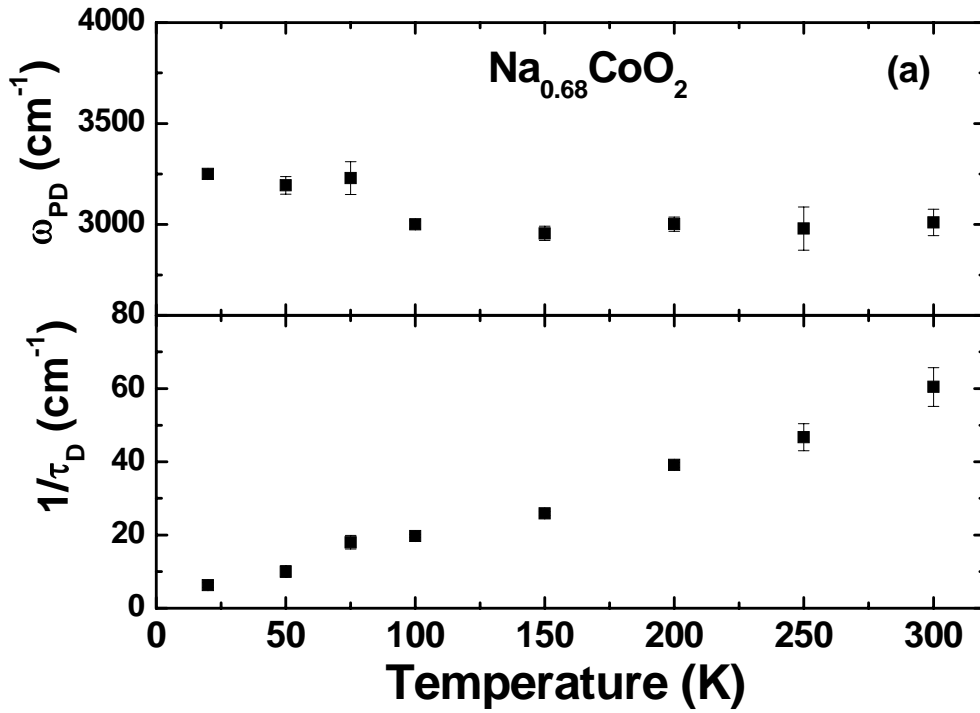


Fig. 5 - 28. (a) Temperature dependence of the plasma frequency ( $\omega_{PD}$ ) and scattering rate ( $1/\tau_D$ ) of  $\text{Na}_{0.68}\text{CoO}_2$  thin film.

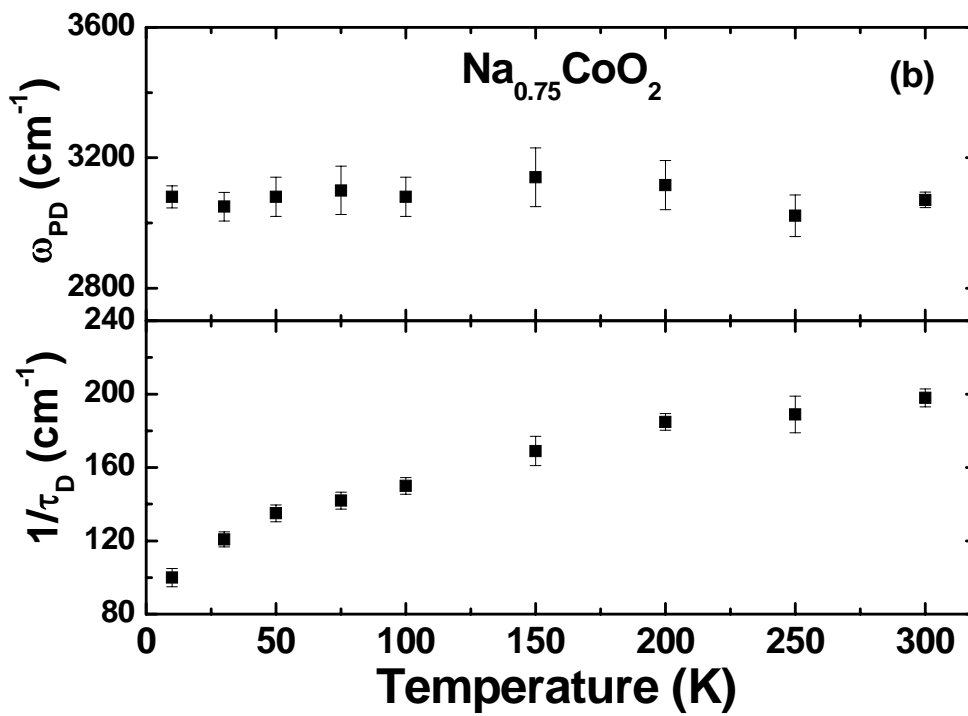


Fig. 5 - 28. (b) Temperature dependence of the plasma frequency ( $\omega_{PD}$ ) and scattering rate ( $1/\tau_D$ ) of  $\text{Na}_{0.75}\text{CoO}_2$  thin film.

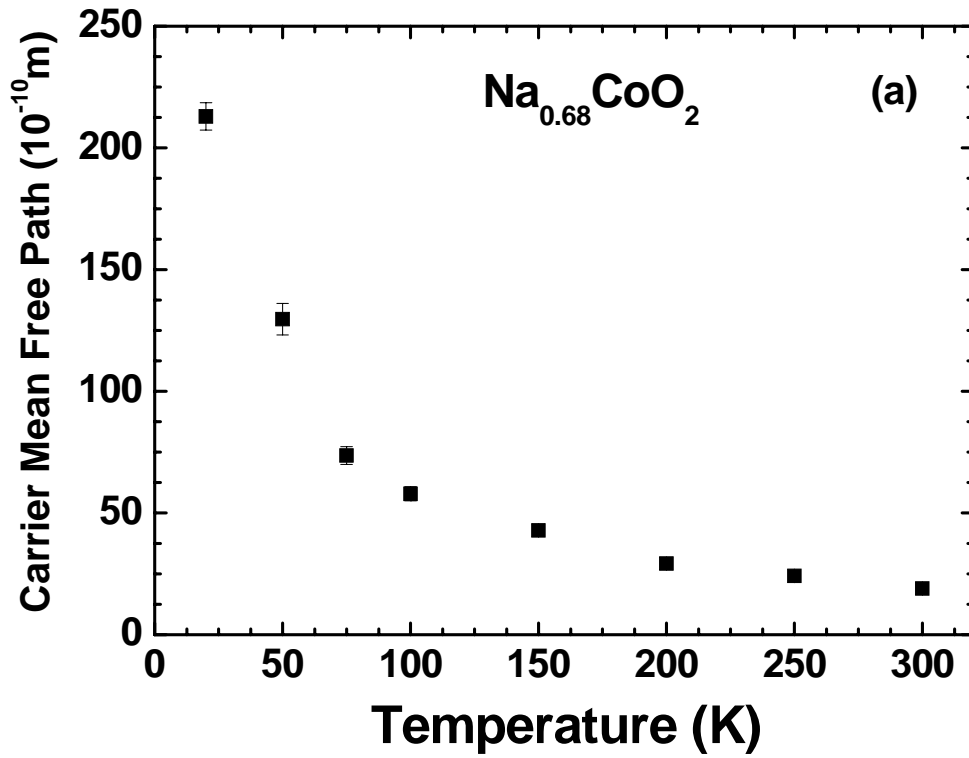


Fig. 5 - 29. (a) Temperature dependence of the carrier mean free path of  $\text{Na}_{0.68}\text{CoO}_2$  thin film.

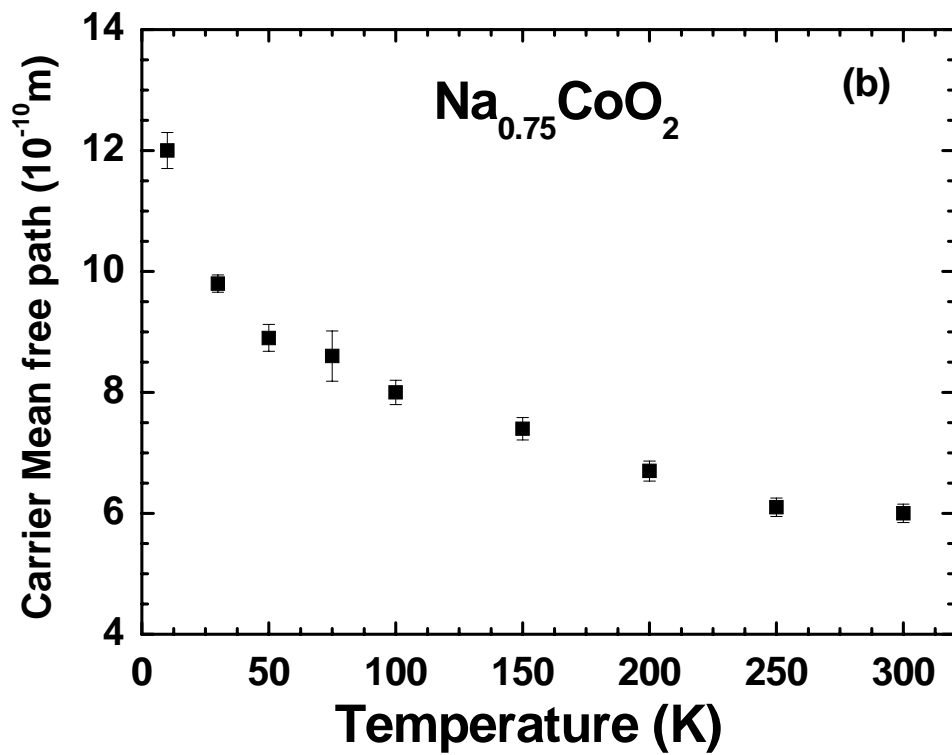


Fig. 5 - 29. (b) Temperature dependence of carrier mean free path of  $\text{Na}_{0.75}\text{CoO}_2$  thin film.

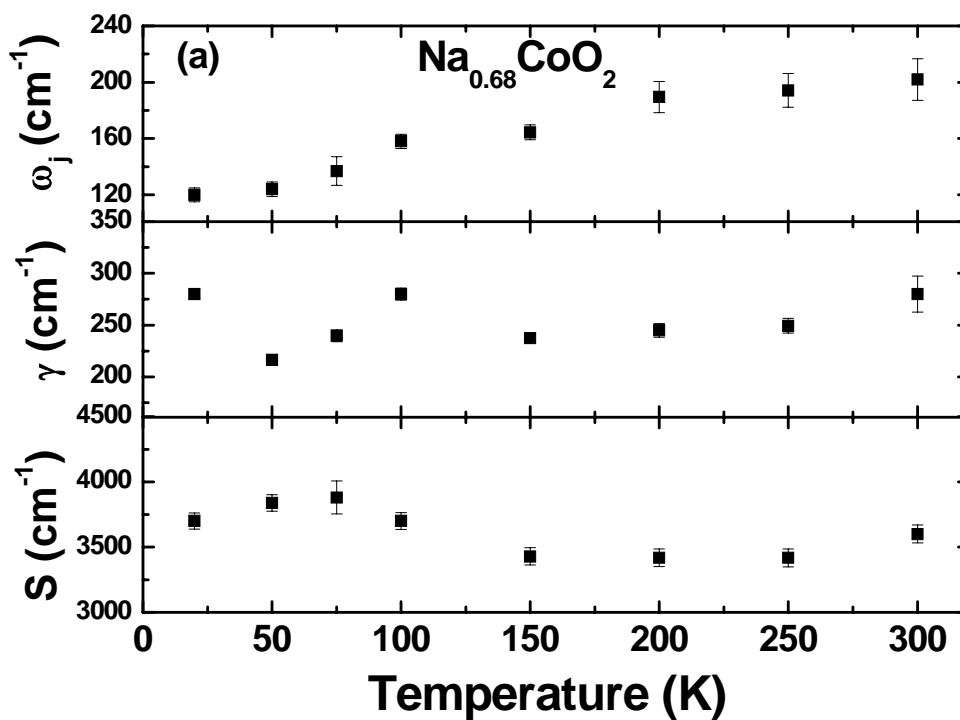


Fig. 5 - 30. (a) Temperature dependence of the frequency ( $\omega_j$ ), linewidth ( $\gamma_j$ ), and spectral weight ( $S_j$ ) of the  $150\text{ cm}^{-1}$  peak of  $\text{Na}_{0.68}\text{CoO}_2$  thin film.

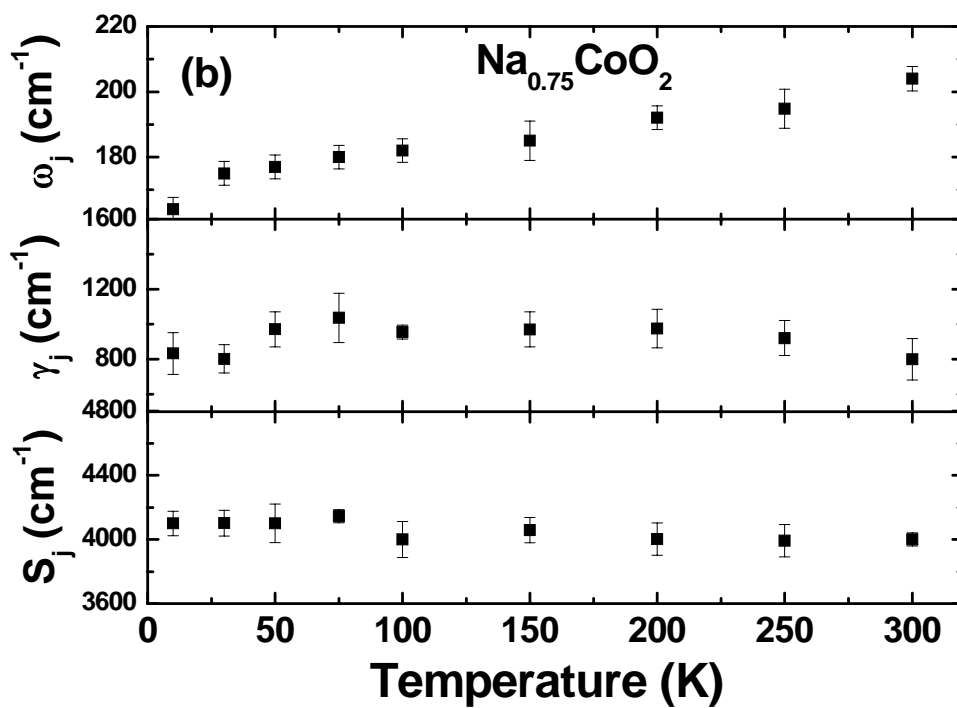


Fig. 5 - 30. (b) Temperature dependence of the frequency ( $\omega_j$ ), linewidth ( $\gamma_j$ ), and spectral weight ( $S_j$ ) of the  $150\text{ cm}^{-1}$  peak of  $\text{Na}_{0.75}\text{CoO}_2$  thin film.

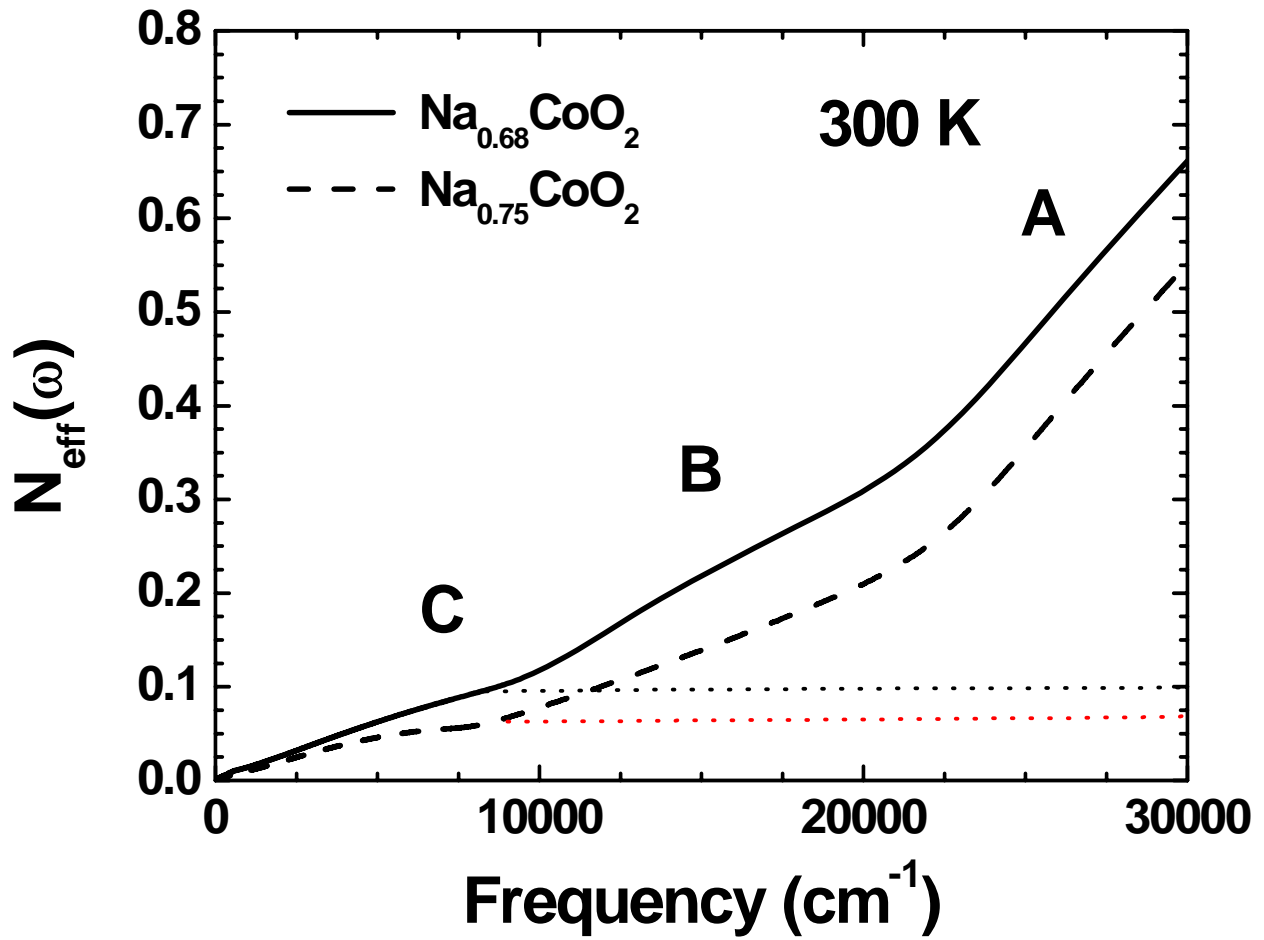


Fig. 5 - 31. Partial sum rule for the two  $\text{Na}_x\text{CoO}_2$  ( $x = 0.68$  and  $0.75$ ) thin films at 300 K. Dashed lines show the extrapolating the flat regions to infinite frequency.

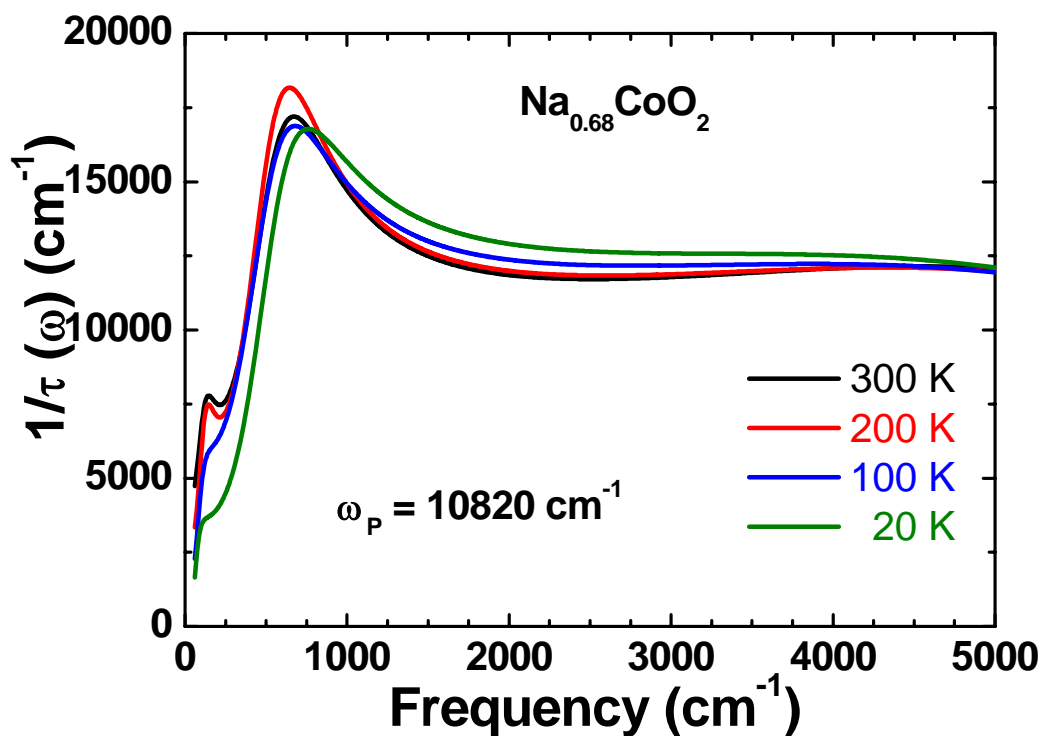


Fig. 5 - 32. Temperature-dependent scattering rate  $1/\tau(\omega)$  spectra of  $\text{Na}_{0.68}\text{CoO}_2$  thin film. Here we subtracted the phonons contributions in order to see the bosonic mode better.

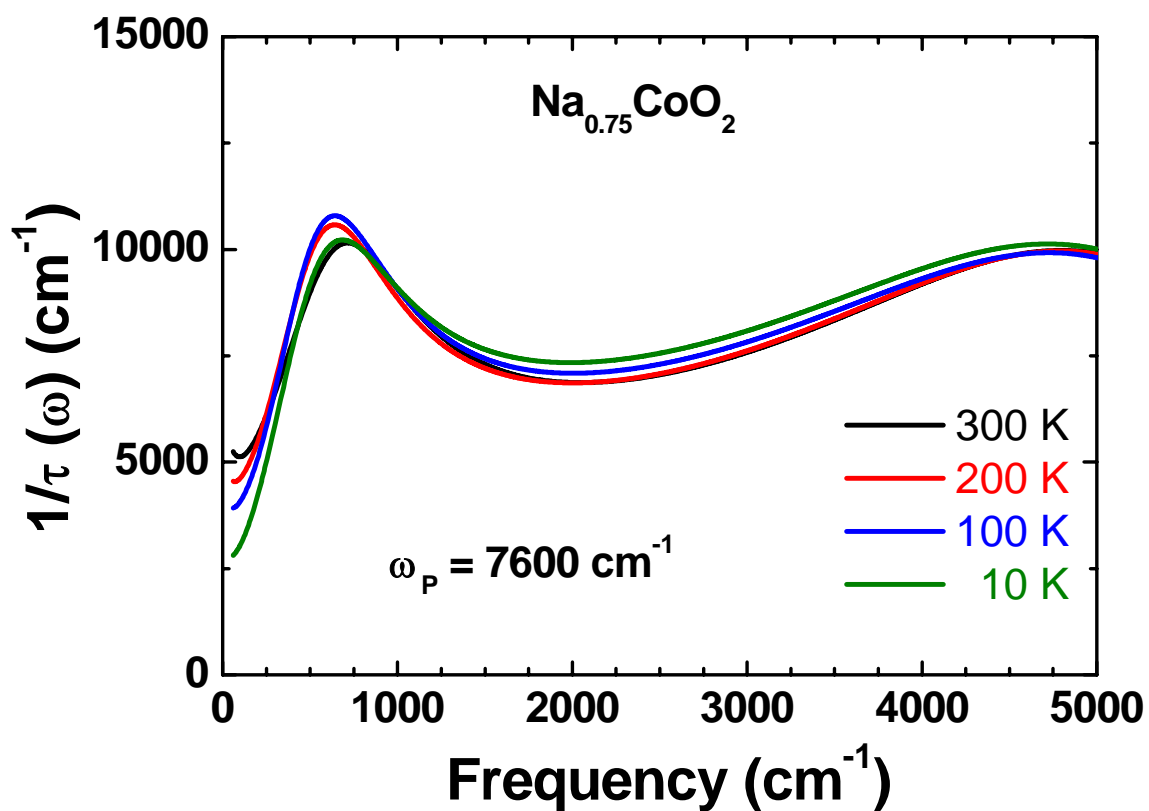


Fig. 5 - 33. Temperature-dependent scattering rate  $1/\tau(\omega)$  spectra of  $\text{Na}_{0.75}\text{CoO}_2$  thin film. Here we subtracted the phonons contributions in order to see the bosonic mode better.

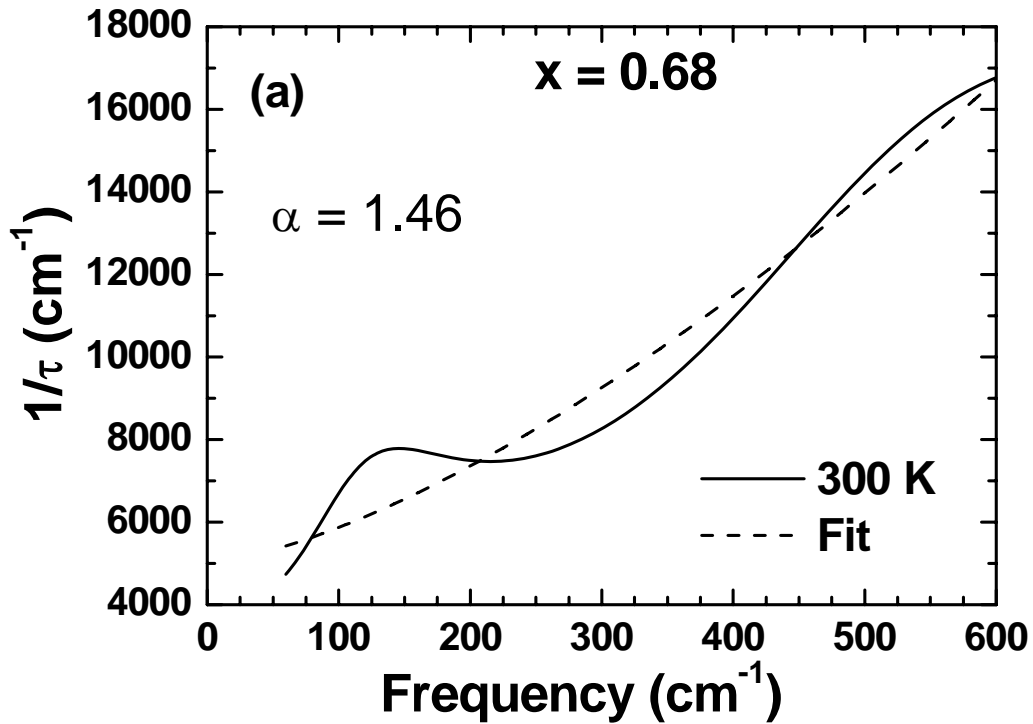


Fig. 5 - 34(a). Temperature-dependent scattering rate  $1/\tau(\omega)$  spectrum of  $\text{Na}_{0.68}\text{CoO}_2$  thin film at low frequencies at 300 K. The fitting curve is based on Eq. (5.2.10).

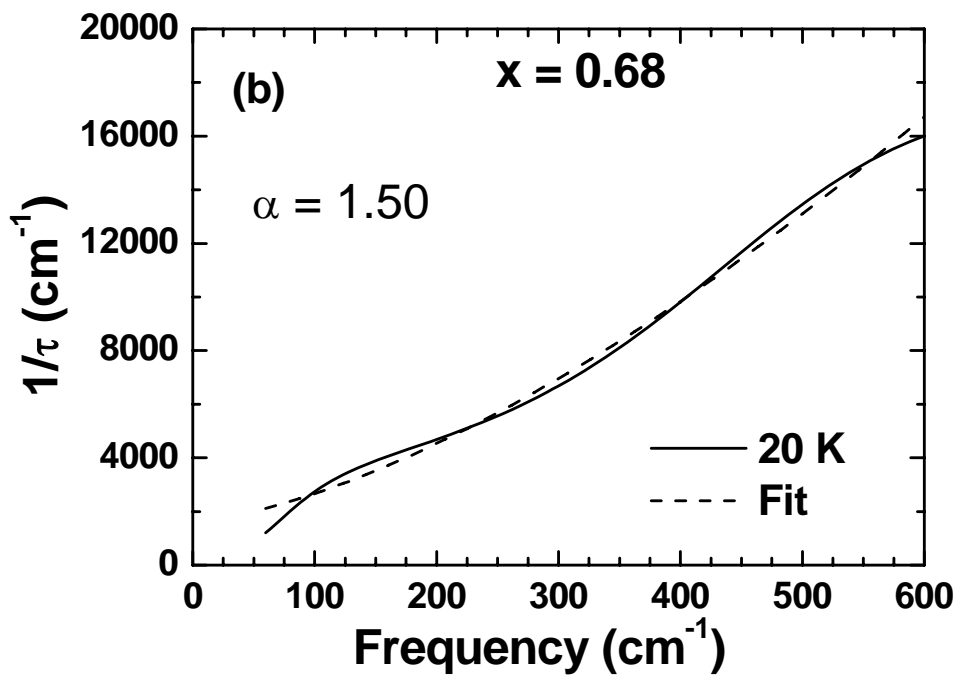


Fig. 5 - 34(b). Temperature-dependent scattering rate  $1/\tau(\omega)$  spectrum of  $\text{Na}_{0.68}\text{CoO}_2$  thin film at low frequencies at 20 K. The fitting curve is based on Eq. (5.2.10).

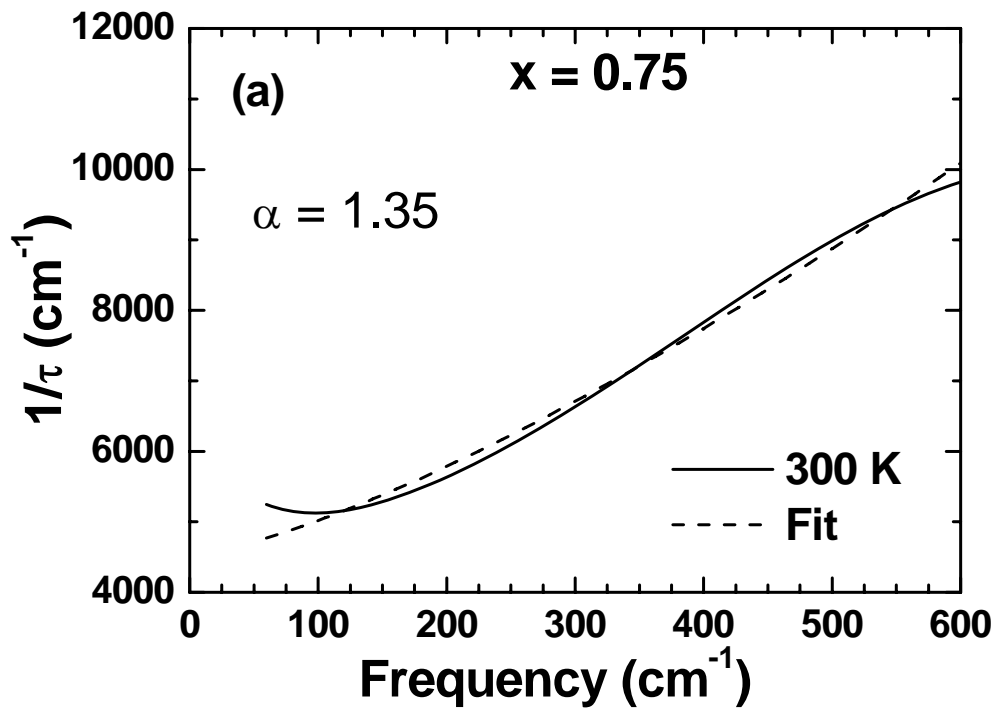


Fig. 5 - 35(a). Temperature-dependent scattering rate  $1/\tau(\omega)$  spectrum of  $\text{Na}_{0.75}\text{CoO}_2$  thin film at low frequencies at 300 K. The fitting curve is based on Eq. (5.2.10).

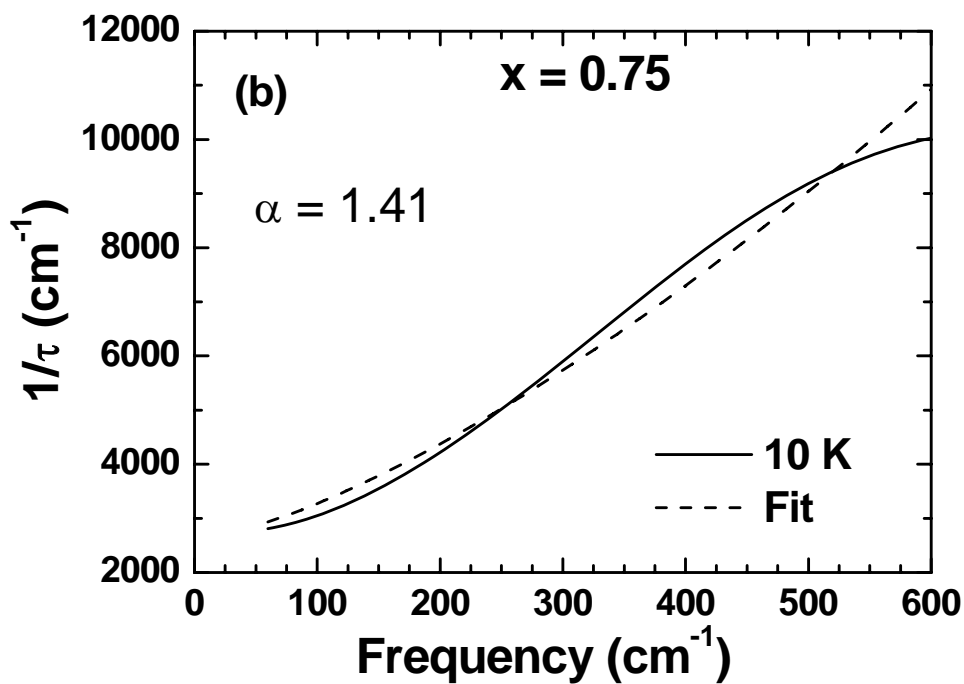


Fig. 5 - 35(b). Temperature-dependent scattering rate  $1/\tau(\omega)$  spectrum of  $\text{Na}_{0.75}\text{CoO}_2$  thin film at low frequencies at 10 K. The fitting curve is based on Eq. (5.2.10).